EFFECT OF CELL ATTACHMENT AND MOLECULAR EVENTS ASSOCIATED WITH FREEZING BIOPHYSICS AND THE "TWO FACTOR" INJURY HYPOTHESIS

A DISSERTATION

SUBMITTED TO THE FACULTY OF THE GRADUATE SCHOOL

OF THE UNIVERSITY OF MINNESOTA

BY

SARAVANA KUMAR BALASUBRAMANIAN

IN PARTIAL FULFILLMENT OF THE REQUIREMENTS

FOR THE DEGREE OF

DOCTOR OF PHILOSOPHY

JOHN BISCHOF, ADVISER

DECEMBER 2011

ACKNOWLEDGEMENTS

I would like to thank all members of the Bioheat and Mass transfer lab for their support and friendship during the course of my dissertation. To mention a select few, I have had the pleasure to work with David Swanlund, Venkat Kalambur, Erin Grassl, Raghav Goel, Ramji Venkatasubramanian, Mie Hagiwara, Arjun Menon, Helena Zec, Emily Ongstad, Rachana Visaria, Jeung Choi, Jing Jang, Mithun Shenoi, and Neha Shah during my graduate school. A special note of thanks to Dr. Wim Wolkers, who inspired me by his calm and intelligent demeanor. I have also had the opportunity to interact with members from other research groups for which I am very thankful.

I have also had the pleasure to interact with a number of faculty members during the course of my thesis. A special note of thanks to all my committee members – Dr. Allison Hubel, Dr, Victor Barocas, Dr. Alptekin Aksan, Dr. Chun Wang and Dr. Steven Girshick. My sincere thanks to all my graduate school professors, who provided me with the right knowledge and tools to succeed.

Most of all, I would like to thank my adviser, Dr. John Bischof, who always pushed me to aim beyond good. Every meeting with him was informative and gave me the tools to succeed. He was always open, honest and forthcoming with his opinions and constructive criticisms, which has constantly pushed me to get better. The best compliment that I can give him is that I have tried to mold myself after him in every facet of my professional life. I sincerely thank you for your patience, support and guidance when I required it the most.

Last but not the least; I want to thank my family for always being there. My in-laws have lent me due support during my long journey. I cannot have done this without the constant support, trust and love of my wife Katya. I am incredibly blessed to have my lovely daughter Amelia by my side at my defense. Lastly, I want to thank my parents who have sacrificed a lot and whose one goal was to see me pursue this dream. Thank you …….

ABSTRACT

Freezing of biological systems is generally intended to maximize cell survival (cryopreservation) or injury (cryosurgery) depending on the application. The biophysical contribution to cellular freeze injury is generally described by the "two factor" injury hypothesis. Slow freezing is associated with "solution effects" injury while rapid freezing is linked to the lethality of intracellular ice formation (IIF). The "two factor" hypothesis has been actively investigated for cell suspensions. While cell suspensions provide a fundamental understanding of cellular biophysics and injury, more complex systems (featuring cell attachment) are needed to potentially link to tissues. The effect of cell attachment in the context of the "two factor" hypothesis has not been extensively investigated especially for water transport biophysics. In addition, the "two factor" injury hypothesis implicates changes to cellular macromolecules (e.g. lipids and proteins) as potential freezing injury mechanisms. Currently very little is known about the molecular events associated with the biophysics of freezing cells.

The specific aims (SA) of the dissertation are listed below, and it addresses some of the limitations identified.

SA 1: Study the effect of cell attachment on the "two factor" hypothesis during freezing

SA2: Investigate the molecular events (lipids and proteins) associated with the "two factor" biophysics of freezing

The effect of cell attachment (SA 1) was studied using two mammalian cell types – human dermal fibroblasts (HDF), and porcine smooth muscle cells (SMC). The cellular systems that were evaluated include suspensions, monolayer (cell-cell interactions), and tissue equivalents (cell-cell and cell-ECM interactions). Cell based biophysical models were then used to compare the predicted biophysics as a function of the attachment state. The molecular events associated with the "two factor" biophysics (SA 2) were studied using three different mammalian cell types – HDF, SMC, and human LNCaP prostate tumor cells. Changes to membrane lipids and proteins during controlled freezing were

evaluated using Fourier Transform Infra-Red spectroscopy (FTIR). The molecular events were then linked to cellular freezing biophysics assessed using cryomicroscope.

The important findings of this dissertation are included below:

1. Cell attachment affects the "two factor" biophysics of freezing. Experimental data shows that IIF is enhanced for cells in the attached state as compared to suspensions. In addition, the results suggest that water transport is enhanced for cells in the attached state as compared to suspensions. However, the impact of increased water transport on cell survival for attached cells is unclear.
2. The study of molecular events shows that slow freezing affects membrane phase transition (liquid crystalline to gel phase), whereas rapid freezing is observed to maintain the high conformational disorder of the membranes.
3. Molecular events (i.e. membrane phase transition) measured using FTIR are linked to cellular biophysics measured using cryomicroscope.
4. The results show a link between cell and lipid membrane dehydration events. It is suggested that membranes can only tolerate dehydration to a certain extent. This connection is suggested as a potential link to a molecular mechanism of cell injury due to "solution effects".

TABLE OF CONTENTS

LIST OF TABLES

LIST OF FIGURES

PERMISSIONS

Letter to Editors

Dear Editor

I, Saravana Kumar Balasubramanian, am finishing up my PhD at the University of Minnesota, Minneapolis. I have authored publications in ABME/Cryobiology/BBA that are listed below.

- Balasubramanian, S.K. Venkatasubramanian, R.T., Menon, A. and Bischof, J.C., "Thermal injury prediction during cryoplasty through in vitro characterization of smooth muscle cell biophysics and viability". Annals of Biomedical Engineering, 2008. 36(1):86-101.
- Balasubramanian SK, Bischof JC, Hubel A. "Water transport and IIF parameters for a connective tissue equivalent"; Cryobiology; 2006 Feb;52(1):62-73
- Wolkers WF, Balasubramanian SK, Ongstad EL, Zec HC, Bischof JC. "Effects of freezing on membranes and proteins in LNCaP prostate tumor cells"; Biochim Biophys Acta. 2007 Mar;1768(3):728-36.
- Balasubramanian SK, Wolkers WF, Bischof JC. "Membrane hydration correlates to cellular biophysics during freezing in mammalian cells"; Biochim Biophys Acta. 2009 May;1788(5):945-53.

I request permission to use the text and figures from my above publications in my doctoral dissertation.

Please let me know if I need to send any additional forms to you.

Thank you.

Saravana Kumar Balasubramanian

Replies from Editors

ABME

- License Number - 2817370983615
- License date - Dec 27, 2011
- Licensed content publisher - Springer
- Licensed content publication - Annals of Biomedical Engineering
- Licensed content title - Thermal Injury Prediction During Cryoplasty Through *In Vitro* Characterization of Smooth Muscle Cell Biophysics and Viability
- Licensed content author - Saravana Kumar Balasubramanian

Cryobiology

Dear Saravana

Many thanks for your email.

You are free to use the material in the doctoral thesis if the published paper is clearly cited/indicated as the source in each instance.

I hope this is helpful.

David Rawson

Editor-in-Chief, Cryobiology

BBA

This should be ok.

Good luck
Yechiel

Yechiel Shai, PhD
Professor of Biochemistry and Biophysics
Dept. of Biological Chemistry
The Weizmann Institute of Science
Rehovot, 76100, ISRAEL
Tel: 972-8-9342711
Fax: 972-8-9344112

TABLE OF SYMBOLS

Symbol	Units	Definition
V	μm^3	Cell volume
T	K or ^oC	Temperature
A	μm^2	Surface Area
L_p	$m^3/N.s$	Hydraulic conductivity of the cell membrane
L_{pg}	$m^3/N.s$	Hydraulic conductivity of the cell membrane at 273.15K
E_{Lp}	kJ/mol	Activation energy for water transport
π	Atm or N/m^2	Osmotic pressure
σ	N/A	Coefficient of reflection – Transport equation
ω	N/A	Coefficient of permeability – Transport equation
ΔP	Atm or N/m^2	Hydraulic pressure gradient
ΔT	K or ^oC	Temperature gradient
T_{fp}^o	K or ^oC	Freezing point of planar ice-water interface

σ_{SL}	N/m	Interfacial tension between ice and liquid water
ν_L	m^3/mol	Molar volume of liquid water
L_f	kJ/mol	Molar latent heat of fusion
Ω	m^2/s	Kinetic parameter of IIF
κ	K^5	Thermodynamic parameter of IIF
$T - T_f$	K or ^oC	Degree of supercooling
η	Kg/(m.s)	Viscosity of the cytosol
k	W/(m.K)	Thermal conductivity
ρ	kg/m^3	Density

1. CELL BIOPHYSICS & THE "TWO FACTOR" INJURY HYPOTHESIS: A REVIEW

This chapter reviews literature to provide an overview of the current understanding of the effect of cell attachment and molecular events associated with the freezing of biological cells in the context of the "two factor" hypothesis.

1.1 BACKGROUND

Cryobiology is the study of biological materials or systems at low temperatures (especially below the freezing point of water). Controlled freezing is used for either the preservation (cryopreservation) or the destruction (cryosurgery) of cells. The first reported successful cryopreservation was the result of an accidental discovery by Polge et al. in 1949 (6). Long term cryopreservation of cells has since been reported for many cells types (7; 8; 9; 10; 11; 12). Freezing is also used to destroy malignant cells or tissues using cryosurgery (13; 14). Detailed reviews of cryopreservation or cryosurgical applications can be found elsewhere (11; 15; 16; 17).

One of the fundamental challenges in cryobiology is to understand the mechanisms of cellular freeze injury. It is known that a temperature range of 0^{o}C to -15^{o}C is probably most lethal to cells, which the cell traverses twice during freezing and warming (18). Ice initially forms in the extracellular media while the cell supercools, presumably since the plasma membrane blocks ice crystals from entering the cell. This creates an osmotic imbalance leading to the outflow of water from the cell. The rate of water movement is dependent on the cooling rate – slow freezing allows cell dehydration whereas rapid freezing traps water that eventually forms intracellular ice (19). Both slow and rapid freezing rates can be damaging to cells though the underlying mechanisms of injury may be different (2; 20).

Cellular freezing biophysics is linked to cell injury by the “two factor” hypothesis as originally proposed by Mazur (20; 19). An inverted U curve relation between cell injury

and cooling rate is purported to result from two opposing damaging factors. Slow freezing rates are linked to "solution effects" injury, and cell injury at rapid freezing rates is attributed to lethal IIF (Figure 1.1) (19; 20). An optimal freezing rate should be low enough to avoid IIF but high enough to minimize solution effects injury. This optimal cooling rate is dependent on cell type as shown in Figure 1.1. Cell biophysics and injury ("two factor" hypothesis) has been well studied for multiple cell types in the unattached state (suspensions) (21; 18; 22; 23; 10; 9; 24; 25; 12; 19). *However, the effect of cell attachment on the "two factor" hypothesis is not well understood.* This is an important link between suspensions and tissues during freezing.

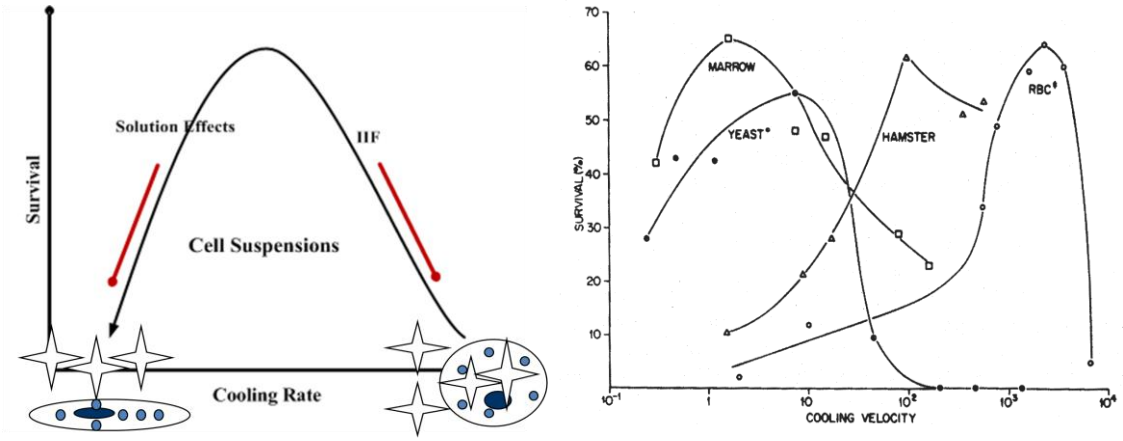

Figure 1.1: (Left) A schematic representation of the "two factor" hypothesis of cell injury. Slow freezing results in cell dehydration and is linked to "solution effects" injury, whereas rapid freezing injury is attributed to the lethality of intracellular ice formation (IIF). (Right) The "two factor" relation is cell type dependant. Adapted from Mazur **(2)**.

The underlying biophysical mechanisms of the "two factor" cellular freeze injury are different. Slow freezing allows water to leave the cell to establish a chemical equilibrium but too slow of a rate is damaging to cells. Lovelock proposed that the increased solute concentration adversely affects the lipid-protein complexes of cell membranes rendering

it permeable to electrolytes, which causes swelling and eventually cell damage (*solute toxicity hypothesis*) (26). Increased solute concentration was also proposed to heighten cell membrane susceptibility to thermal shock at lower temperatures (27). Meryman proposed that injury results from cells being unable to shrink below a minimum volume due to compressive stresses on the plasma membrane (*minimum volume hypothesis*) (28). Steponkus and Lynch proposed a mechanistic explanation involving *membrane phase transition and destabilization* as the cause for injury in plant cells (29). Muldrew proposed that cell injury results from breaking of protein salt bridges leading to a glut of intracellular ions that may swell the cell past its elastic limit due to water influx (*protein "salting in" hypothesis*) (30). A detailed discussion of the above theories and others is done elsewhere (2). In contrast, cell injury during rapid freezing is attributed to the formation of lethal ice inside the cell. Mechanisms of damage are attributed to the mechanical effects of the ice crystal (19; 31; 32), solution effects and thermal shock (33), osmotic injury (34), protein denaturation (35), and gas bubble formation (36; 37). The actual mechanism of cell injury during freezing is potentially multi-factorial, and one or more of the theories discussed above may act in conjunction to cause cell damage. *Though many of the above theories implicate molecular events as potential cell injury mechanisms, its measurement in the context of the cell freezing biophysics & its relation to the "two factor" hypothesis is not well studied.*

The focus of this dissertation is to address some of the limitations identified above. Firstly, the effect of cell attachment on the "two factor" hypothesis is studied. Secondly, molecular events (lipid and protein changes) associated with the "two factor" hypothesis

are studied. A brief review of the current understanding of cell attachment effect and the molecular events during freezing is done below.

1.2 CELL BIOPHYSICS

The "two factor" hypothesis is well studied for cells in suspension. The biophysical response of cells depends on the ability of water to move across the cell membrane (or cell permeability). Biophysical models are thus useful to determine and predict cell membrane permeabilities for imposed thermal conditions. A discussion of cellular freezing biophysical models and experimental techniques is done below.

1.2.1 Cell Dehydration

Extracellular ice concentrates the extracellular media, thus creating an osmotic pressure difference across the semipermeable cell membrane that drives the ex-osmosis of water from the cell. Slow freezing rates allow adequate time for intracellular water to move out, thus dehydrating the cell (18). The rate of water movement is affected by the cell membrane permeability and the chemical potential gradient. A simplified model for cell dehydration was proposed by Mazur (18) in 1963 (Eqn. 1.1).

$$\frac{dV}{dT} = \frac{L_p ART}{B\upsilon_W}\left[\ln\frac{(V-V_b)}{(V-V_b)+\upsilon_W\upsilon_s n_s} - \frac{\Delta H_f}{R}\left(\frac{1}{T_{ref}} - \frac{1}{T}\right)\right] \quad (1.1)$$

The above equation is based on the coupled transport equations originally proposed by Kedem and Katchalsky in 1958 (38) for bulk water movement.

Osmotic water transport is limited by the temperature dependence of the cell membrane permeability. This is modeled using an Arrhenius relation as proposed by Levin et al. (39) as given below.

$$L_p = L_{pg} \exp\left[\frac{-E_{Lp}}{R}\left(\frac{1}{T} - \frac{1}{T_{ref}}\right)\right] \qquad (1.2)$$

Water transport across the cell membrane can be predicted using these cell specific biophysical parameters (reference cell permeability - L_{pg} & activation energy - E_{Lp}). In general, changes to permeability (L_p) shift the dehydration curves from left to right without affecting their overall profile (Figure 1.2). A change to activation energy (E_{Lp}) affects the profile and shifts the curve. Selected dehydration parameters for multiple cell types are included in Table 1.2.

It is to be noted that Mazur's water transport model was originally proposed for cell suspensions (18). It does not account for interactions that would occur in attached cellular systems. There are other limitations to the model, which is discussed in detail elsewhere (18; 40; 41; 42). Subsequently, other biophysical models have been proposed that attempt to address limitations of Mazur's original model (43; 44; 45; 46; 47).

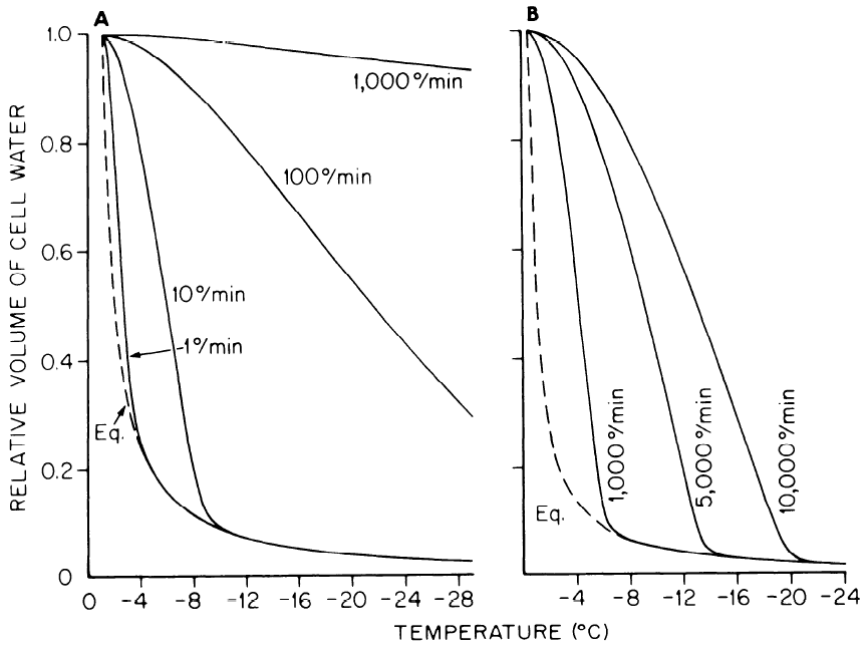

Figure 1.2: Calculated fraction of intracellular water remaining in yeast (A), and human red blood cells (B) as a function of temperature at indicated cooling rates. Adapted from Mazur **(48)**

1.2.2 Intracellular Ice Formation (IIF)

Intracellular ice formation (IIF) results from intracellular water supercooling faster than it can exosmose out of the cell. There are three major theories to describe how IIF occurs in cells.

- **Membrane damage theory**

  This theory contends that IIF is a consequence of the loss of cell membrane integrity and not a precursor to membrane damage (49).

- **Pore theory**

  The theory postulates that at a particular freezing temperature, extracellular ice crystals are small enough to advance through aqueous pores (protein pores or gap junctions) in the plasma membrane and nucleate the intracellular media (50; 51; 52).

The equilibrium ice crystal radius needed to advance through the pores was theoretically predicted as shown below.

$$\Delta T = \frac{2v_1^L T_{fp}^o \sigma_{SL} \cos\theta}{aL_f} \quad (1.3)$$

Based on calculations, an ice crystal was deemed small enough to pass through 0.8nm pores below -10^{o}C if the contact angle of ice-water interface with the pore wall was ~75^o (50; 52; 53).

- **Surface catalyzed nucleation (SCN) theory**

  The SCN theory postulates that the plasma membrane, interacting with extracellular ice, acts as an intracellular nucleation site (44).

In this dissertation, the SCN theory is used to study IIF biophysics in cellular systems. Toner et al proposed this mechanistic model to assess IIF in biological cells (44; 54). Ice nucleation rate (I) is modeled as:

$$I = \Omega \exp\left(\frac{\kappa}{(T - T_f)^2 T^3}\right) \quad (1.4)$$

$$\Omega = \Omega_0 \left(\frac{T}{T_{fo}}\right)^{1/2} \left(\frac{\eta}{\eta_o}\right)\left(\frac{A}{A_0}\right) \quad (1.5)$$

$$\kappa = \kappa_0 \left(\frac{T_f}{T_{fo}}\right)^4 \quad (1.6)$$

The probability of intracellular ice formation (PIF) is then predicted as given below.

$$PIF^{SCN} = 1 - \exp\left(-\int_0^t AI_{SCN}\,dt\right) \qquad (1.7)$$

The SCN model for IIF in cells has assumptions and limitations to its application. The nature of the interaction of ice with the plasma membrane is broad – chemical, physical, electrical, ionic, thermal or mechanic. It is unknown if a particular underlying interaction is predominant or if a combination of the above plays a critical role. Experimental evidence showing the plasma membrane as the originator of IIF is lacking. Additionally, this model was originally developed for cell suspensions and does not account for cell attachment effects like cell-cell interactions. There have been other models proposed to study IIF in cell suspensions, which include both mechanistic and phenomenological models (20; 55; 56; 57). Though fundamentally different in their approaches, the end results are reported to be similar (45).

A tabulation of the thermodynamic and the kinetic parameters from a survey of literature is provided in Table 1.1 for different cell types based on the SCN theory of IIF.

Table 1.1: Selected literature summary of cell IIF biophysical parameters evaluated using the IIF model proposed by Toner et al. **(44)**

CELL TYPE	$\Omega_O \times 10^{-8}$ ($M^2\ S^{-1}$)	$\kappa_O \times 10^{-9}$ (K^5)	REFERENCE
Hepatocytes			
Pig	13.0	0.48	(58)
Pig (Spheroids)	5.9	3.0	(59)
Rat (Freshly Isolated)	110	1.4	(60)

Rat (Digested)	237	0.33	(60)
Rat (Lewis)	110.0	1.4	(54)
Human	10.8	1.04	(61)
Human	7.6	0.75	(58)
Tumor Cells			
Rat ELT – 3 Fibroid	3.6	4.3	(62)
LNCaP Prostate	27.7	2.23	(3)
Miscellaneous Cell Types			
Lymphocytes (Genetically Modified)	3500	55	(63)
Porcine Smooth Muscle Cells	1.1	1.6	(4)
Human Dermal Fibroblasts	0.92	1.2	(5)
Human Microvascular Endothelial Cells	6.8	8.3	(62)
Mouse Embryo (One Cell)	0.8	7.8	(64)
Mouse Oocyte	3.6	4.6	(65)
Hematopoietic Progenitor Cells ($CD34^+$)	2337	43.9	(66)
Monkey Oocyte	8.0	2.2	(67)

1.2.3 Experimental Techniques

Cell freezing biophysics is commonly studied using a cryomicroscope (54; 62; 4; 65). The historical development of the cryomicroscope and its applications to cryobiology is discussed elsewhere (68; 69; 70; 71; 72; 73). Current designs of the cryomicroscope are

modifications of the initial work by Diller and Cravalho who invented the convection based thermal cryomicroscope where cooling rate and temperature could be programmed independently (74). A modified version of the stage based on radial conduction was later proposed by McGrath as an enhancement to the original design (75). A more detailed review of the engineering contributions to cryobiology can be found elsewhere (76; 77).

A cryomicroscope is used to track cell volume (using projected area) as a function of temperature during freezing. An important assumption is that the cells are circular, and cell volume can be calculated using a simple circle-sphere relation. Figure 1.3 monitors the dehydration of mouse embryos using a cryomicroscope (64). Cell volume measurement during freezing are obtained either manually or using algorithms developed to automatically track and calculate volume changes (78; 79; 80). Major limitation of the cryomicroscope is its inability to map cell volume as a function of temperature for non-spherical cells (e.g. sperm), and attached cells.

The cryomicroscope can also be used to track IIF in cells (Figure 1.3). IIF is classically described as a sudden "flashing" of the cell attributed to a change in the optical transparency of light as cellular water converts to ice. IIF is sometimes described as "twitching" - a "very sudden and small volume increase" - of the cell with no perceptible darkening of the cellular cytoplasm (81; 21). There is a degree of subjectivity associated with tracking IIF using a cryomicroscope since "flashing" is affected by the experimental setup (amount of water/ice in the system), and user interpretation of optical changes to the cell during freezing. Additionally, it is difficult to ascertain if the mechanistic events causing IIF precede or succeed the "flashing or twitching" of the cells.

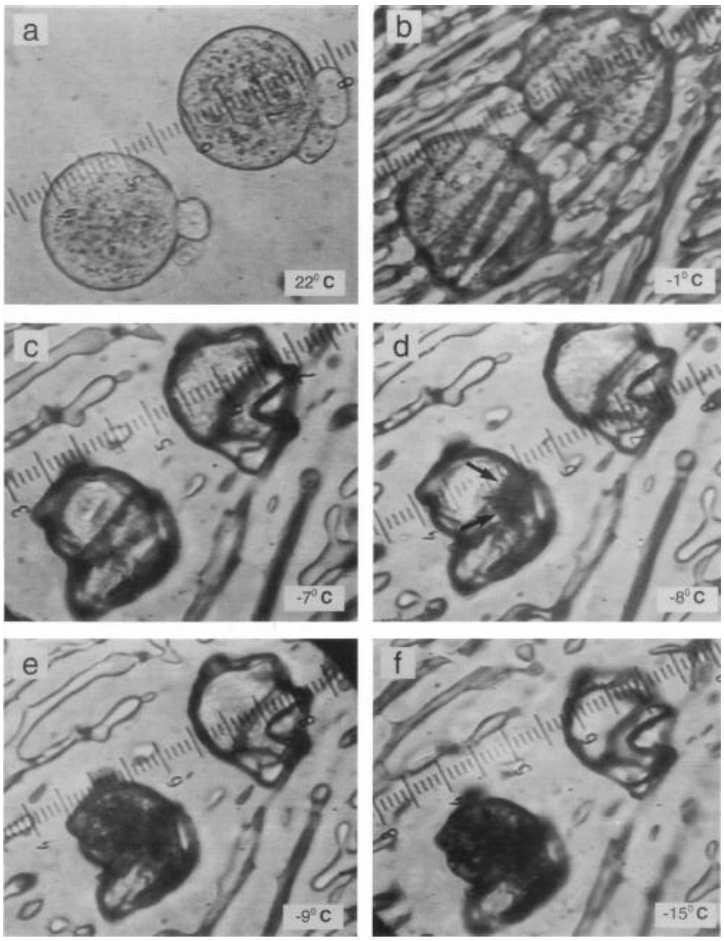

Figure 1.3: Cell dehydration during freezing of one-cell mouse embryos as seen using a cryomicroscope. Ice was nucleated at -1°C and the cooling rate is 2°C/min. One cell is seen to form IIF (darkens at -8°C), which spreads rapidly as temperature declines further. Adapted from Toner et al. **(64)**

Technological advances to the cryomicroscope have aided in the study of IIF biophysics in cells. Recently, Stott and Karlsson used high speed video cryomicroscopy in micropatterned tissues to challenge the conventional acceptance of "flashing" as an indication of IIF (82). Using high frame rates (8000 – 16000 frames/s), they showed that intracellular ice growth originated at a point source within the cell, which then manifests as a single advancing front (Figure 1.4). The typical "flashing" associated with IIF was shown to be a secondary event that occurred after the ice front had traversed the cell (82).

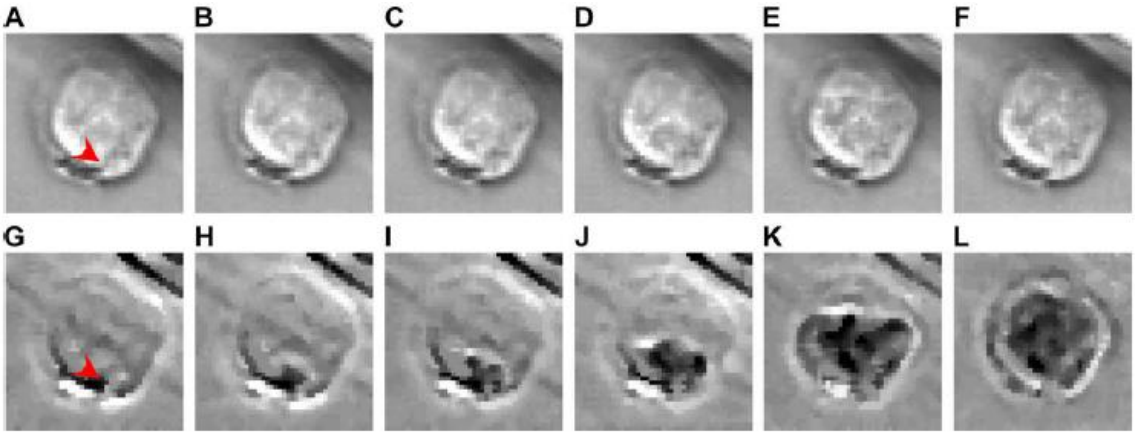

Figure 1.4: High speed video of IIF in an adherent BPAEC cell in a micropatterned tissue construct. The frame rate used was 8000 fps compared to standard frame rates of 100 – 300 fps. (A-F) are original unprocessed video frames whereas (G – L) are obtained following image processing. The cooling rate of the sample was 130^{o}C/min, and the stage temperatures at the start and end of the above sequence was -14.1^{o}C and -14.2^{o}C respectively. These images were adapted from Stott and Karlsson **(82)**

Amongst other available experimental techniques, the differential scanning calorimeter (DSC) is used to quantify cell biophysics (especially water transport) during freezing. Changes to the cell volume are tracked by measuring the difference in the heat release between intact and lysed cells (83). Unlike the cryomicroscope, the DSC technique is not limited by the size or the shape of the cells (non spherical). However, it is an indirect measurement method, and it has not been advanced to quantify IIF biophysics. A detailed review of the applicability, technical advantages and limitations of the DSC for biophysical evaluations is done elsewhere (84). Other experimental techniques that have been used to study cell dehydration in non-isotonic solutions (not freezing) include diffusion and perfusion chambers (85; 86; 87), spectrophotometers (88; 89; 90), photomicroscope (91), and electronic particle counters (92; 93; 94). A selected summary of cell suspension dehydration parameters is provided in Table 1.2 below.

Table 1.2: Selected literature summary of cell dehydration biophysical parameters. The measurement techniques that were used are included. Conversion to SI units is included in parenthesis for all measurements.

CELL TYPE	L_{PG} μM/MIN.ATM ($\times 10^{14}$ M^3/N.S)	E_{LP} KCAL/MOL (KJ/MOL)	TECHNIQUE	REF
Human Granulocytes	0.41 (6.8)	51.9 (217.1)	Cryomicroscope	(95)
Human Microvascular Endothelial Cells	0.05 (0.8)	14.8 (61.9)	Cryomicroscope	(62)
Liposomes	1.82 (30.0)	10.6 (44.4)	Cryomicroscope	(96)
Human Lymphocytes (EBVT Transformed)	0.10 (1.7)	15.5 (64.9)	DSC	(83)
Lymphocytes (Genetically Modified)	0.27 (4.5)	41.4 (173.2)	Cryomicroscope	(63)
Human Monocytes	0.82 (13.5)	14.3 (59.8)	Cryomicroscope	(97)
Hematopoietic Progenitor Cells	0.08 (1.3)	24.6 (102.9)	Cryomicroscope	(66)
Human Keratinocytes	0.035 (0.6)	10.7 (44.8)	Cryomicroscope	(98)
Hamster Fibroblasts	0.12 – 0.24 (2.0 – 4.0)	-	Cryomicroscope	(99)
Human Dermal Fibroblasts	0.13 (2.2)	43.5 (182.0)	Cryomicroscope	(5)
Mouse Embryo (One cell)	0.08 (1.3)	19.3 (80.8)	Cryomicroscope	(64)
Porcine Smooth Muscle Cells	0.12 (2.0)	24.1 (100.8)	Cryomicroscope	(4)
Articular Cartilage Chondrocytes	0.06 (1.0)	8.23 (67.8)	Cryomicroscope	(100)
Pig Hepatocytes	3.51 (57.9)	115.0 (481.2)	Cryomicroscope	(58)
Rat Hepatocytes (Freshly Isolated)	9.3 (153.5)	81.5 (341.0)	Cryomicroscope	(60)
Rat Hepatocytes (Digested)	0.38 (6.3)	57.0 (238.5)	Cryomicroscope	(60)
Rat Hepatocytes	2.7 (44.6)	75.9 (317.6)	Cryomicroscope	(101)

Human Hepatocytes	2.8 (46.2)	79.0 (330.5)	Cryomicroscope	(61)
Human Hepatocytes	0.97 (16.0)	51.6 (215.9)	Cryomicroscope	(58)
AT – 1 Prostate	2.7 (44.6)	55.4 (231.8)	Cryomicroscope	(102)
ELT-3 Leiomyomas	0.27 (4.5)	26.4 (110.5)	DSC	(103)
LNCaP Prostate	0.21 (3.5)	25.1 (105.0)	Cryomicroscope	(3)
Mouse Oocyte	0.036 – 0.052 (0.59 – 0.86)	10.8 – 15.8 (45.2 – 66.1)	Cryomicroscope	(65)
Monkey Oocyte	0.23 (3.8)	33.8 (141.4)	Cryomicroscope	(67)
Bovine Oocyte	0.31 (5.1)	7.8 (32.6)	Cryomicroscope	(104)
Equine sperm	0.02 (0.3)	32.7 (136.8)	DSC	(12)
Boar sperm	0.02 (0.3)	29.3 (122.6)	DSC	(105)
Canine sperm	0.003(0.05)	15.3 (64)	DSC	(106)
Bovine sperm	0.036 (0.59)	42.1 (176.1)	DSC	(107)
Rat sperm	0.007 (0.12)	17.8 (74.5)	DSC	(108)
Mouse sperm	0.01 (0.17)	22.5 (94.1)	DSC	(109)
Rhesus Monkey sperm	0.002 – 0.003 (0.03 – 0.05)	10.6 – 18.3 (44.4 – 76.6)	DSC	(110)
Human sperm	0.14 (2.31)	85.5 (357.7)	DSC	(111)
Southern Platyfish sperm	0.005 – 0.009 (0.08 – 0.15)	9.8 – 29.0 (41.0 – 121.3)	DSC	(112)

1.3 EFFECT OF CELL ATTACHMENT

Cell suspensions provide a fundamental understanding of the effects of freezing on the "two factor" injury hypothesis. However, more complicated cellular systems featuring cell attachments are needed to link to tissue freezing responses. The benefits and applications of the cellular systems used in the current study are discussed in Table 1.3. This section reviews literature to assess the effects of cell attachment on freezing.

Table 1.3: *In vitro* model systems used for experimental evaluation of cell freezing

CELLULAR SYSTEM	PURPOSES/APPLICATION	SAMPLE REFERENCES
Cell Suspension 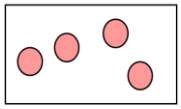	• Fundamental understanding of biophysics – Cellular & Molecular • Quantification of "Two factor" biophysics & viability • Cell cryopreservation (eg. Gamete)	**(20; 21; 113; 114; 18; 19; 115; 65; 54; 12)**
Cell Monolayer 	• Features cell-cell & cell-substrate interactions • Fundamental understanding of the effect of cell attachment on "Two factor" biophysics	**(116; 117; 118; 92; 119; 120; 121)**
Artificial Tissue (In collagen/fibrin gel) 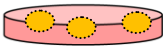	• Tissue like environment featuring cell-cell and cell-matrix interactions • Preferred model system for understanding fundamentals of tissue effects (Biophysics and functional aspects) • Cryopreservation applications (eg. Dermal constructs)	*Cell Biophysics & Viability:* **(60; 122; 123; 124)** *AT Functional Performance* (125; 126; 127; 128)

1.3.1 Cell Morphology & Expression

Cell attachment is anticipated to affect the biophysics of freezing in comparison to cells in suspension. This could a result of the differences in the environment and interactions of the cell with its surroundings. Cell attachment is known to affect the morphology, and the phenotype (129; 130; 131). The extracellular matrix (ECM) is known to provide structural integrity and functional assistance to cells. In fact, it is argued that the ECM is an extension of the cells and an active participant in the regulation of cell function (132; 131). Currently, substantial evidence has been obtained showing cell-cell and cell-ECM interactions are essential organizing principles that define the nature of an artificial tissue (133). In addition, the cytoskeleton of the cell affects the structure of the cell membrane, morphology, membrane tension, mechanical properties and osmotic responses (134; 135; 136; 137). Actin is a major protein present in the cytoskeleton of cells (Figure 1.5), and is known to play a critical role in cell volume regulation (136; 138). Defects to the cytoskeleton are known to cause membrane instability (139). Hence, events that can cause extensive depolymerization of the actin cytoskeleton may increase the vulnerability of cells to injury (140). Freezing could disrupt these interactions, and currently there is minimal understanding of its impact on the “two factor” hypothesis.

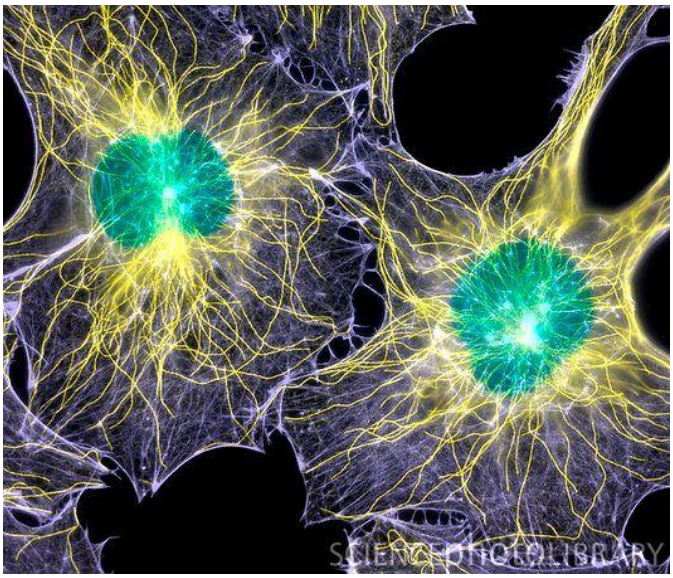

Figure 1.5: Fluorescent light micrograph of two fibroblast cells showing their nuclei (green) and cytoskeleton. The cytoskeleton is made up of microtubules (yellow) and filaments of actin (blue). (www.sciencephoto.com)

1.3.2 Cell Biophysics & Injury

Experimental Approaches

The propagation of IIF is influenced by cell-cell and cell-matrix interactions. This was first reported in plant tissues where a strong relationship between cell interactions and increased IIF was noted (141; 142; 49; 73). Subsequently, this phenomenon has been reported for other cellular systems (143; 92). Acker et al. demonstrated the effect of attached cell interactions on IIF using four different *in vitro* cellular systems of hamster fibroblasts. These systems included cells in suspension, attached to a glass surface (cell-surface interactions), colonies of cells attached to glass with both cell-cell and cell-surface interactions, and multi-cellular spheroids with extensive cell-cell interactions (Figure 1.6) (116).

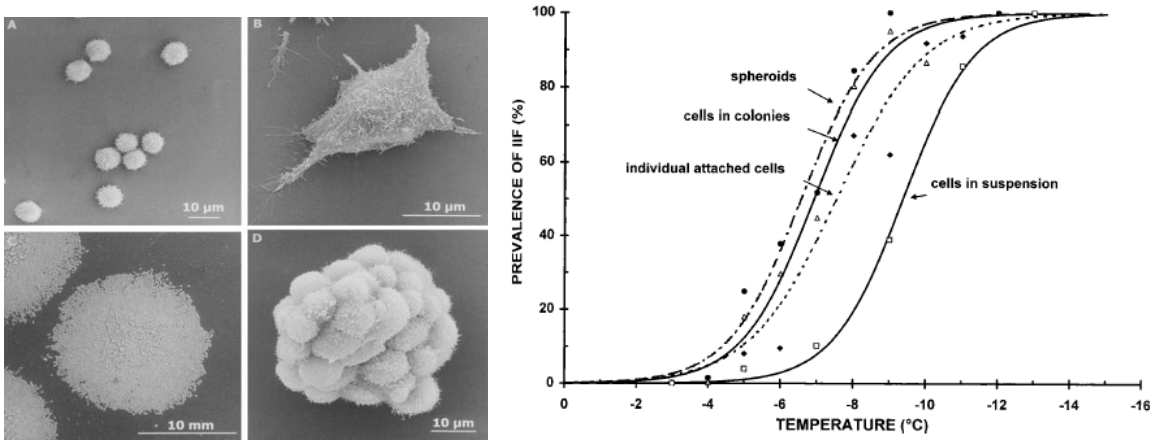

Figure 1.6: The impact of cell attachment state on freezing biophysics was evaluated using four model systems. (Top panel) – Hamster fibroblasts in (A) Suspension; (B) Individual cells attached to glass; (C) Cells in colonies; (D) Cells forming a spheroid. (Bottom panel) – The probability of IIF (%) as a function of temperature in the model systems evaluated. Adapted from Acker et al. (116)

A significant increase in IIF was noted in the presence of cell-cell contact. In addition, a significant decrease in the time to reach 50% IIF for cells in suspension as compared attached cells was observed (116). This data showed that cell-cell and cell-surface interactions alter IIF biophysics as compared to cell suspensions.. One reason for the increase in IIF was attributed to the presence of gap junctions, which facilitated ice propagation through intercellular interactions (53).

Though cell attachment was clearly shown to increase the probability of IIF in comparison to suspensions, its effect on cell damage is unclear. Acker and McGann showed that MDCK cell survival in monolayer is greater than 65% even though the cells exhibited 100% IIF (Figure 1.7) (119). The authors attributed this to the protective action of intracellular ice formed by propagation through gap junctions. In contrast, the tenets of the "two factor" hypothesis would have predicted a higher percentage of cell injury. In

contrast, Irimia and Karlsson did not observe a benefit to cell viability in the presence of intercellular ice propagation (120). More studies are needed to understand the impact of cell attachment on the "two factor" hypothesis of cell injury.

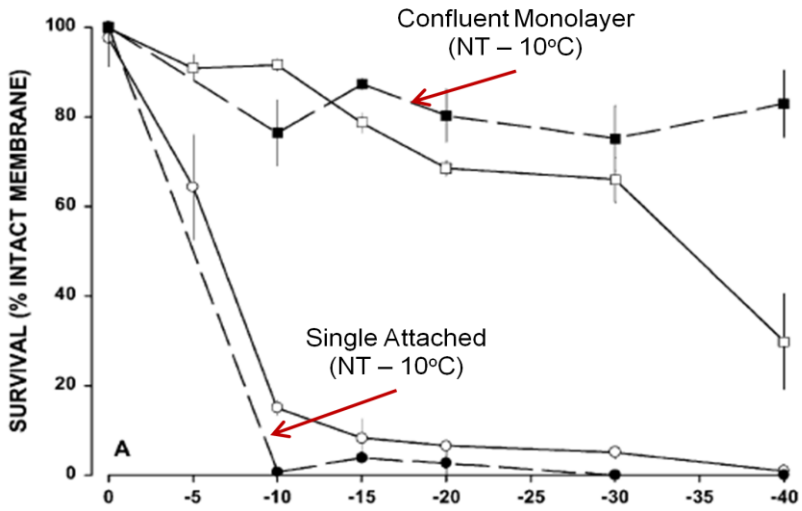

Figure 1.7: The impact of cell attachment state on survival of MDCK epithelial cells. A comparison of single attached cells and confluent monolayer at two different ice nucleation temperatures (-5°C solid line & -10°C dashed line) is shown. Adapted from Acker & McGann (119)

There are very few studies that have been reported for water transport biophysics for attached cells during freezing. One main reason is the limitation of experimental techniques that are currently incapable of measuring cell volume changes in the 3D configuration for attached cells. This limits the scope of both experimental and numerical methods in predicting attached cell dehydration biophysics. Recently, Choi and Bischof studied the "two factor" biophysics of freezing fibroblasts in suspension vs. monolayer. Water transport is predicted to be higher for fibroblasts in monolayer as compared to suspensions at slow freezing rates. This would indicate that "solution effects" injury should be higher for the cells in monolayer per the "two factor" hypothesis. However,

cell survival is significantly higher in monolayer vs. suspension (144). A possible explanation is that cells in suspension are squeezed into unfrozen channels and exposed to high solute concentrations but not all the cell surface area may be accessible to solutes in the case of attached cells (Figure 1.8). This indicates that the slow freezing biophysics of attached cells might be mechanistically different when compared to suspensions.

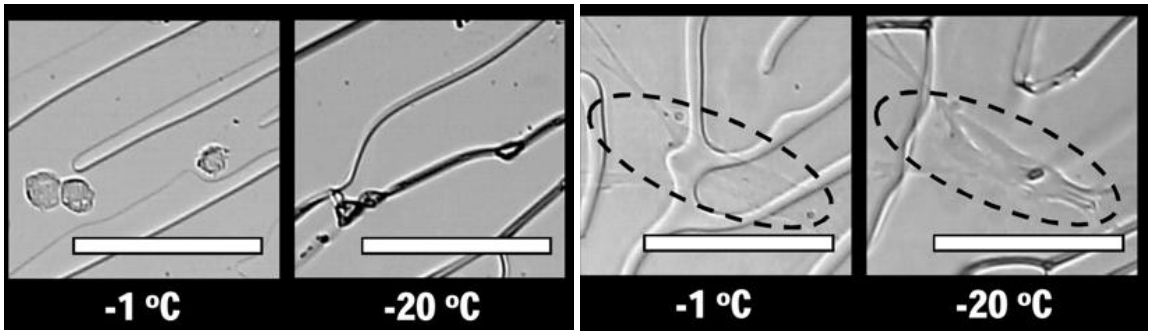

Figure 1.8: Cryomicroscope images of fibroblast cells during freezing for suspensions and attached cells when cooling at 5°C/min. Adapted from Choi et al. **(144)**

Biophysical Models

The water transport model proposed for cell suspensions has limitations in its application to attached cells. The model does not account for cell-cell and cell-ECM interactions, and is constrained by experimental techniques since they are unable to measure cell volume in 3D configuration. *In spite of these limitations, the cellular biophysical model for water transport can still be reasonably used to assess the dehydration kinetics of attached cells.*

Yarmush et al. used the cellular models to predict attached cell biophysics by decoupling the kinetics of IIF from cell dehydration at rapid freezing rates. This provided relevant IIF biophysical parameters, which were then assumed as constant at lower freezing rates.

Cell dehydration biophysical parameters were then predicted using coupled water transport and IIF models (60). We have used this approach in this dissertation to quantify the biophysics of IIF and cell dehydration in the attached cellular systems. Other biophysical models for attached cell water transport have been proposed but they are limited to specific applications or cellular systems (145; 39; 146; 147; 148; 149; 150).

Similarly, the biophysical models of IIF developed for cell suspensions may be applied to study cells in the attached state (60). We have adopted this approach in this dissertation to study IIF kinetics of multiple cell types as a function of cell attachment. Recently, other approaches have been proposed to model IIF kinetics in the attached state by accounting for cell-cell interactions. Irimia and Karlsson used micropatterned cells to propose a theoretical model to predict the IIF kinetics in a group of cell pairs as shown below (120).

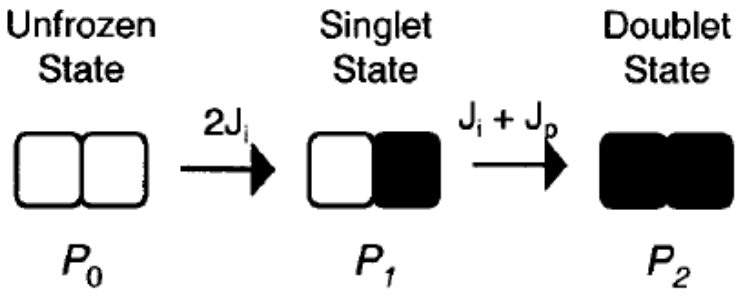

Figure 1.9: Schematic depiction of IIF formation in the presence of cell-cell interactions. Open blocks indicate unfrozen cells, while filled blocks indicate IIF. The transitions are modeled as first order reactions with given rate constants. P_o represents the unfrozen state, P_1 the singlet frozen state, and P_2 the doublet frozen state. Adapted from Irimia and Karlsson **(120)**

The rate of singlet ice formation – primarily a random and probabilistic event – and the effect of intercellular ice propagation (the rate of doublet formation) are given below.

$$\frac{dN_o}{dt} = -2J_1N_o \; ; \; \frac{dN_2}{dt} = (J_1 + J_p).N_1 \quad (1.10)$$

In the above, J_1 is the average rate of independent ice formation events per unfrozen cell, t is the time, J_p is the average rate of intercellular ice propagation events per unfrozen cell given that ice is present in the adjacent cell. A scaled up version of the same model was proposed subsequently using Monte Carlo simulation techniques to extend to artificial tissues (121). These models account for cell interactions and hence, are potentially useful in the future for the analysis of IIF for attached cells. A further discussion of the assumptions and limitations associated with these models is presented elsewhere (121).

In summary, a review of literature shows a limited understanding of the biophysics of freezing cells in an attached state especially for water transport. This study focuses on understanding the impact of cell attachment state (cell-cell and cell-ECM interactions) on the "two factor" hypothesis of freezing. In addition, the cell attachment state affects the molecular expression of cells (e.g. lipids and proteins). Recently, Ragoonan et al. showed that osmotic cell dehydration affects both the membrane and the cytoskeleton potentially resulting in cell injury (140). The long term goal is to understand the implications of cell attachment and the molecular events on the "two factor" hypothesis. However, firstly a fundamental understanding of the molecular events associated with the "two factor" hypothesis needs to be developed using simpler cellular systems (i.e. cell suspensions).

1.4 MOLECULAR EVENTS DURING FREEZING

The lack of understanding of molecular events (proteins and lipids) associated with the biophysics of freezing cells (cell dehydration vs. IIF), and its role in the mechanisms of cellular freeze injury remains an important area of research. Specifically, changes to membrane lipids and proteins are an area of interest. This section reviews the current state of understanding of the molecular events associated with freezing of biological systems.

1.4.1 Cellular Water

Two forms of water are generally described for biological systems – bulk water that is a universal solvent and bound or hydration layer of water attached to cell components including proteins and membrane lipids (151). The physical, chemical, and thermodynamic properties of water are different in its two forms. Freezing affects both these forms of water but in different ways. The previous sections focused on reviewing the impact of freezing on the biophysics of bulk water movement across the cell membrane. This section reviews what constitutes bound water, and its potential role in defining molecular events during freezing.

Water is a polar molecule that influences the structure and conformation of biological molecules (thereby its function) inside the cell (e.g. lipids and proteins) (152; 153). The properties of water around lipids and proteins change as a result of hydrogen bonds that promote an ordering of the water molecules (154). Hydrophobic interactions between water and the macromolecules result in hydration layer(s) of water, which is known to

affect its structure. Early works by Jacobson contended that the structuring effects extend beyond the first hydration layer and may involve long range hydration structures (155). The polarizing effects of water lead to an induction field that actually causes the water molecules and hydrophobic macromolecules to attract each other, thus stabilizing the hydration layers (156; 157).

Freezing converts bulk water to ice but its effect on bound water is debatable. The freezing point of water has been shown to be different for bulk and bound water (using water trapped in nanopores) (158). Unfrozen water was detected in the nanopores to temperatures as low as 135K (or -138^{o}C), which potentially indicates that water bound to membranes and proteins may behave differently compared to bulk water (159). Using calorimeter experiments, Wood and Rosenberg noted that about 10% of water in yeast cells was incapable of freezing (160). Similar studies have also indicated the presence of "unfreezable" water in membranes, polymers and intact cells (161; 162; 163; 164). In contrast, Bronshteyn and Steponkus used DSC to show that the majority of bound water freezes in membrane vesicles (DPPC) below homogeneous ice nucleation temperature (-40^{o}C) (165). Hseih and Wu used NMR to show that a few molecules of bound water associated with the lipid head groups freeze when temperatures were reduced to -70^{o}C (166).

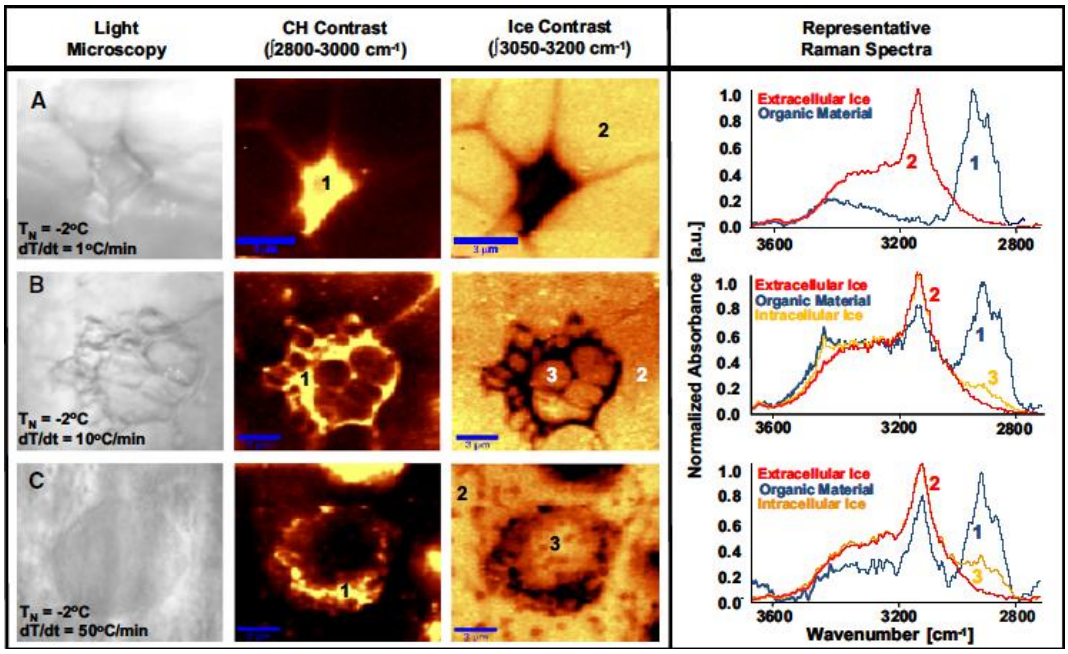

Figure 1.10: Light microscopy & confocal Raman microscopy (CRM) images of fibroblasts during freezing. The images were taken at 100X magnification at -50°C after ice nucleation at -2°C, and after specified cooling rates. Ice contrast images show ice in a lighter color, whereas CH images show organic materials in lighter colors. Adapted from Dong et al. **(167)**

In this dissertation, we do not quantify or measure changes to the bound water directly but assess its potential impact on lipids and proteins during freezing. Macromolecular associated water may disassociate and join the bulk phase as a result of temperature or dehydration stresses. Destabilization of the plasma membrane due to the removal of the bound water has been proposed as a possible cell injury mechanism in plant cells (29). Devireddy et al. implicated the removal of bound water to contribute to increased enthalpy during cell dehydration as compared to IIF using DSC (83). Forcible removal of the bound water is also known to impact cell viability and function (168). Bound water removal is generally associated with slow freezing, but Dong et al. used confocal Raman microscopy to show rapid freezing (that causes IIF) removed bound water from the intra-

cellular structures. Paradoxically, this caused a higher dehydration effect to intracellular macromolecular structures as compared to slow cooling (Figure 1.10). This is hypothesized to be a possible mechanism for cellular freeze injury during rapid freezing (167). In summary, the role of water associated with cellular lipids and proteins is potentially critical for the functioning of the cell, and needs to be understood in the context of the "two factor" hypothesis.

1.4.2 Lipid Membrane Transition

Mammalian cell membranes are semipermeable by nature and provide structural integrity to the cell (169; 170). Membrane lipid structures are arranged with their hydrophobic tails sequestered together and away from water whereas the hydrophilic head groups face the aqueous environment. This arrangement is preferred thermodynamically as it minimizes free energy (171). Any change to the external environment – physical, chemical, thermal and/or biological – disturbs this fragile equilibrium and is expected to affect the membrane structure. This section briefly reviews literature to assess current knowledge of the effect of low temperature and hydration on cell membranes.

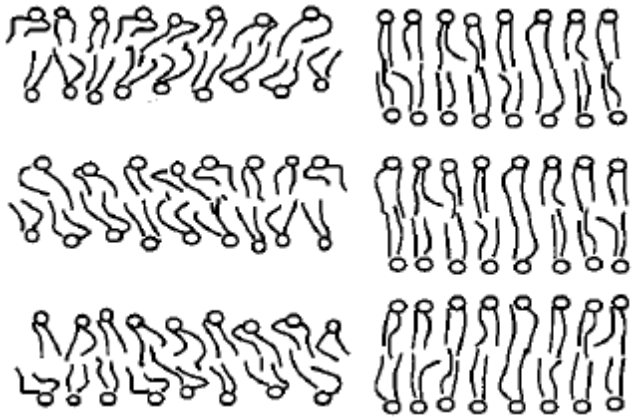

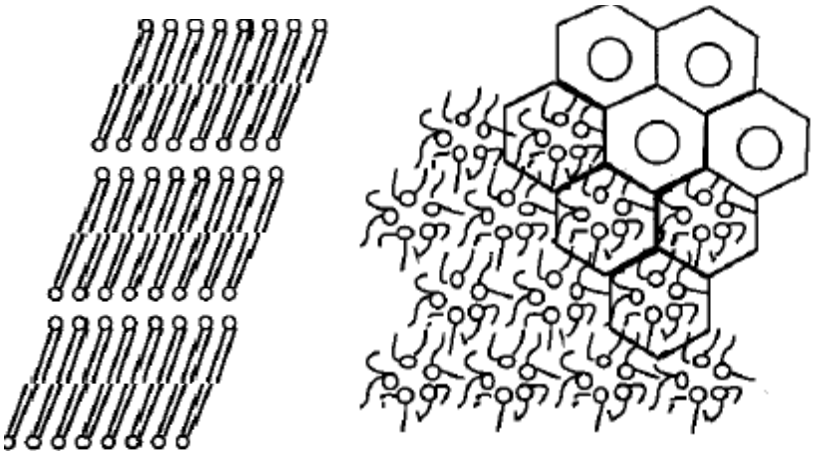

Figure 1.11: Membrane lipid phases as a function of hydration (Top panel) Lamellar fluid phase (liquid crystalline) at high hydration; Decreased interlamellar distance but fluid phase at low hydration; (Bottom Panel) Lamellar phase transition to gel phase at low hydration; Lamellar phase transition to Hexagonal II phase under extreme dehydrations in some cases. Adapted from Wolfe & Bryant **(172)**

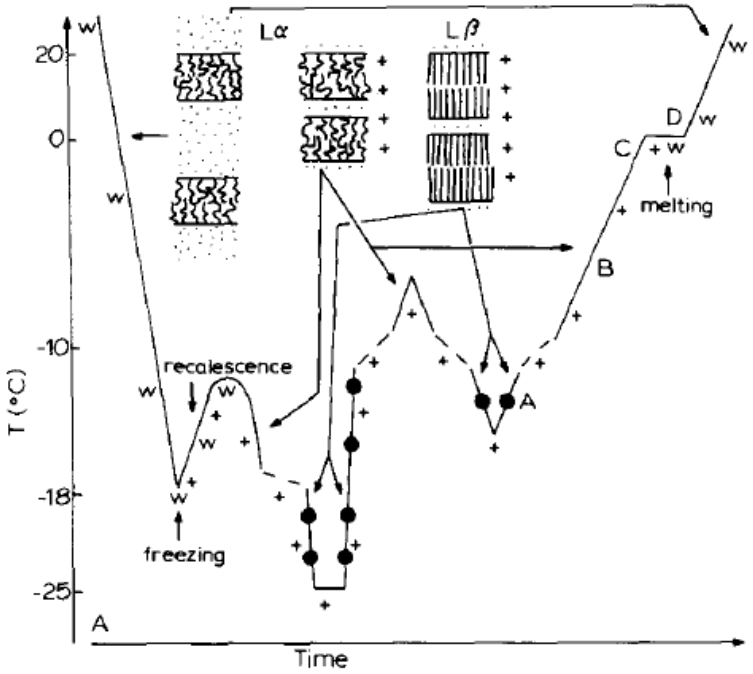

Figure 1.12: A schematic view of phase change undergone by the lipid and fluid component of the system is represented for dioleoylphosphatidylserine (DOPS). Lipid membrane hydration changes as a function of temperature are noted to occur from a liquid crystalline to a gel phase. Adapted from Caffrey M **(173)**

Lipid membrane changes during freezing can be studied using simple membrane-water systems, single or multi component lipid systems (e.g. liposomes), or biological cells (174; 172; 175; 176; 177; 173). Phospholipids are well known to bind to significant amounts of water (178). At room temperatures, the structure of the lipid membrane of cells is considered to be liquid crystalline (Figure 1.11 & Figure 1.12). Using simple membrane-water systems, temperature decrease during freezing is observed to result in membrane phase transition from liquid crystalline to an ordered gel phase structure (172). In general, the diffusion rate of water across biological membranes in the liquid crystalline state is $(2 - 50) \times 10^{-4}$ cm/s (179). As the membrane changes phase, the diffusion rate is noted to increases initially but then drops significantly till there is no water transport in the gel phase (180; 181; 182; 173). Additionally, the gel phase is characterized by increased compressive stress on the membrane, decreased lipid head group spacing, elevated lipid-water phase transition temperature, increased order of the acyl chains, and an increased bilayer thickness (183; 184; 185; 186; 172; 187; 188). Phase diagrams for simple membrane-water systems and phospholipids have been created as shown in Figure 1.12 (173; 189).

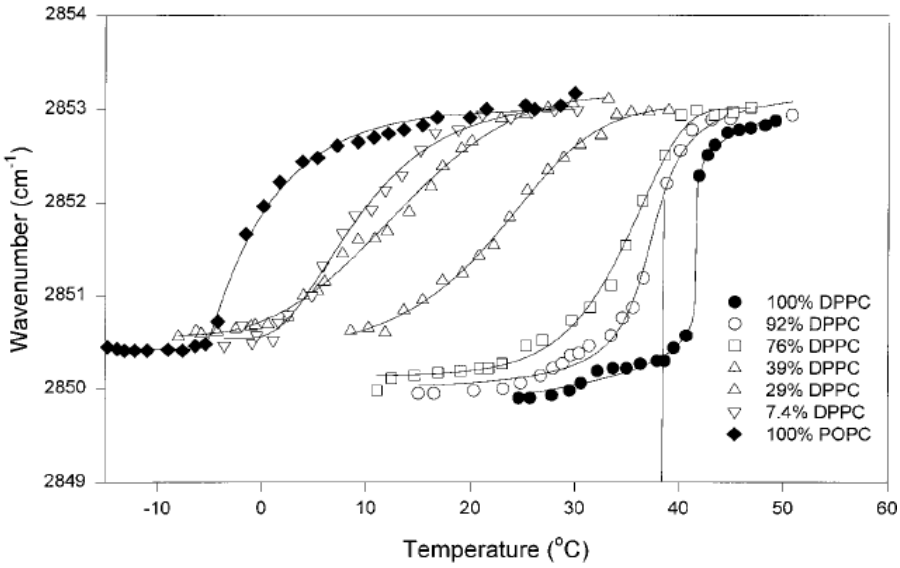

Figure 1.13: Impact of freezing on the temperature of phase transition in indicated mixtures of DPPC and POPC. Adapted from Crowe et al. **(190)**

Biological cell membranes are more complex in comparison to lipid systems since it is constituted of multiple lipid types that interact and affect the overall outcome. Using a mixture of DPPC and POPC, Crowe et al. showed that the phase transition temperature changes, and the temperature range of transition widens for lipid mixtures as compared to pure lipids. Hence, both liquid crystalline and gel phases are anticipated to coexist (demixing) for such lipid mixtures in the temperature range of phase transition. The phase boundaries for such coexistence are known to be leaky, and the maximum rate of leakage has been correlated to the phase transition temperature in liposomes (191). This could potentially affect and damage biological cell membranes.

Under extreme conditions of dehydration, the lamellar layer could phase separate and form an inverse hexagonal II phase (192; 193; 29). The lamellar to hexagonal lipid phase transition has been implicated as a possible injury mechanism for the freezing of plant

protoplasts (Figure 1.14) (194; 29). However, the formation of inverse hexagonal phase has not been reported for mammalian cell types. Crowe et al. implicated lipid phase transition events as a potential mechanism of chilling (not freezing) injury for platelets (190). However, in general there is very little information on membrane events during freezing of mammalian cells especially in the context of the "two factor" biophysics.

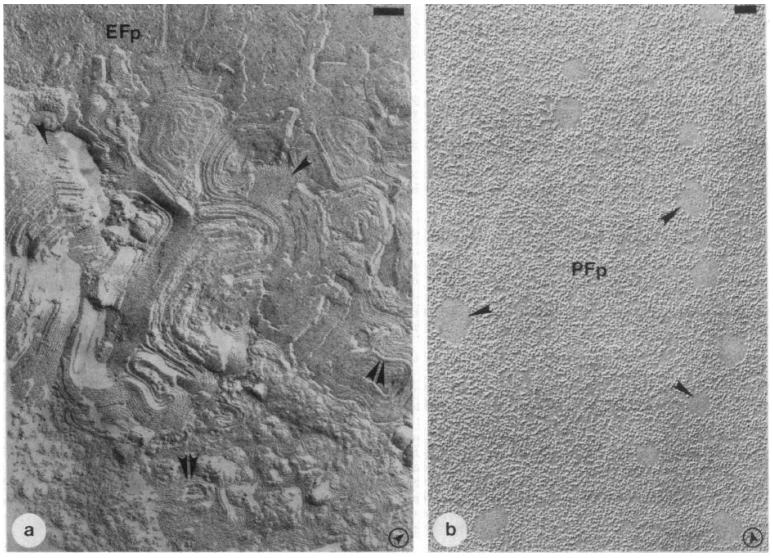

Figure 1.14: Freeze fracture images: (a) Stages of lamellar-to-hexagonal phase transition in the plasma membrane of a non-acclimated plant protoplast hypertonically contracted. Highly ordered hexagonal regions (single arrowhead), and less ordered striations or cylinders (double arrowheads) are shown. (b) Plasma membrane of a non-acclimated protoplast supercooled to -10^{o}C. Small areas of phase separation (arrowheads) are shown. Adapted from Gordon-Kamm and Steponkus **(194)**

1.4.3 Protein Denaturation

Cellular protein functions are governed by their structure, which exists at multiple levels from primary (linear) to quaternary (i.e. globular structure in 3D) (195). Hydrogen bonding is critical in the formation of secondary structures of proteins, while hydrophobic and electrostatic interactions stabilize the tertiary structures of proteins. Denaturation is defined as the loss of this structure (without breaking of peptide bonds)

due to internal or external stimuli including temperature and hydration effects (196). Variations in the strength of the hydrogen bond interactions – in particular the hydrophobic interactions – affect protein denaturation (171).

Proteins are known to denature at both high and low temperatures (197; 198; 199). The kinetics of protein denaturation can generally be modeled as a first-order irreversible reaction going from a native to a denatured state (200). When the changes to the protein structure are achieved at low temperatures it is termed as cold denaturation. Cold denaturation of pure proteins (not necessarily freezing) has been studied extensively (199; 198). A cold denaturation temperature of approximately -30^{o}C is predicted for typical biological proteins in solution (201), and 0 – 10^{o}C for cellular proteins (199). This is reversible in most cases for biological proteins when the temperature is increased back to its original state (199).

However, the study of cellular proteins during freezing is complicated due to its interactions with other components (e.g. lipid interactions) of the cell. Very few studies have looked into cellular protein denaturation during freezing of mammalian cells. Bischof et al. used FTIR to assess protein denaturation in AT-1 Dunning cells for different freezing conditions (Figure 1.15). Irreversible protein denaturation was linked to cell injury at -80^{o}C, but protein denaturation was noted to be reversible when frozen to -20^{o}C. Freezing induced protein denaturation is suggested to be a result of the temperature and the dehydration of the cell that leaves it exposed to concentrated salts. The study was limited by the uncontrolled nature of freezing but it still showed that protein denaturation

is reversible under certain freezing conditions (202). More studies are needed to assess cellular protein denaturation in the context of the "two factor" freezing biophysics.

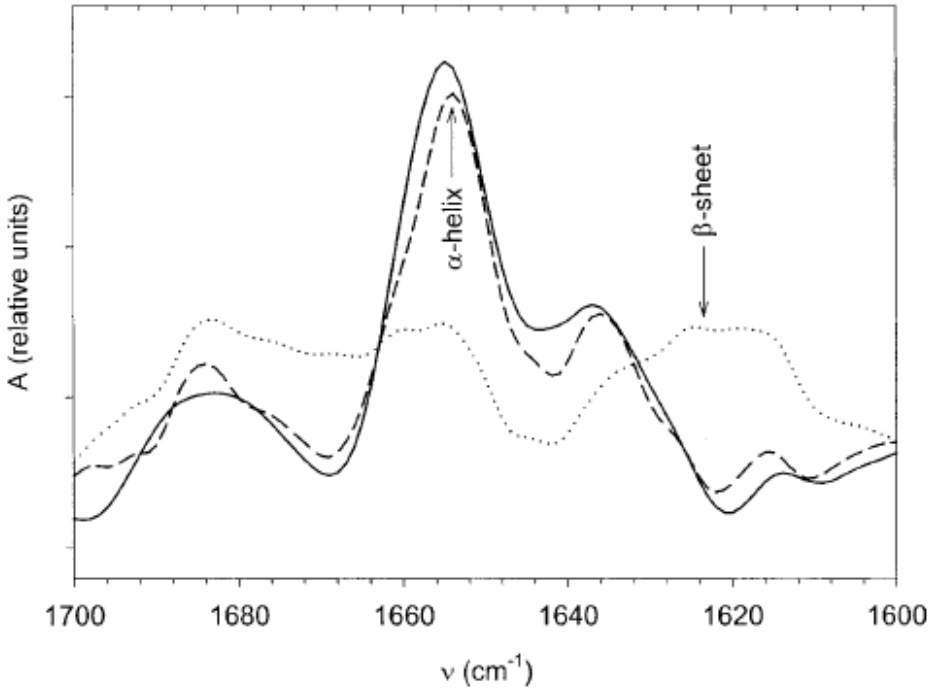

Figure 1.15: Protein denaturation assessed using amide I band profile from FTIR spectroscopy. Denaturation is monitored by recording changes to the α-helix and the β-sheet band locations for control cells (solid line), cells incubated for 1hr at -20°C (dashed line), and cells incubated for 1hr at -80°C (dotted line). All spectra were obtained at 20°C after exposure to above conditions. Adapted from Bischof et al. **(202)**

1.5 SUMMARY & SPECIFIC AIMS

The "two factor" freezing hypothesis links cell biophysics to injury – solute effects at slow freezing rates, and IIF at rapid freezing rates. This has been well studied for cell suspensions, but cell attachment effects need to be studied to link the understanding to tissues. In addition, molecular events have been implicated as potential cellular freeze injury mechanisms but very few studies have studied this in the context of the "two factor" hypothesis.

The specific aims of this dissertation are structured to develop some of these limitations identified above (schematically represented below).

SA1: Study the effect of cell attachment on the "two factor" hypothesis during freezing – *Chapters 2 & 3*

SA2: Investigate the molecular events (lipids and proteins) associated with the "two factor" biophysics of freezing – *Chapters 4 & 5*

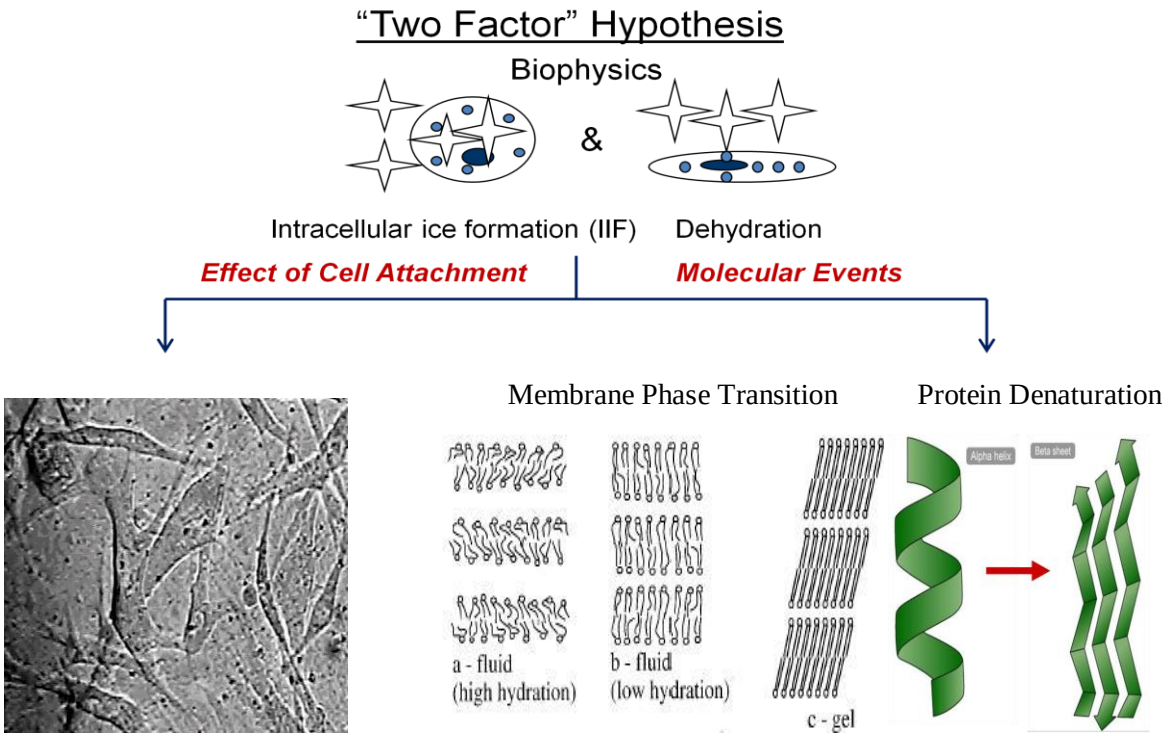

Figure 1.16: Schematic representation of the specific aims of the dissertation. The effect of cell attachment, and molecular events associated with the "two factor" hypothesis of freezing are studied for different mammalian cell types

1.6 OUTLINE OF DISSERTATION

This dissertation is organized into four chapters that address the specific aims listed above. An overview of the goals of each chapter is provided below.

Chapter 2: **Cellular biophysics as a function of model system during freezing of human dermal fibroblasts (HDF)**

This chapter describes the experimental and numerical analysis performed to assess the impact of cell attachment state/model system on the "two factor" biophysics of freezing human dermal fibroblasts (HDF). The cell model systems that were studied include cell suspensions and tissue equivalents (TE). Tissue equivalents (TEs) were formed by entrapping human dermal fibroblasts (HDFs) in either collagen or in fibrin gels. Freezing studies were conducted using a Linkam cryostage fitted to an optical microscope allowing observation of the TEs cooled under controlled rates between 5 – 130^{o}C/min. Experimental data were fitted in numerical models to extract parameters that governed water permeability, E_{Lp} and L_{pg}, and intracellular ice nucleation, Ω_o and κ_o. Results indicate significant differences exist between freezing HDFs in suspension and tissue equivalents. The resultant biophysics indicates that cell-cell and cell-matrix interactions play a major role in ice propagation in TEs.

The results from this chapter were included as part of the following publication:

- Balasubramanian SK, Bischof JC, and Hubel A (2006) "Water transport and IIF parameters for a connective tissue equivalent" *Cryobiology* 52 (1); pp 62 – 73

Chapter 3: Cellular biophysics & viability as a function of model system during freezing of porcine smooth muscle cells (SMC)

This chapter characterizes the "two factor" injury hypothesis as a function of cell attachment for porcine smooth muscle cells (SMC). Cells isolated from porcine femoral arteries was used in suspensions and attached *in vitro* systems (monolayer and fibrin gel). Cell biophysics and viability experiments were conducted using a cryomicroscope as a function of different freezing rates. Cell biophysical models are used to show that water transport and IIF are potentially enhanced in the attached state (ECM > monolayer) as compared to suspensions. One possible reason for the differences in IIF kinetics was verified to be the presence of gap junctions, which facilitate cell-cell connections through which ice can propagate. This is reflected by the change in the predicted IIF parameters when a gap junction inhibitor was added in monolayer. SMC viability was affected by the model system (lower viability in attached systems), the thermal conditions and the biophysics. SMC viability was found to be the least in fibrin TE (most % IIF) and the most in suspensions (least % IIF) at all cooling rates. The outputs from this chapter are applied to Cryoplasty - a clinical procedure to treat peripheral arterial disease.

The results from this chapter were included as part of the following publication:

- Balasubramanian SK, Venkatasubramanian RT, Menon A, and Bischof JC (2008) "Thermal injury prediction during cryoplasty through in vitro characterization of smooth muscle cell biophysics and viability" *Annals of Biomedical Engineering* 36 (1); pp 86 – 101

Chapter 4: Effects of freezing on membranes and proteins in LNCaP prostate tumor cells

This chapter studies molecular events – membrane phase transition & protein denaturation - associated with the biophysics of freezing malignant prostate tumor cells (LNCaP) using Fourier transform infrared spectroscopy (FTIR). Cell pellets were monitored during cooling at 2°C/min while the ice nucleation temperature was varied between -3 and -10°C. The predicted incidence of intracellular ice formation (IIF) rapidly increases at ice nucleation temperatures below -4°C and cell survival is an optimum at a nucleation temperature of -6°C. The ice nucleation temperature was found to have a great effect on the membrane phase behavior of the cells. The liquid crystalline to gel phase transition coincided with the ice nucleation temperature. In addition, ice nucleation at -3°C resulted in a much more co-operative phase transition and a concomitantly lower membrane fluidity in the frozen state compared to samples that were nucleated at -10°C. These observations were explained by the effect of the nucleation temperature on the extent of cellular dehydration and IIF. Amide-III band analysis revealed that proteins are relatively stable during freezing.

The results from this chapter were included as part of the following publication:

- Wolkers WF, Balasubramanian SK, Ongstad EL, Zec HC, and Bischof JC (2007) "Effects of freezing on membranes and proteins in LNCaP prostate tumor cells" *Biochimica et Biophysica Acta* 1768 (3); pp 728 - 736

Chapter 5: Membrane hydration correlates to cellular biophysics during freezing in mammalian cells

This chapter characterizes the molecular events associated with the "two factor" biophysics for multiple cell types. Specifically, the molecular state of the membrane and the surrounding water is linked to cellular biophysical events for three different mammalian cells types: human prostate tumor cells (LNCaP), human dermal fibroblasts (HDF), and porcine smooth muscle cells (SMC) using Fourier Transform Infrared spectroscopy (FTIR). Variable freezing rates were achieved by controlling the degree of supercooling prior to ice nucleation (between -3°C and -10°C) while the sample was cooled at a set rate of 2°C/min. Membranes displayed a highly cooperative fluid to gel phase transition under dehydrating conditions (i.e. NT = -3°C), which was not observed under IIF conditions (NT = -10°C). Spectral analysis showed a consistently greater amount of ice forming during dehydrating vs. IIF conditions in all cells. This is hypothesized to be due to the extreme loss of membrane hydration in dehydrating cells that exhibits itself in excess water available for phase change. Interestingly, membrane dehydration correlates strongly with cellular dehydration as assessed by cryomicroscopy. A strong correlation was found between the activation energies for freezing induced lyotropic membrane phase changes determined using FTIR and the water transport measured by cryomicroscopy.

The results from this chapter were included as part of the following publication:

- Balasubramanian SK, Wolkers WF, and Bischof JC (2009) "Membrane hydration correlates to cellular biophysics during freezing in mammalian cells" *Biochimica et Biophysica Acta* 1788 (5); pp 945 – 953

Appendix A: Protein denaturation and membrane phase transition during thermal treatments of Mammalian Cells: An FTIR study

The previous chapters showed that molecular events during freezing are cell specific responses. This chapter shows that heating of cells also exhibits unique molecular events that can be quantified using Fourier transform infrared (FTIR) spectroscopy. The cell types studied include cardiovascular cells (SMC and HDF), and malignant (LNCaP prostate tumor) cells. Protein denaturation is found to be a cell specific response during heating. Distinct denaturation temperatures and cooperativity of denaturation are identified per cell type. Freezing induced cold denaturation of proteins is found to be reversible for HDF and LNCaP cells but not for SMC. This suggests that the proteins are more stable (or less susceptible to freeze injury) in LNCaP and HDF as compared to SMC. The cells display similar membrane phase behavior during heating that lack a distinct thermotropic phase transition. Protein denaturation during heating is suggested as a potential method to thermal fingerprint mammalian cells.

The results of this chapter are currently being compiled for publication:

- Balasubramanian SK, Wolkers WF, and Bischof JC (In preparation) "Protein denaturation and membrane phase transition during thermal treatments of mammalian cells: An FTIR study"

2. CELLULAR BIOPHYSICS AS A FUNCTION OF MODEL SYSTEM DURING FREEZING OF HUMAN DERMAL FIBROBLASTS (HDF)[1]

This chapter describes the biophysics of freezing human dermal fibroblast (HDF) cells in different model systems (or attachment states). The present author performed all the experimentation work and data analysis. The results from this chapter have been compiled, edited and published in the following citation:

I. Balasubramanian SK, Bischof JC, and Hubel A (2006) "Water transport and IIF parameters for a connective tissue equivalent" *Cryobiology* 52 (1); pp 62 – 73

[1]This work was supported by institutional funds and a Forstrom Fund Fellowship. The authors would like to acknowledge David Swanlund and Dr. Bumsoo Han for technical assistance provided. Curtis Anderson and Dr. Uwe Kortshagen are also acknowledged for developing the plasma treatment technique of the coverslips used for collagen tissue equivalent (TE) preparations.

This chapter describes the experimental and numerical analysis performed to assess the impact of cell attachment state/model system on the biophysics of freezing human dermal fibroblasts (HDF). The model systems that were studied include cell suspensions and tissue equivalents (TE). Tissue equivalents (TEs) were formed by entrapping human dermal fibroblasts (HDFs) in either collagen or fibrin gels. Freezing studies were conducted using a Linkam cryostage fitted to an optical microscope allowing observation of the TEs cooled under controlled rates between 5 – 130^{o}C/min. Typically, freezing of cellular systems results in two biophysical processes that are both dependent on the cooling rate: dehydration and/or intracellular ice formation (IIF). Experimental data were fitted in numerical models to extract parameters that governed water permeability, E_{Lp} and L_{pg}, and intracellular ice nucleation, Ω_o and κ_o. Results indicate significant differences exist between freezing HDFs in suspension and tissue equivalents. The resultant biophysics indicates that cell-cell and cell-matrix interactions may play a major role in ice propagation in TEs.

2.1 INTRODUCTION

Living tissue replacements, fabricated from a combination of living cells and scaffolds (either biological or synthetic), have found successful applications in clinical practice (203; 204). For instance, tissue equivalents fabricated for replacement of skin, blood vessels and ligaments have been studied extensively (205; 204; 206; 207). Currently, there are many FDA approved tissue engineered products in the market including Apligraf (Organogenesis Inc.), Dermagraft (Advanced Tissue Sciences, Inc), Carticel (Genzyme Corp.) and InFUSE bone graft (Medtronic) to name a few. With the continued interest and investment in tissue engineered products, the development of preservation technologies – including cryopreservation - for economical and efficient long term storage is critical. For successful cryopreservation, a better understanding of the underlying biophysics at both the cellular and artificial tissue level is necessary.

Freezing injury at the cellular level is often ascribed to two biophysically mediated responses to cooling rate: extreme dehydration at slow cooling rates and intracellular ice formation (IIF) at high cooling rates (19). Freezing of isolated and cultured cells has been extensively studied for various cell types using both experimental methods and predictive numerical models (62; 21; 83; 65). In addition, freezing studies in attached model systems - in monolayer or in an extracellular matrix (e.g. collagen gel) – have been shown to result in higher incidences of IIF when compared to freezing cells in suspension (116; 92; 120). Acker et al. experimentally demonstrated that cell-cell interactions increase the incidence of IIF while gap junctions may play a role in the propagation of IIF in cultured monolayer (116; 53). However, de Freitas and Diller noted that the IIF trends

determined during freezing of pancreatic islets could be predicted using the theoretical models proposed by Toner et al. for cellular suspensions (208; 44). Limitations to the aforementioned studies include low cell densities unlike tissues, and highly controlled interactions (e.g. micro patterned tissues).

The objective of the present study is to assess the biophysics of freezing in three different model systems using human dermal fibroblasts (HDFs). Freezing of HDFs in a collagen/fibrin TE matrix are evaluated, and compared to HDFs in suspension. Cellular biophysical models were used to predict the water transport and IIF parameters in all the model systems studied. The results are then compared and contrasted to existing biophysical parameters for other cell types.

2.2 BIOPHYSICAL MODELS

The biophysical models for water transport and IIF used in the current study are discussed in Chapter 1. Briefly, water transport across the cell membrane occurs to maintain the osmotic balance between the intracellular compartment and the extracellular media as the solute concentration increases during freezing. The IIF biophysical model used in the current study is based on the formulations developed by Toner et al. (44). Briefly, for a thermodynamic system composed of identical biological cells, the probability of IIF (PIF) by surface catalyzed nucleation (SCN) is a function of cooling rate and the degree of supercooling of the intracellular media to name a few factors. Further details regarding the assumptions and the details of the biophysical models are discussed in Chapter 1.

2.3 MATERIALS & METHODS

2.3.1 Human Dermal Fibroblasts (HDF) Culture

Normal HDFs were obtained from cryopreserved stock (Cambrex Corporation, East Rutherford, NJ) and thawed in a warm water bath at 37^{o}C. The cells were centrifuged at 500xg for 10 minutes and then suspended in cell media. The cell media contained Dulbecco's modified Eagle medium (DMEM) with 10% fetal bovine serum (FBS) and 5mL/L penicillin-streptomycin. The cells were grown in 75cm^2 T-flasks and incubated at 37^{o}C and 5% CO_2 for 72 hrs before either experimentation or splitting. The HDFs used for experiments were between passages three to six.

HDFs were trypsinized (1.5mL) to remove them from the tissue culture flask (0.05% Trypsin/0.53mM EDTA). The concentration of the cells was determined using a hemocytometer under a light microscope. A specific volume of the suspension was taken, according to the desired concentration of cells required, and centrifuged at 500xg for 10minutes. The cell pellet was then resuspended in culture media and held on ice (~2^{o}C to 4^{o}C) for the time period of the experiments. For freezing studies of HDFs in suspension, the cells were used as such.

2.3.2 Collagen Tissue Equivalent (TE) Preparation

Collagen gels were prepared at a final concentration of 2mg/mL (Organogenesis, Canton, MA) and were polymerized according to manufacturer's instructions. Briefly, HDFs were suspended in cold collagen gel at a concentration of 2×10^5 cells/mL. The cells/collagen

solution (10μL) was transferred to tissue culture treated glass cover slips (Fisher Scientific, Hampton, NH) and incubated at 37^{o}C for 1hr to form a TE. At the end of incubation, 5mL of cell media was added to the Petri dish to cover the TE entirely. The TE was then incubated at 37^{o}C for 24hrs prior to experimentation. To enable the collagen gel to attach to the glass surface, the coverslips were plasma treated before plating the gels. A "nonthermal" Helium gas at ~ 300K was applied using a 75W @ 13.56MHz RF power source for a period of 30s to treat the coverslips.

2.3.3 Fibrin Tissue Equivalent (TE) Preparation

Bovine fibrinogen was mixed with the cell solution and bovine thrombin at a ratio of 4:1:1 at room temperature. The final cell concentration in the mixture was 2×10^{5} cells/mL. 10μL of the cells/fibrin gel solution was placed on the surface of a 12mm tissue culture treated glass cover slip (Fisher Scientific, Hampton, NH) and incubated at 37^{o}C for 1hr to allow it to gel. Cell media (3mL) was then added and the fibrin TE was incubated for a further period of 24hrs prior to experimentation.

2.3.4 Cryomicroscope Setup and Freezing Protocol

Controlled freezing of the samples was carried out in the Linkam Scientific conduction type cryostage (Linkam Corporation, United Kingdom). An Olympus BX50 fluorescent microscope (Tokyo, Japan) was used to observe the freezing and the images obtained during freezing were recorded by a 1 chip CCD camera connected to a VCR. The cryostage had a silver block, where the samples were placed for freezing, to which platinum RTD's were attached for temperature measurement. Liquid nitrogen was the

coolant used for freezing, and an inbuilt heating system controlled thawing. A circular quartz crucible was mounted on the cryostage to hold the samples (cell suspension/TE) during freezing. For cooling rates of 1-130^{o}C/min, the error in temperature measurement was less than 0.1^{o}C. In addition, since the volume of the sample was small (10μL), spatial variation of concentration and temperature was minimized.

Prior to freezing, the cells in suspension, monolayer or in TEs were stained with Hoechst 33342 (Sigma, St. Louis, MO) (a membrane permeable nucleic acid binding dye) solution diluted to 1/1000 with culture media. This was done to facilitate locating the cells prior to and during freezing. During the cooling protocol, temperature was decreased at 10^{o}C/min to -2^{o}C where ice was seeded (T_{seed}) by touching a chilled needle to the edge of the sample. The temperature was then increased to just below the phase change temperature before a specified linear cooling rate (130, 100, 75, 50 and 30^{o}C/min) was imposed. The chosen end temperatures were -30^{o}C and -80^{o}C for the water transport and the IIF studies respectively. The cells were thawed back to room temperature at 130^{o}C/min.

2.3.5 Water Transport Measurement

Water efflux from the HDFs in suspension was measured at cooling rates of 5, 10 and 30^{o}C/min. Three to five cells in the field of view were selected per experimental run. Three to five experiments were pooled together to represent the cellular water transport data at a particular cooling rate. Area measurements of the cells during freezing were obtained and analyzed using Image-Pro software (Media Cybernetics, Silver Spring, MD). This was done by manually tracing the outer cell membrane three times and taking

an average. This denoted the final projected area for a particular cell at a specific temperature. Only cells that maintained their spherical shape during freezing were included in the final analysis. The area of the cells was related to the volume by a $2/3^{rd}$ power dependence as given by $(A/A_o) = (V/V_o)^{2/3}$.

To determine the inactive cell volume (V_b), nucleated cell suspension samples were cooled at 2^oC/min and held at specific temperatures (e.g. -2^oC, -3^oC, -5^oC etc.) for 5 minutes to establish equilibrium between the intracellular and the extracellular space. The minimum volume attained by the cells then was taken to be the osmotically inactive cell volume. The limitations of the model may include permeability differences between individual cells, volume calculation using two-dimensional information and an assumption of perfect spherical geometry of the cells.

2.3.6 Measurement of IIF

The kinetics of IIF for HDFs in suspension, collagen TE and fibrin TE was determined for a range of cooling rates (130, 100, 75 and 50^oC/min). During experimentation, IIF was characterized either by "darkening" or by "twitching". Darkening was observed by the sudden opaque "flashing" at a particular temperature indicating formation of large ice crystals in the cell. PIF in the cells was assumed to be equal to the ratio of cumulative number of cells exhibiting darkening to total number of cells in the sample population. The recorded images were analyzed for the cumulative fraction of IIF in each of the experiments performed. Data from the freezing responses of 50-70 cells were then pooled together to obtain the IIF kinetics.

Twitching was characterized by a sudden vibration of the cell with no darkening. Even though twitching has been reported earlier, it is yet to be explained by an appropriate model (62; 209). Hence, in the present study IIF data is only reported based on the measurements due to the darkening effects in the cell.

2.3.7 Numerical Model for Biophysics Estimation

The experimental data was fit to the previously given equations to determine WT and IIF parameters. The Marquardt optimization scheme (210) was used as previously described in Toner et al. (44). Briefly, it minimizes the variance between the experimental data (y_i) and the theoretical fit/data ($y_{fit,i}$) and maximizes the R^2 value (≥ 0.97 in this case) of the fit as represented as shown below.

$$R^2 = 1 - \frac{\sum \left(y_i - y_{fit,i}\right)^2}{\sum \left(y_i - \bar{y}\right)^2} \qquad (2.1)$$

2.4 RESULTS

2.4.1 Intracellular Ice Formation

The kinetics of IIF for HDFs in suspension, collagen TE and fibrin TE is determined at 50, 75, 100 and 130^{o}C/min. IIF is characterized by the "darkening" of the cells attributed to ice crystallization. Figure 2.1 depict the "darkening" effect as a consequence of IIF for HDFs in a collagen TE cooled at a rate of 50^{o}C/min. The micrographs depict HDFs before (-1^{o}C) and after ice nucleation (-20^{o}C) in the TE.

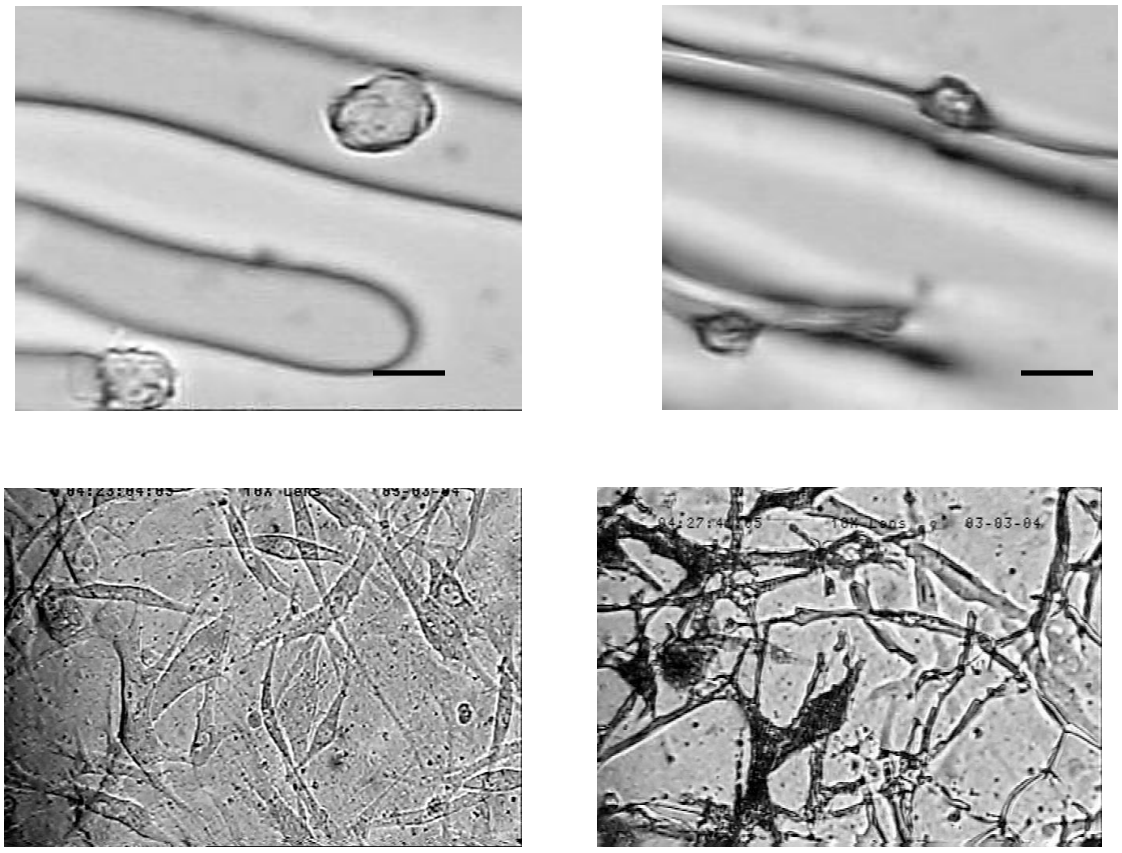

Figure 2.1: (Top Panel) Cryomicroscope images of HDF frozen in suspension at a cooling rate of 5°C/min. (Left) Cells at -1.0°C, (Right) Cells at -20°C. (Bottom Panel) HDFs frozen in collagen TE at a cooling rate of 50°C/min. (Left) Cells at -1.0°C, and (Right) Cells at –20°C. IIF within HDFs in the collagen TE is characterized by cell darkening. Bar represents a scale of 20 μm.

The cumulative fraction of IIF increases with decreasing temperature for all the model systems at the cooling rates studied (Figure 2.2). IIF is observed to occur in the temperature range between -6°C and -17°C. In addition, the cumulative fraction of IIF in the cells increases with increasing cooling rate for all the model systems. However, the data indicates clear differences in the kinetics of IIF amongst the three model systems studied. At the highest cooling rate studied (130°C/min), HDFs exhibited 100% IIF in all model systems except in the cell suspension where only 55% IIF in recorded. The fraction of cells with IIF is distinctly higher in the TEs when compared to suspensions at

all the imposed cooling rates. Between the TEs, there are no major observed differences in the maximum cumulative fraction of IIF (Figure 2.3).

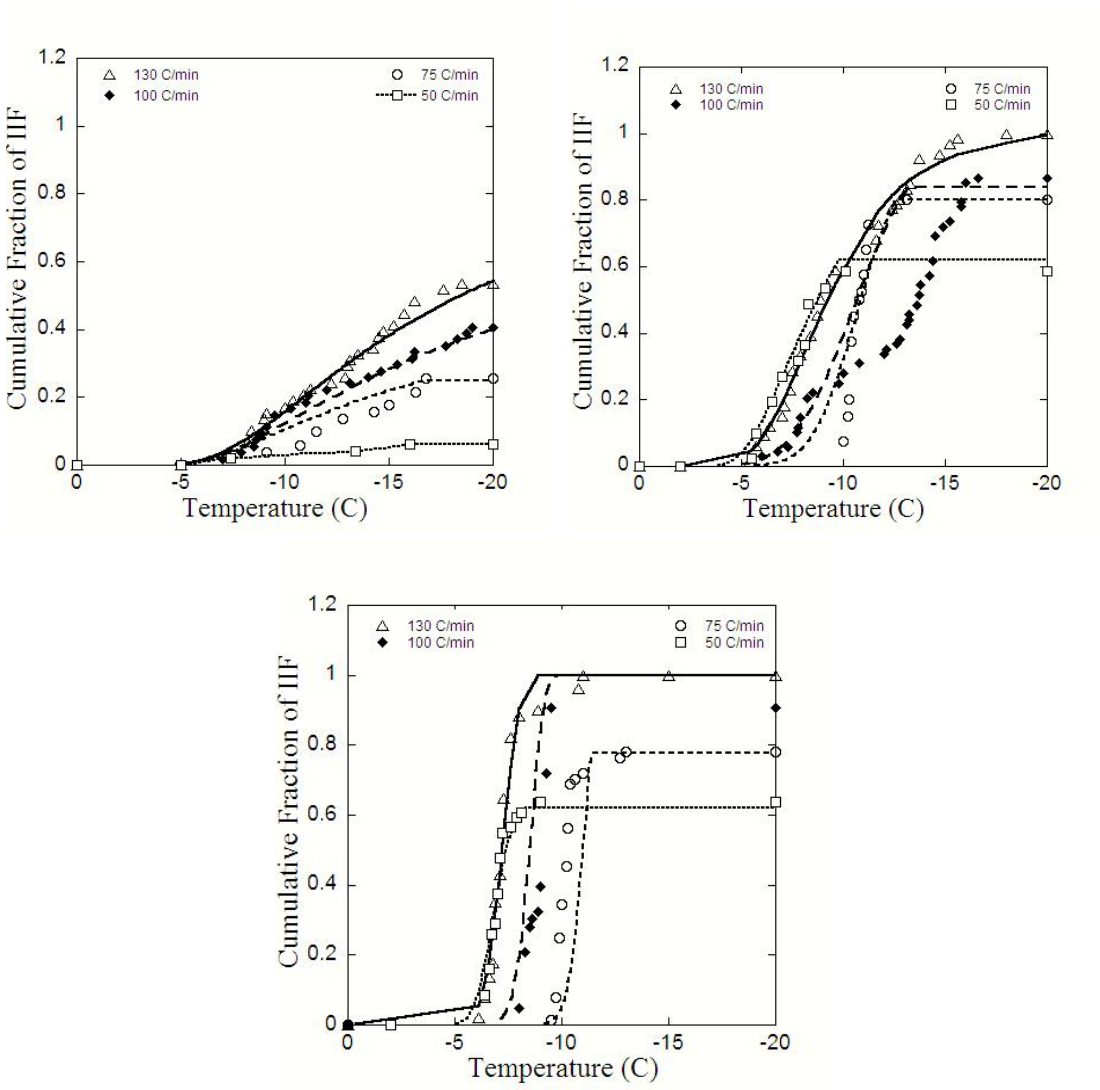

Figure 2.2: Cumulative fraction of IIF as a function of temperature at different cooling rates (130, 100, 75 and 50°C/min) for (A) HDF in suspension; (B) HDF in a collagen TE; and (C) HDF in a fibrin TE. Lines represent the theoretical predictions based on inverse fitting to obtained experimental data.

An estimate of the kinetic and thermodynamic parameters, Ω_o and κ_o for the TE model systems is done at 130°C/min. At this freezing rate, water transport across the cell

membrane is assumed to be minimal. The IIF nucleation parameters for HDFs are found to be $\Omega_o = 3.6 \times 10^9 (m^2.s)^{-1}$ and $\kappa_o = 1.03 \times 10^9 K^5$ in collagen TE; and $\Omega_o = 9.81 \times 10^{11}$ $(m^2.s)^{-1}$ and $\kappa_o = 4.04 \times 10^9 K^5$ in fibrin TE. A good fit is obtained between the model predictions and the experimental observations ($R^2 > 0.97$ in all cases).

For HDFs in suspension that were frozen at 130°C/min, the IIF-water transport models cannot be decoupled since not all cells form IIF. Hence, the biophysical parameters for IIF are determined by a coupled IIF-water transport analysis using the water transport parameters obtained at lower cooling rates. The estimated IIF biophysical parameters for HDFs in suspension are $\Omega_o = 9.2 \times 10^7 (m^2.s)^{-1}$ and $\kappa_o = 1.20 \times 10^9 K^5$ at 130°C/min. A summary of all the determined IIF parameters for the cellular model systems studied is provided in Table 2.1.

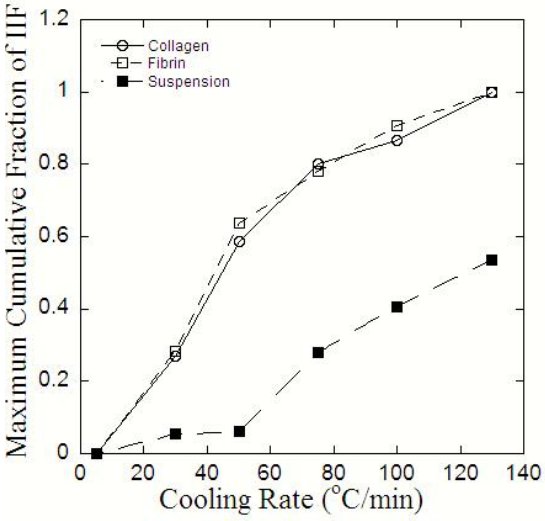

Figure 2.3: Comparison of the maximum cumulative fraction of IIF for HDFs in tissue equivalents (TEs) to HDFs in suspension to illustrate the potential impact of cell-cell and cell-ECM interaction on IIF

Table 2.1: Estimates of the IIF biophysical parameters (κ, Ω) for HDFs in different model systems.

MODEL SYSTEM	$\Omega_o \times 10^{-8}$ ($1/M^2.S$)	$\kappa_o \times 10^{-9}$ (K^5)	R^2
Collagen TE	36	1.03	0.99
Fibrin TE	9814.6	4.04	0.97
Monolayer*	105	2.35	0.99
Cell suspension	0.92	1.20	0.98

*Data obtained from Choi et al. (144)

2.4.2 Water Transport

The mean diameter of HDFs at room temperature is estimated to be 12.12 ± 1.72μm (n=63). Thus, the average initial volume of the cells (V_o) is 932.32μm^3. An estimate of V_b, based on Boyle Von't Hoff method, is done by freezing the cells at 2°C/min to -30°C with 5min hold time at intermediate temperatures to allow the cells to equilibrate with the ECM. The minimum volume reached by HDFs is determined to be $V_b = 0.24V_o$.

Micrographs of the dehydration of HDFs during freezing are depicted in Figure 2.4(a, b). At 10°C/min cells undergo dehydration but a few instances of IIF are noted. The normalized volume of the cell as a function of temperature at the three different cooling

rates (5, 10, 30°C/min) is given in Figure 2.4(a-c) with a composite curve given in Figure 2.4(d). The data is inverse fit to the water transport models to determine the dehydration parameters (L_{pg}, E_{Lp}) at each cooling rate (Table 2.2). The average of the three values is estimated to be $L_{pg} = 4.34\times10^{-14} \pm 2.93\times10^{-14}$ m^3/N.s and $E_{Lp} = 170 \pm 11$ kJ/mol.

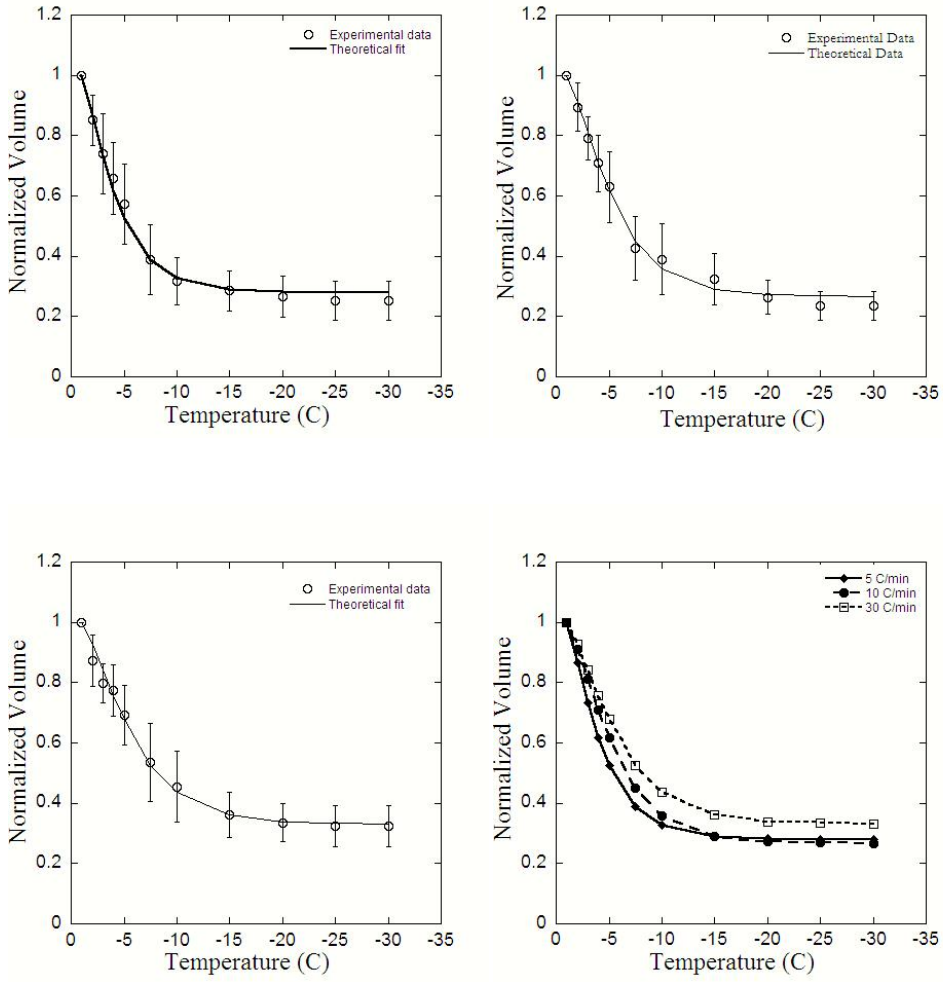

Figure 2.4: Normalized cell volume as a function of temperature for HDF in suspension at a cooling rate of (A) 5°C/min; (B) 10°C/min; (C) 30°C/min; and (D) 5, 10 and 30°C/min. Open circles indicate average experimental data (n = 10 to 30 cells) and error bars represent SD. Predicted lines based on biophysical parameter estimates are included.

Table 2.2: Water transport parameters (L_{pg} & E_{Lp}) for HDFs in suspension at 5, 10 and 30°C/min.

COOLING RATE (°C/MIN)	L_{PG} $\times 10^{14}$ (M^3/N.S)	E_{LP} (KJ/MOL)	R^2
5	2.17	182	0.99
10	3.17	161	0.99
30	7.67	166	0.99

The water transport parameters for HDFs in the fibrin and collagen TEs cannot be determined through conventional cryomicroscopy observations since the cells are attached. Hence, an indirect approach is taken to assess water transport of HDFs in the attached state. Cell dehydration parameters for TEs are numerically estimated from a coupled analysis of the dehydration and IIF kinetics at rapid cooling rates (e.g. 100, 75 and 50°C/min). This method has been previously suggested by Yarmush et al. for hepatocytes embedded in a collagen matrix (60). Briefly, the IIF parameters determined at the highest cooling rate (130°C/min) are assumed to be a constant at all other rates. Water transport parameters are then estimated from IIF kinetics at slow cooling rates where water transport and/or IIF would occur. Using this method, the average water transport parameters for the collagen and fibrin TEs are determined to be L_{pg} = 105 ± 50 ($\times 10^{14}$) m^3/N.s and E_{Lp} = 301 ± 60 kJ/mol, and L_{pg} = 152 ± 100 ($\times 10^{14}$) m^3/N.s and E_{Lp} = 334 ± 199 kJ/mol respectively (Table 2.3).

Table 2.3: Water transport parameters (L_{pg} and E_{Lp}) for HDFs in a monolayer*, collagen and a fibrin TE at 50, 75, 100 and 130°C/min.

Cooling Rate °C/min	Monolayer*			Collagen TE			Fibrin TE		
	L_{PG} $\times 10^{14}$ $M^3/N.S$	E_{LP} KJ/MOL	R^2	L_{PG} $\times 10^{14}$ $M^3/N.S$	E_{LP} KJ/MOL	R^2	L_{PG} $\times 10^{14}$ $M^3/N.S$	E_{LP} KJ/MOL	R^2
130	19.7	294	0.99	100	262	0.99	207	477	0.99
100	6.3	63	0.94	143	334	0.93	168	384	0.97
75	36.2	221	0.90	140	368	0.98	225	433	0.95
50	20.9	200	0.97	36.7	239	0.99	6.8	40	0.98

*Data obtained from Choi et al. (2011) (144)

2.5 DISCUSSION

Cell biophysical responses to freezing HDFs in collagen and fibrin TEs were experimentally characterized using cryomicroscopy, and numerically predicted using a coupled water transport and IIF model. These parameters were then compared to freezing HDFs in suspension to elucidate quantitative differences. The estimated biophysical parameters are then compared to illustrate the impact of cellular model system on biophysics.

2.5.1 Water Transport

The biophysical model used in this study for predicting cell permeability parameters were from the formulations developed by Mazur (18). This model did not account for the effect of cell-cell and cell-matrix interactions on cell dehydration during freezing.

However, this model is still useful as an indirect technique to compare cell biophysics in different attached states. Levin et al studied the influence of cell-cell interactions on water transport for a closely packed cluster of erythrocytes (39). Devireddy et al. and Korniski and Hubel developed similar models to study water transport in liver cells (146; 150). They determined that transport depends on the location of the cell in the tissue and on the duration of exposure to freezing.

The calculated permeability L_{pg} for HDFs in suspension was 4.34×10^{-14} $m^3/N.s$ and the activation energy E_{Lp} was 170 kJ/mol. The permeability values determined were similar to those reported earlier for fibroblasts (99), and comparable to digested rat hepatocytes and lymphocytes (60; 21). The activation energy for HDFs was lower when compared to human and rat hepatocytes but similar to equine sperm (12). A more comprehensive compilation of the dehydration parameters for multiple cell types is given in Table 1.2.

The data given in Figure 2.1 and Figure 2.4 suggest that the cells experience equilibrium freezing for cooling rates $\leq 10^{o}C/min$ where some intracellular water was retained at $30^{o}C/min$. Experimental results for HDFs in suspension suggest that the volumetric response to freezing induces osmotic stress that can be explained by semi-permeable membrane limited diffusion of water (47). In addition, previous studies have shown that the biophysical models were more sensitive to E_{Lp} and relatively insensitive to L_{pg} (18; 211). However, for the HDF cell diameter ($12.12\mu m \pm 14\%$), E_{Lp} was relative insensitive ($\pm0.1\%$) as compared to L_{pg} ($\pm10\%$).

Table 2.4: Water transport and IIF parameters for HDFs in suspension, collagen TE and fibrin TE compared to hepatocytes removed from a collagen gel **(60)**.

BIOPHYSICAL PARAMETER		**CELL SUSPENSION**	**COLLAGEN TE**	**FIBRIN TE**	**ADULT RAT HEPATOCYTES** (60)
Water transport parameters (Average)	$L_{pg} \times 10^{14}$ (m^3/N.s)	4.34	105	152	21.6
	E_{Lp} (kJ/mol)	170	301	334	76.4
IIF parameters	$\Omega_o \times 10^{-8}$ ($1/m^2$.s)	0.92	36	9814.6	54
	$\kappa_o \times 10^{-9}$ (K^5)	1.20	1.03	4.04	0.30

The permeability parameters for HDFs in the TEs were nearly 20 times higher as compared to suspensions. The current results are compared to the water transport parameters obtained by Yarmush et al. for intact rat hepatocytes cultured in a sandwich configuration in Table 2.4 (60). An increase in both the water transport (permeability) and IIF kinetics is observed for cells in the attached state as compared to suspensions. In the TEs, this increase in the permeability value seems to be offset by a substantial increase in the activation energies. The result is that the PIF was still greater for TEs as compared to HDFs in suspension at a given cooling rate. The higher activation energy of water transport for HDFs in the TEs could be a reflection of the influence of diffusion of water through the extracellular matrix. The estimates obtained in this investigation represent a somewhat 'lumped parameter' model for water transport. The differences in water permeability estimates for fibrin and collagen TE suggests that the microstructure

of the extracellular matrix may play an important role in modifying water transport and IIF in the TE systems. Further studies (both experimental and numerical) are needed to elucidate the influence of the microstructure characteristics on water transport.

2.5.2 Intracellular Ice Formation

During freezing, IIF is described by either "darkening" or "twitching" in the model systems studied. The difference between the two modes of IIF likely depends on the cooling rate and the nucleation temperature. Twitching has previously been reported during freezing of granulocytes at rates greater than 30^{o}C/min, and in human micro vascular endothelial cells (HMECs) (209; 62). It is characterized by small ice crystals that recrystallize to form larger ice crystals especially during thawing.

Toner et al. proposed the surface catalyzed nucleation theory (SCN) to mechanistically predict IIF in cells during freezing (44). Acker et al. and Irimia and Karlsson have shown that cell-cell interactions contribute to increase IIF based on cell attachment (116; 53; 120). Additionally, Irimia and Karlsson proposed a mathematical model to predict IIF in a micro-patterned hepatocytes tissue construct that accounts for cell-cell interactions. However, the applicability of this simplified model is limited to model systems with controlled cell-cell interactions. This approach may be appropriate for epithelial tissue but becomes increasingly difficult to extend to connective or artificial tissues where cell density is relatively low but ECM density is high.

Freezing in TE may be affected by spatial and temporal gradients of temperature. The TEs used in this investigation were designed to be uniform volume/thickness while

minimizing the thickness to permit visualization of the cell biophysics. As such, we do not anticipate significant temperature gradients. This is corroborated by a simple scaling analysis that shows that time constant for heat transfer in a TE sample is of the order of 0.0001s as compared to mass transfer time constant of ~100s. The results suggest that the extracellular matrix influences the diffusion of water. As such concentration gradients (specifically NaCl) may be present. These gradients will be highest during the initial crystallization phase when the cells are engulfed by the advancing ice front. After that point (which is the majority of the experiment), concentration gradients within the TE are expected be minimal.

The kinetics of IIF (slope of the CIIF as a function of temperature) was higher for TEs as compared to suspensions. Acker et al. reported a similar increase in the kinetics of IIF for cell monolayer when compared to suspensions (116; 53). They concluded that cell-to-cell contact had a strong influence on observed IIF. This is evident during freezing of TEs where a clear demarcation is observed between intracellular or "slow" independent IIF, and intercellular or "rapid" IIF propagation due to cell contact. Both studies show that the impeding diffusion of water out of the cell - either through the presence of an extracellular matrix or because of high cell density - increases the probability of IIF.

The results of the study suggested that a cooling rate of 5°C/min may help maximize HDF viability since it simultaneously appears to avoid excessive dehydration and IIF. This prediction of an optimal cooling rate is consistent with previous observations by Devireddy et al. for post thaw survival of cells in collagen based TEs (124). Further studies are needed to verify the relationship between cooling rate and cell survival for

TEs. Additionally, more studies are also needed to establish a link between cell damage and biophysics for TEs.

2.6 SUMMARY

The impact of cell attachment state on the freezing biophysics of HDFs was assessed in three different model systems – suspensions, fibrin and collagen tissue equivalents (TE). Controlled freezing experiments were conducted for cooling rates of 5 – 130^{o}C/min using a cryomicroscope. Cell biophysical models were then used to compare the biophysics of cells in suspensions vs. TE. The results from this study are summarized below:

i. The kinetics of IIF is enhanced in TEs as compared to cell suspensions. At a given temperature and cooling rate, the incidence of IIF is higher in the attached state vs. suspensions.

ii. The biophysical models suggest that both IIF and water transport in TEs is enhanced as compared to cell suspensions. The biophysical parameters (IIF and water transport) for TEs were significantly higher than in suspensions.

The cell biophysical models are applied indirectly to compare the freezing biophysics of HDFs in TEs vs. suspensions. The exact factors that affect increased IIF and water transport in TEs may not be known but cell-cell and cell-ECM interactions are generally implicated. In addition, the impact of these biophysical changes on cell viability as a result of the attachment state needs to be studied. This is done in Chapter 3 where the impact of cell type and attachment state on the biophysics and cell survival is evaluated.

3. CELLULAR BIOPHYSICS & VIABILITY AS A FUNCTION OF MODEL SYSTEM DURING FREEZING OF PORCINE SMOOTH MUSCLE CELLS (SMC)[2]

This chapter describes the biophysics of freezing porcine smooth muscle cells (SMC) in different model systems (or attachment states). The biophysics is linked to cell injury post freeze thaw for the model systems studied. The present author and Arjun Menon performed all the experimentation work and data analysis related to the cell biophysics and viability. Ramji Venkatasubramanian performed the computer simulations and data analysis for thermal modeling. The results from this chapter have been compiled, edited and published in the following citation:

I. Balasubramanian SK, Venkatasubramanian RT, Menon A, and Bischof JC (2008) "Thermal injury prediction during cryoplasty through in vitro characterization of smooth muscle cell biophysics and viability" *Annals of Biomedical Engineering* 36 (1); pp 86 - 101

[2]The research work pertaining to this chapter was made possible by financial support from Boston Scientific, and scientific & technical assistance from Daniel Lafontaine and David Swanlund.

This chapter characterizes the freezing biophysics and viability of porcine smooth muscle cells (SMC) in different model systems. Cryoplasty, a novel technique involving simultaneous stretching and freezing of the peripheral arteries using a cryogen filled balloon catheter, has shown the potential to combat restenosis. However, evaluation of the thermal and biophysical mechanisms that affect cellular survival during cryoplasty is lacking. To achieve this, the thermal history in arteries was predicted for different balloon temperatures using a thermal model. Cellular biophysics was then characterized, using *in vitro* model systems, based on the thermal model predictions. The thermal and biophysical effects on cell survival were eventually determined. Smooth muscle cells (SMC) isolated from porcine femoral arteries was used in suspensions and attached *in vitro* systems (monolayer and fibrin gel). The thermal model predicted cooling rates from 2200 to 5^{o}C/min in the artery. The biophysical parameters (WT & IIF) were higher for SMCs in attached systems as compared to suspensions. One possible reason for the differences in IIF kinetics was verified to be the presence of gap junctions, which facilitate cell-cell connections through which ice can propagate. This is reflected by the change in the predicted IIF parameters when a gap junction inhibitor was added in monolayer. SMC viability was affected by the model system (lower viability in attached systems), the thermal conditions and the biophysics. SMC viability was found to be the least in fibrin TE (most % IIF) and the most in suspensions (least % IIF) at all cooling rates. Using fibrin TE results (suggested as the best *in vitro* system to mimic restenosis), conservative estimates of injury regimes in the artery during cryoplasty is predicted.

3.1 INTRODUCTION

The most common types of vascular disease in the peripheral arteries (i.e. PAD) are blocked arteries due to fatty deposits that affected about 8-12 million people in the United States in 2006 (212). Endovascular techniques such as percutaneous transluminal angioplasty (PTA) are used to treat PAD. However, typically 30-40% of angioplasties result in restenosis (213; 214). This occurs because PTA causes substantial injury to the vessel wall during dilation of the arterial blockage. This disrupts not only the plaque but also the endothelium, the internal elastic lamina and the media, which can lead to aggressive proliferation of SMCs resulting in neointimal hyperplasia or restenosis (215). To offset these drawbacks, alternative treatment procedures for PAD are being actively investigated (216). Drug coated stents have been introduced as an option over PTA. However, there is durability issues associated with the treatment (e.g. material sloughing, restenosis over time etc.) (217). This suggests the need for continued research and development in restenosis treatments.

One new and promising method is the use of controlled freezing to treat stenotic vessels (Cryoplasty) using a cryogen filled balloon catheter. The choice of the cryogen includes liquid N_2, Freon, nitrous oxide, CO_2 gas and in certain cases saline solution mixed with ethanol (218). Freezing of the stenotic vessel can help predict the survival of the proliferating SMCs and also prevent elastic recoil of the artery, which could result in restenosis (218). Other advantages of freezing include maintenance of ECM structure (219), the minimally invasive approach and lack of coagulation effects, i.e. thermal fixation (220). Recently, a thermal model analyzing the temperature distribution in

arteries during cryoplasty was reported (221). However, an assumption of constant thermal properties for tissues during freezing will affect predicted temperatures and cooling rates. Though promising, there is still a lack of clear understanding of the extent and distribution of thermal injury during freezing in arteries that limits its informed use.

The use of freezing for the treatment of tumors in various tissues and organs has been well documented in the literature (222; 223; 224; 225). The interpretation of results during freezing is limited by the choice of the model system (i.e. *in vitro* or *in vivo*). *In vivo* models are complicated since freezing results in both cellular and host mediated (vascular and immunological) injury (226; 214). Though *in vivo* animal models are ultimately needed to demonstrate the efficacy of the treatment, the proper *in vitro* model system can help elucidate the mechanism of freeze injury (126). In addition, *in vitro* models are simpler to handle and can provide a basic understanding of the cellular biophysical responses during freezing.

The effects of freezing in the arterial system have been reported using both *in vivo* and *in vitro* systems. Reported effects of direct freezing using *in vivo* systems include early arterial cell loss, late intimal hyperplasia and increased collagen production for a 10 week post freeze study using the rabbit iliac artery model (226). Also, recovery of microvascular perfusion and endothelial cell injury was reported for a 7 day post freeze study using myocardial cryothermia in rats (227). However, there is a lack of quantitative information linking the effect of freezing direct cell injury. To address this, tissue and cellular level studies have been reported for arterial cells. Previous cellular freezing studies in monolayer have shown that endothelial cells are more resistant to freezing and

have increased proliferation post freeze/thaw as compared to SMCs (228). Separately different *in vitro model* systems were also used to study the freezing effects on SMCs from different animal cell lines including rat, pig and human SMCs. It was concluded that porcine SMCs behave similarly to human SMCs on freezing (125). In spite of these previous efforts, the mechanisms of freeze injury (cellular/molecular) during freezing and the appropriate thermal thresholds are still not completely understood. In addition, an attempt to quantify the molecular mechanisms of injury was reported for human SMCs and endothelial cell suspensions. Necrotic injury and to a lesser extent apoptotic cell injury were observed at temperatures below -20^{o}C and between -5 & -15^{o}C respectively (229). Further challenges then involve quantifying the thermal, biophysical and molecular events (mechanisms) responsible for cell injury during freezing.

The aim of this chapter is to quantify and predict the thermally driven biophysics of injury during freezing. A thermal model is first used to predict temperature distribution in femoral and popliteal arteries (two common targets) during freezing. Based on these predictions, *in vitro* model systems are then employed to characterize cell biophysics. The model systems studied include suspensions (simplest), monolayer (cell-cell interactions) and fibrin TE (cell-cell and cell-ECM interactions). The study variables include the model system, the cooling rate, the end temperature and the time post freeze/thaw. Results from the thermal model and cell viability are used to obtain conservative estimates of thermal injury regimes in a simulated artery.

3.2 THEORETICAL MODELS

3.2.1 Thermal Model

The energy equation was modified to account for phase change using the enthalpy method (1; 13) and to predict the thermal history of the artery during freezing. Similar use of the model was reported for a variety of tissue systems as reviewed recently (200). The governing partial differential equation is given by:

$$\frac{1}{r}\frac{\partial}{\partial r}\left(kr\frac{\partial T}{\partial r}\right)=\rho\frac{\partial H}{\partial t} \qquad (3.1)$$

The tissue was considered frozen for all $T < T_s$, unfrozen for all $T > T_l$ and a mushy zone considered for $T_s < T < T_l$ where T_s = -40^{o}C and T_l = -0.53^{o}C. The thermal properties used in the model, outside the mushy zone, are listed in Table 3.1. The calculation of the thermal properties and the enthalpy inside the mushy zone has been discussed elsewhere (13; 101). Briefly, the thermal properties and the enthalpy in the mushy zone were calculated as follows:

$$X_i = X_s + f(T)^*(X_l - X_s) \qquad (3.2)$$

$$f(T)=\frac{\left(\frac{T_s}{T}-1\right)}{\left(\frac{T_s}{T_l}-1\right)} \qquad (3.3)$$

In the above equations, X_s and X_l are the thermal property or enthalpy at T_s and T_l respectively and f (T) the release pattern describing the relation between temperature and

the unfrozen tissue within the mushy zone. An Euler forward one dimensional finite difference analysis with time step of 10^{-5}s and element size 0.025mm was constructed and run to solve the thermal model (230). The results were additionally verified using finite element analysis (ANSYS 10.0, Canonsburg, PA).

Table 3.1: Thermal properties used in the model. Tissue properties from previously reported studies were assumed true for arteries. All the latent heat of the artery was assumed to be from only water, which constitutes 60-65% of the tissue.

PROPERTY	VALUES	UNITS
k_l	0.6	W/m-K
k_s	$2.24+ 5.975 \times 10^{-3} \times (-T)^{1.156}$	W/m-K
C_l	4100	J/Kg-K
C_s	7.16(T-273.15)+138	J/Kg-K
ρ_l	999	kg/m^3
ρ_s	921	kg/m^3
L	210	kJ/kg

The thermal model predicted the temperature distribution in simulated geometries corresponding to femoral and popliteal arteries. Figure 3.1 depicts the arterial geometry modeled and the boundary conditions imposed. A lumen radius of 3mm for popliteal and 5.5mm for femoral artery was used while the arterial thickness was assumed to be 2mm for both the arteries (231; 232). The arteries were assumed to be perfect cylinders and the heat transfer was assumed to be radial. Cryoplasty involves freezing of the artery to approximately -15 to -20^{o}C for about 60s (233). Thus, a constant boundary temperature of -15^{o}C and -20^{o}C was separately applied for each case at the inner artery wall for a time of 60s. The entire artery was assumed to be at an initial temperature of 37^{o}C.

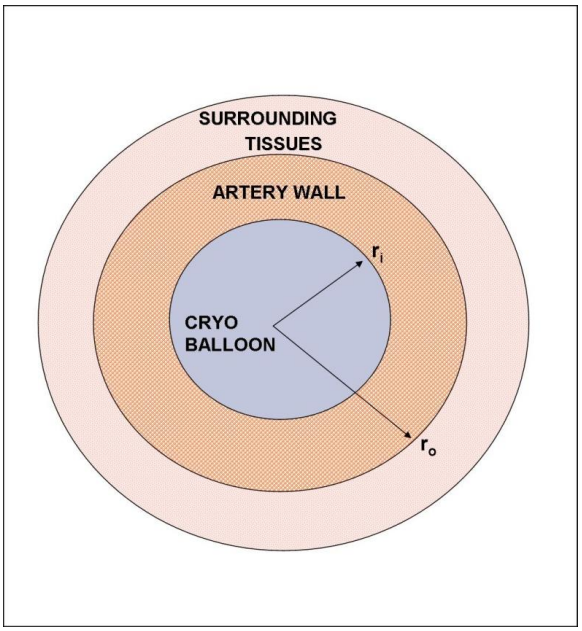

	r_i (mm)	r_o (mm)	T (r_i) (^oC)	T (r_o) (^oC)
Femoral Artery	5.5	7.5	-15 or -20	37
Popliteal Artery	3	5	-15 or -20	37
Extreme Case	5.5	15.5	-15 or -20	37

Figure 3.1: Artery geometry used in the thermal model for the prediction of temperature distribution during cryoplasty. The geometrical dimensions and the imposed boundary conditions for the thermal model are listed.

Both the femoral and the popliteal arteries are surrounded by blood perfused muscle fibers. Assuming that the blood flow in the surrounding tissues maintains the outer arterial wall temperature at 37^{o}C, a constant temperature boundary condition was imposed at the outer wall. In another case, as an extreme situation, the surrounding tissues were included in the model and a constant temperature (37^{o}C) boundary condition imposed at 15.5mm from the lumen center. The surrounding tissues were also assigned

the same thermal properties as the arteries. It is expected that the *in vivo* situation would fall in between the two boundary conditions described.

3.2.2 Biophysical Models

The biophysical models for water transport and IIF used in the current study are discussed in Chapter 1. Briefly, water transport across the cell membrane occurs to maintain the osmotic balance between the intracellular compartment and the extracellular media as the solute concentration increases during freezing. The IIF biophysical model used in the current study is based on the formulations developed by Toner et al. (44). Briefly, for a thermodynamic system composed of identical biological cells, the probability of IIF (PIF) by surface catalyzed nucleation (SCN) is a function of cooling rate and the degree of supercooling of the intracellular media to name a few factors. Further details regarding the assumptions and the details of the biophysical models are discussed in Chapter I.

3.2.3 Numerical Model for Biophysics Estimation

The experimental data was fit to the biophysical models to determine WT and IIF parameters. The Marquardt optimization scheme (210) was used as previously described in Toner et al. (44). Briefly, it minimizes the variance between the experimental data (y_i) and the theoretical fit/data ($y_{fit,i}$) and maximizes the R^2 value of the fit as represented as shown below .

$$R^2 = 1 - \frac{\sum \left(y_i - y_{fit,i}\right)^2}{\sum \left(y_i - \bar{y}\right)^2} \qquad (3.4)$$

Theoretical predictions for WT in cell suspensions are generally reported in two ways: theoretical value at a particular cooling rate and a "combined" fit parameter obtained by fitting of the complete dehydration data from all cooling rates as previously described **(102)**. Accuracy of fit (WT "combined" fit & IIF parameters) was ascertained by comparing the experimental data at a new rate to model predictions.

3.2.4 Statistical Analysis

Viability data are represented as mean ± standard deviation of at least three samples. Student t-test was used to determine significant differences with a minimum confidence level of $p < 0.05$.

3.3 MATERIALS & METHODS

3.3.1 Smooth Muscle Cell Culture

SMCs used for the experiments were isolated from adult pig femoral arteries as described elsewhere (125; 234). Briefly, the arteries were cut into small pieces, placed in a Petri dish and covered with media to allow SMCs to migrate from the tissue to the dish and grow. The cell media contained Dulbecco's modified Eagle medium (DMEM) (Gibco, Grand Island, NY) supplemented with 10% fetal bovine serum (FBS), 1% penicillin-streptomycin and 1% L-Glutamine. The cells were grown in 75cm^2 T-flasks and incubated at 37^{o}C and 5% CO_2 for 3-4 days before either experimentation or splitting.

Before experiments, SMCs were trypsinized (0.5mL) to remove them from the tissue culture flask (0.05% Trypsin/0.53mM EDTA). The cells were then centrifuged at 500xg for 7mins, and the cell concentration was measured using a hemocytometer. It was observed that SMCs show a 10-20% decrease in viability between passages 4 and 5 immediately after freeze/thaw (< 1 hr) at different cooling rates to an end temperature of -20^{o}C (data not shown). Hence, a single cell passage (passage 4) was maintained in all experiments for consistency of results.

3.3.2 Monolayer Preparation

SMCs in monolayer were prepared on sterilized coverslips (12mm diameter, Fisher Scientific, Hampton, NH) and cultured in a Petri dish covered with 10mL of media (cell concentration of 2×10^5 cells/mL). The cells were incubated at 37^{o}C and 5% CO_2 for 4 days to allow them to proliferate before experimentation.

3.3.3 Fibrin Tissue Equivalent Preparation

Bovine fibrinogen was mixed with cell solution and bovine thrombin at a ratio of 4:1:1 at room temperature. The final cell concentration in the mixture was 2×10^5 cells/mL. 10μL of solution was placed on a 12mm diameter tissue culture treated glass cover slip and incubated at 37^{o}C for 1hr to allow it to gel. Cell media (3mL) was then added and the fibrin TE was incubated for 4 days prior to experimentation.

3.3.4 Cryomicroscope Setup & Freezing Protocols

Controlled freezing of the samples was carried out on a Linkam Scientific conduction type cryostage (Linkam Corporation, UK). An Olympus BX50 fluorescent microscope (Tokyo, Japan) was used to observe freezing. Briefly, samples were mounted on a quartz crucible with a coverslip on top for freezing in the cryomicroscope. The freezing protocol included temperature decrease at 10^{o}C/min to -2^{o}C when ice was seeded (T_{seed}) using a chilled needle at the edge of the sample, temperature increase to -0.6^{o}C and then progressive decrease at the desired cooling rate to the desired temperature end point. Instrumentation error in temperature measurement was less than 0.1^{o}C for all controlled cooling rates. The cells were thawed back to room temperature at 130^{o}C/min.

3.3.5 Cellular Water Transport & IIF

Cell Suspensions

Cell volume changes during freezing were measured at cooling rates of 5, 10 and 25^{o}C/min for suspensions. The data was averaged for $n \geq 15$ cells at each of these cooling rates. The projected cell area was measured manually using Image-Pro Plus software (Media Cybernetics, Silver Spring, MD). Briefly, the projection of the outer cell membrane was traced three times and averaged for a particular cell at a specific temperature. Only cells that maintained their spherical shape during freezing were included in the final analysis. The osmotically inactive cell volume (V_b) was determined using a Boyle-Van't Hoff plot as described previously (5; 62). Individual WT parameters at 5, 10 and 25^{o}C/min were obtained by fitting the experimental data using the theoretical

model. A "combined" fit parameter was then obtained by fitting all three experimental data sets simultaneously into the theoretical model (62). The accuracy of the "combined" fit was verified by comparing model predictions to the experimental data at 10^{o}C/min.

The kinetics of IIF for cells in suspension was determined for a range of cooling rates (130, 100, 75 and 50^{o}C/min). IIF was characterized by the sudden "darkening" or opaque "flashing" in the cells at a particular temperature that indicated the formation of large ice crystals. PIF in cells was defined to be the ratio of the cumulative number of cells exhibiting IIF to the total number of cells in the sample population. Data from $n > 50$ cells were pooled to obtain the final IIF kinetics for each group.

Monolayer & Fibrin TE Model Systems

IIF in the attached cell model systems was assessed exactly as in the case of suspensions described above. However, it was not possible to obtain direct quantitative measurements of WT in attached cell systems (monolayer and fibrin TE) since the cells are no longer circular. To circumvent this, WT parameters were predicted from the analysis of the IIF data at slower rates where both IIF and WT is present (5). Briefly, IIF nucleation parameters were determined at 130^{o}C/min assuming minimal water movement. These parameters were then assumed constant at all cooling rates (i.e. same at 50, 75 and 100^{o}C/min). A coupled IIF-WT equation was then used with WT parameters selected to best fit the IIF data. In brief, despite assignment of constant IIF parameters, the IIF kinetics shift at lower cooling rates due to WT. These WT parameters were then used to

verify that cell volume decrease is minimal (≤5%) at 130°C/min, an important assumption for the initial fit of the IIF parameters.

It should be noted that both the WT and the IIF models were developed for cell suspensions. Hence, WT and IIF for attached cell systems should be used with the caveat that the model does not account for cell-cell or cell-ECM effects. One important change in attached model systems is the possibility of gap junction mediated intercellular IIF, which tends to increase the rates of IIF. To verify this effect, a comparison of the biophysics was done for normal SMC monolayer and SMCs were treated with 10mM of gap junction inhibitor carbenoxolone disodium (Sigma-Aldrich Co., St Louis, MO). The use of inhibitors and its general implications have been previously reported (235; 236).

3.3.6 Cell Viability Analysis

Cell viability was assessed at four different time points: immediately (< 1hr), 3, 24 and 72hrs after freeze/thaw using Hoechst 33342 (Sigma, St. Louis, MO) and propidium iodide (PI) (Molecular Probes, Eugene, OR). The control and frozen/thawed cells were incubated for 30min in cell media with Hoechst and PI at 1:1000 and 5:1000 assay-media ratio respectively.

$$\text{Percent Viability } (\%) = \frac{\text{Total Number of Live Cells}}{\text{Total Number of Cells}} \times 100 \qquad (3.5)$$

The samples were then placed on a microslide, coverslipped and analyzed under the cryomicroscope. Hoechst stains all cells whereas PI stains only dead (membrane

compromised) cells. Three to five fields with 30-40 cells per field were counted for every model system. Cell viability is calculated as percent viability as defined by Eqn 3.5.

3.4 RESULTS

3.4.1 Thermal Model

The temperature distribution in the artery vs. radial distance was estimated using a finite difference model. For a constant boundary temperature condition (Figure 3.2), the ice ball edge grew up to approximately half the arterial thickness (~1mm) in each case. For example, in the femoral artery, at a constant boundary temperature of -20^{o}C at the inner wall (r_i = 5.5mm), the ice ball is predicted to grow to r = 6.7mm within 12s. Cooling rate at different radial locations in the artery is determined from the slope of the temperature variation over the first 15-20s as transients at any location reduces significantly after that time point (Figure 3.2). For the popliteal artery, the estimated cooling rates range from 2500 to 5^{o}C/min at different radial locations. Table 3.2 provides data on end temperatures and cooling rates predicted at different locations within the artery for different initial balloon temperatures. In addition to the different conditions listed in Table 3.2, the thermal response during constant boundary condition at r_o = 15.5mm (extreme case) is also studied. Figure 3.2 plots temperature vs. radial distance at different times for this extreme case. While the initial cooling rates did not change significantly, sub-zero temperatures are predicted in the entire artery and the ice ball edge grew beyond the artery wall. Hence, the *in vivo* thermal history is expected to be captured in between the two extreme cases considered in the thermal model. This thermal

information is used to construct the *in vitro* biophysics study, and quantify the expected biophysics in the different regions of the artery.

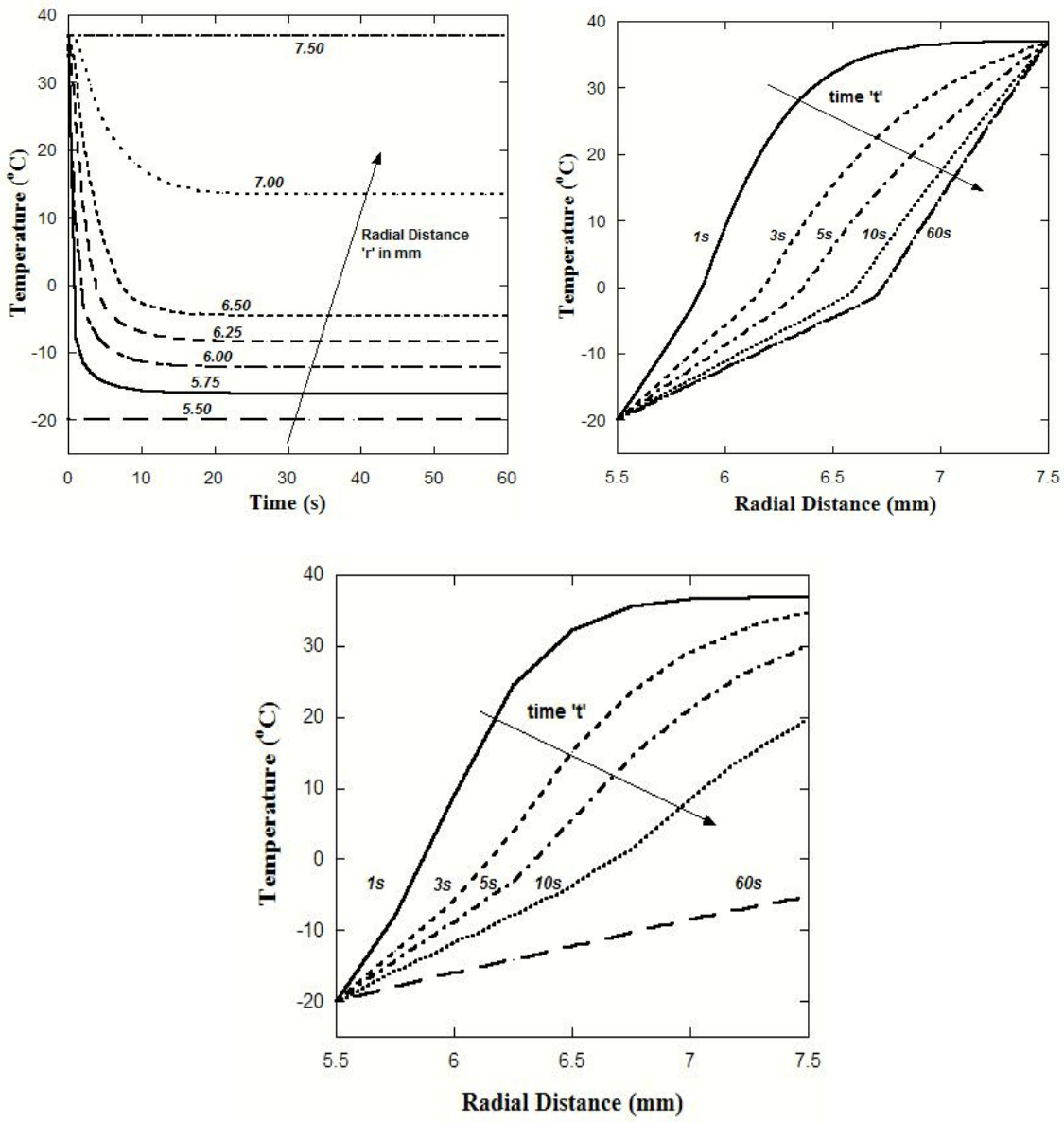

Figure 3.2: Thermal history within the simulated femoral artery (r = 5.5mm) wall during cryoplasty. (Top Panel) Temperature as a function of radial distance at different times, and as a function of time at different locations (Bottom Panel) Temperature as a function of radial distance during the extreme case (i.e. constant boundary condition (37^{o}C) at r_o = 15.5 mm)

Table 3.2: Summary of the thermal injury following cryoplasty in the femoral and the popliteal artery models. BT: Balloon temperature (^oC), r: radius (mm), IBE: Ice ball edge (mm), NZ: Necrotic zone (mm), AZ: Apoptotic zone (mm), CR: Cooling Rate (^oC/min) & ET: End Temperature (^oC).

BT (^oC) (@`R = 5.5 MM)	FEMORAL ARTERY								
	IBE (MM)	RADIUS (r) (MM)						NZ (MM)	AZ (MM)
		5.9	6.3	6.6	5.9	6.3	6.6		
		CR (^oC/MIN)			ET (^oC)				
-15	6.6	530	100	-	-10	-5	0	5.5 - 5.9	5.8 - 6.6
-20	6.7	400	190	90	-14	-8	-3	5.5 - 6.2	6.2 - 6.7

BT (^oC) (@ R = 5.5MM)	POPLITEAL ARTERY								
	IBE (MM)	RADIUS (r) (MM)						NZ (MM)	AZ (MM)
		3.3	3.6	4.0	3.3	3.6	4.0		
		CR (^oC/MIN)			ET (^oC)				
-15	4.0	2300	220	-	-11	-7	0	3 - 3.3	3.3 - 4
-20	4.2	2500	380	80	-15	-10	-4	3 - 3.6	3.6 - 4.2

3.4.2 Cell Biophysics

Water Transport

At room temperature, the mean diameter of SMCs is estimated to be 11.1 ± 2.2μm for n=76 cells. The initial cell volume (V_o) is calculated to be 716.2 ± 5.6μm^3. Also, the osmotically inactive cell volume fraction (V_b) for SMCs is determined to be 0.24V_o.

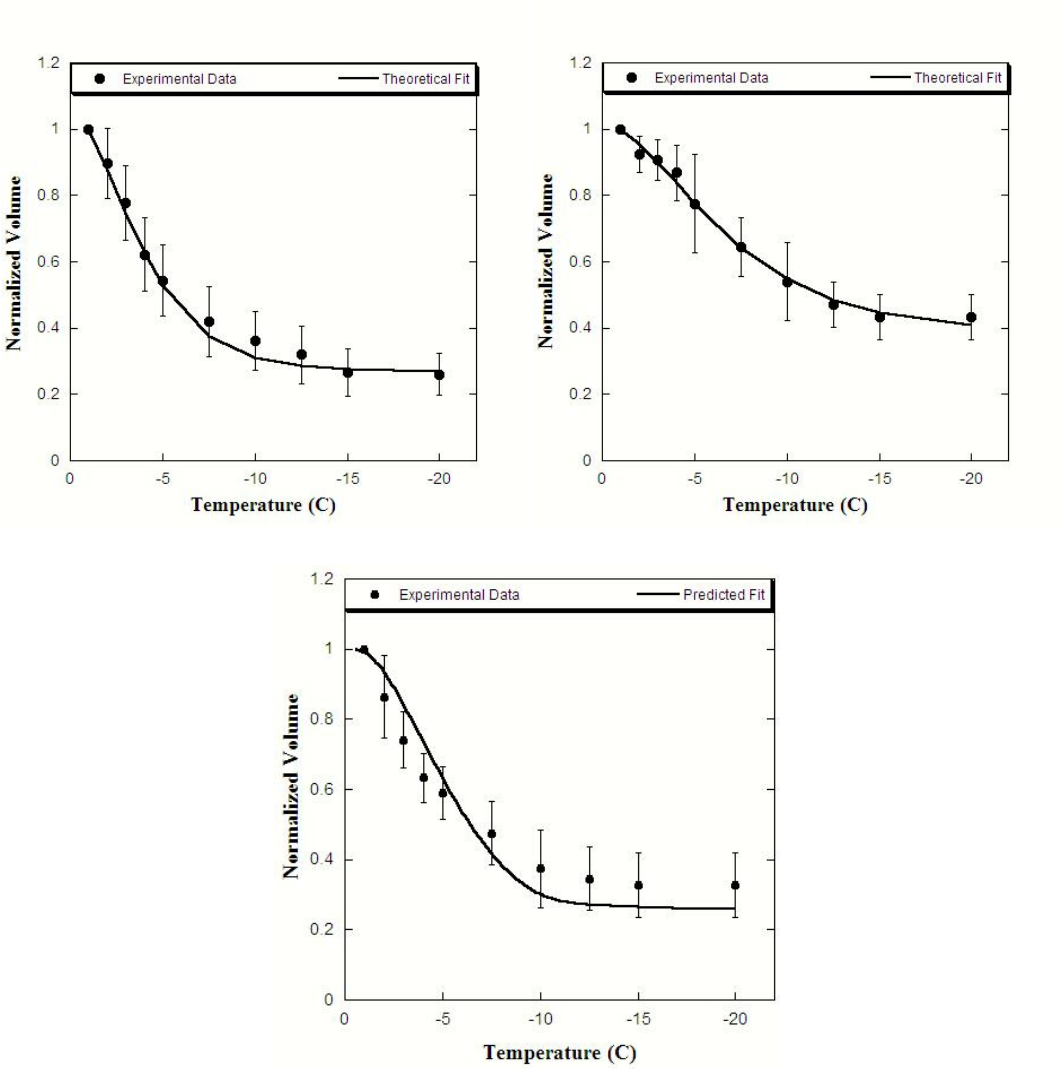

Figure 3.3: Normalized SMC volume as a function of temperature in suspension at a cooling rate of (a) 5°C/min, (b) 25°C/min and (c) 10°C/min. Dark circles indicate experimental data (n = 10 to 30 cells) and error bars indicate SD. The solid lines represent the theoretical fit (a, b) obtained by fitting experimental data to the biophysical model, and the predicted volume change from the estimated "combined fit" parameters (c).

Figure 3.3 depicts the dehydration biophysics of SMCs in suspension during freezing. Cell volume changes are depicted as a function of temperature at 5, 10 and 25°C/min. The biophysical parameters for water transport at 5 and 25°C/min (Figure 3.3 (a, b)) are estimated from the biophysical models (Table 3.3). The "combined fit" parameters are

estimated to be L_{pg} = 0.12μm/min.atm and E_{Lp} = 24.1kcal/mol. Using these parameters, the dehydration response at 10°C/min is predicted and compared to the experimental results in Figure 3.3 (c). A good correlation (R^2 = 0.96) is obtained between the predicted and the experimental data. For SMCs in monolayer and fibrin TE, the WT parameters are estimated as described previously and included in Table 3.5.

Table 3.3: Water transport parameters (L_{pg} and E_{Lp}) for SMCs in suspension at 5, 10 and 25°C/min.

COOLING RATE (°C/MIN)	L_{PG} (μM/MIN.ATM)	E_{LP} (KCAL/MOL)	R^2
5	0.13	45.2	0.99
10	0.28	54.2	0.99
25	0.20	32.5	0.99
Combined fit	0.12	24.1	0.96

Intracellular Ice Formation

IIF kinetics is studied at cooling rates of 130, 100, 75 and 50°C/min. Figure 3.4 depicts the variation of maximum cumulative fraction of IIF with cooling rate for each model system studied. The maximum cumulative fraction of IIF increases with the cooling rate for all model systems. However, the incidence of IIF for SMCs in the attached states is higher as compared to suspensions. For example, at 130°C/min SMCs in monolayer and fibrin TE show 100% IIF but only 46% of SMCs form IIF in suspensions.

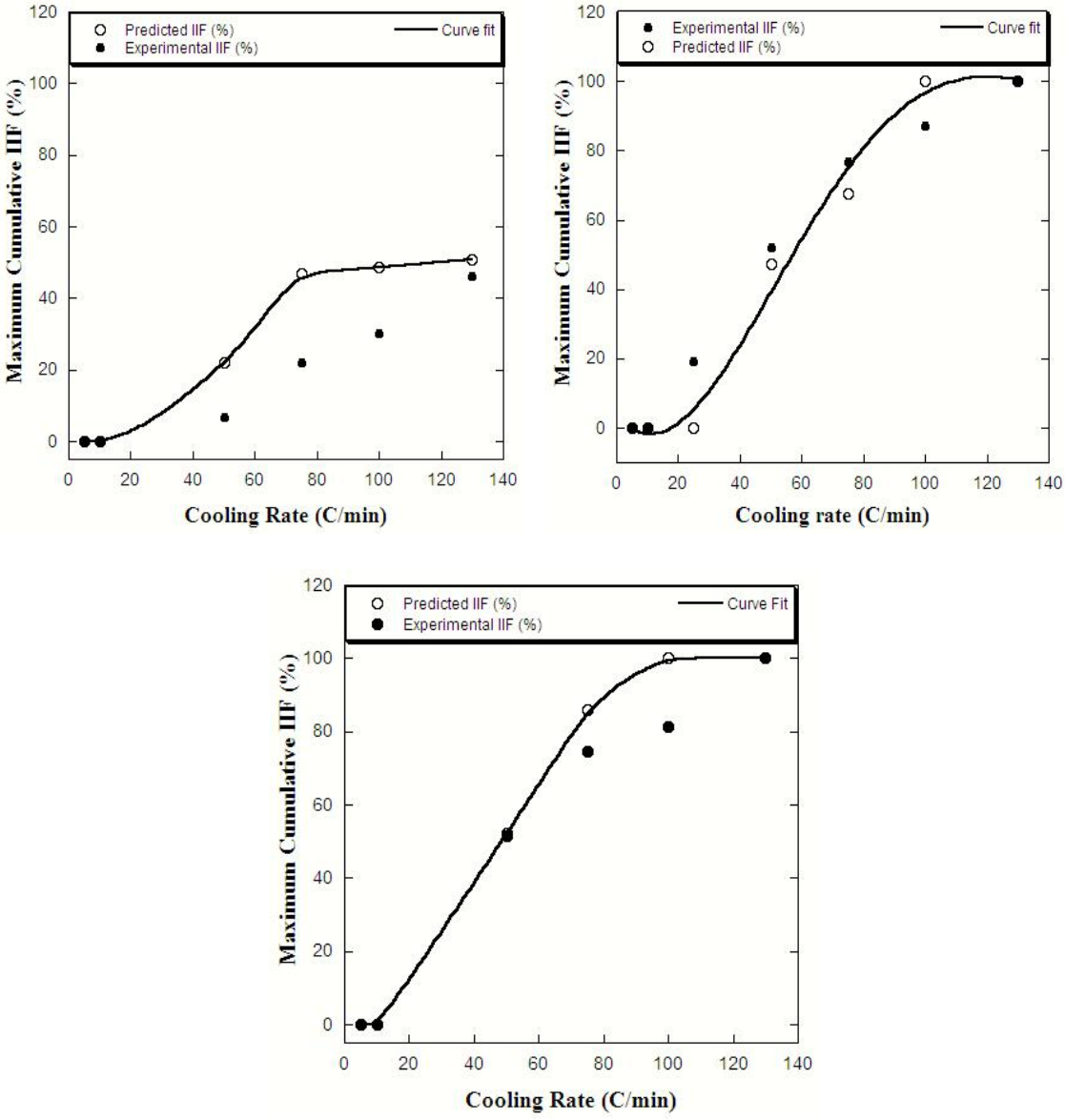

Figure 3.4: Maximum cumulative fraction of IIF as a function of cooling rates to an end temperature of -20°C for SMCs in (a) suspension, (b) monolayer and (c) fibrin TE. Dark circles represent the experimental data, open circles represent the predicted data fit at the corresponding cooling rates and the solid line represents the best fit curve predicted data.

Additionally, a difference in the IIF kinetics is observed between SMCs in attached state vs. suspension. Figure 3.5 depicts the IIF kinetics at 130°C/min for all the model systems studied. Ice propagates faster among cells in the attached states as compared to cells in

suspension. SMCs in monolayer were treated with gap junction inhibitor carbenoxolone disodium and the resultant IIF kinetics is evaluated to assess the role of gap junctions on IIF. The IIF kinetics change significantly in the presence of the inhibitor (Figure 3.5), which is corroborated by the predicted biophysical parameters (Table 3.4). The values indicate that the kinetics of IIF is slower (Ω_o = 58.1 vs. 354) as compared to a normal monolayer of cells. This is presumed to be a result of decrease in intercellular ice formation due to the presence of the gap junction inhibitors.

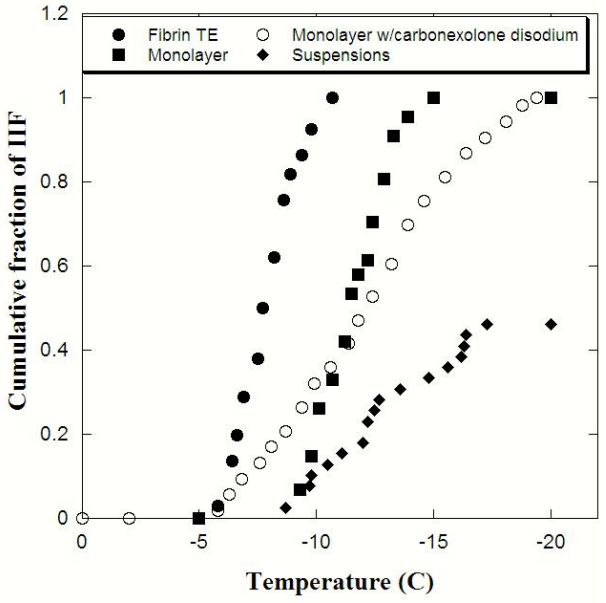

Figure 3.5: A comparison of the IIF kinetics during freezing of SMCs in suspension, monolayer, fibrin tissue equivalent and monolayer with gap junction inhibitor carbenoxolone disodium at a cooling rate of 130^{o}C/min to end temperature of -20^{o}C.

A comparison of the experimental vs. the predicted values of IIF is done using the biophysical parameters estimated. For cells in suspension, the combined fit WT parameters and IIF parameters at 130^{o}C/min were used for these predictions. For monolayer and fibrin TE systems, the biophysical parameters estimated at 130^{o}C/min

were assumed constant for the IIF predictions. A comparison of the cumulative incidences of IIF is obtained as shown in Figure 3.4. It is to be noted that the fit R^2 for suspensions is not great since the influence of coupled water transport and IIF affect the predictions more than in the attached cellular model systems. The goodness of fit (R^2) is reported in Table 3.4 for all the model systems.

Table 3.4: Estimates of the IIF biophysical parameters for SMCs in suspension, monolayer, monolayer with gap junction inhibitor carboxolene disodium and fibrin TE at a cooling rate of 130°C/min. R^2 (fit) represents the goodness of fit between the predicted and the experimental incidences of IIF for each of the model systems studied

MODEL SYSTEM	$\Omega_o \times 10^{-8}$ ($1/M^2.S$)	$\kappa_o \times 10^{-9}$ (K^5)	R^2 (130°C/MIN)	R^2 (FIT) (5-130°C/MIN)
Suspension	1.13	1.6	0.98	0.30
Monolayer	354	1.8	0.99	0.94
Monolayer (w/gap junction inhibitor)	58.1	2.1	0.99	--
Fibrin TE	378	2.1	0.98	0.95

3.4.3 Cell Viability

Effect of End Temperature & Cooling Rate

After freeze/thaw, SMCs in suspension shows a 10-20% variation in viability between passages 4 & 5 at different cooling rates to an end temperature of -20°C (data not shown). To maintain consistency, all viability experiments were performed using SMCs from passage 4. Figure 3.6 shows the effect of end temperature on SMC viability in a monolayer and a fibrin TE at 3hrs post freeze/thaw. The viability drops as the cooling rate increases and the end temperature decreases in most cases. In the monolayer (Figure 3.6(a)), at an end temperature of -10°C, 81% of the SMCs are viable at a cooling rate of

130°C/min whereas only 37% of the SMCs survive to an end temperature of -20°C. Similarly, for the fibrin TE model system (Figure 3.6 (b)), only 3% of the cells survive freeze/thaw to an end temperature of -20°C at a cooling rate of 130°C/min. Additionally, The fibrin TE exhibits inverted U shape viability vs. cooling rate dependence during freezing. Figure 3.7 compares the cooling rate effect on cell viability (to -20°C) across the model systems studied. Cell survival is observed to be the highest for SMCs in suspension and lowest in the fibrin TE at all rates (except 10°C/min).

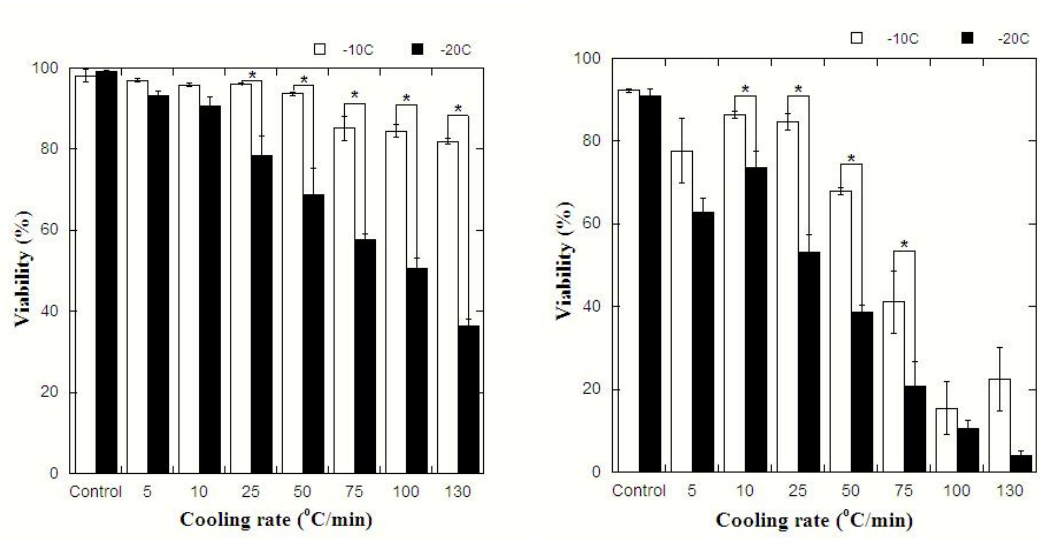

* p < 005

Figure 3.6: The effect of end temperature (-10 & -20°C) on SMC viability at different cooling rates determined 3hrs post thaw in (a) monolayer and (b) fibrin TE. Statistical analysis using student t-test shows significant difference for $p < 0.05$.

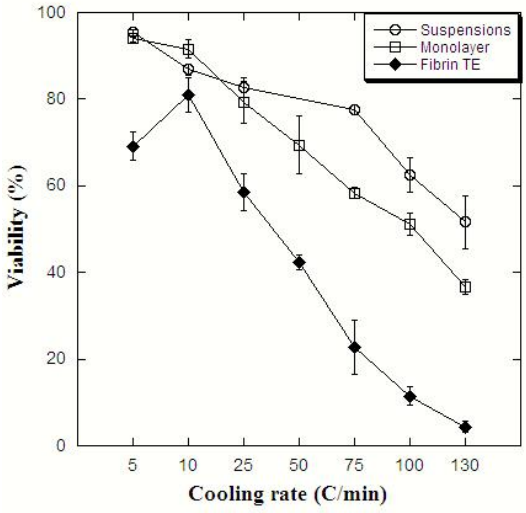

Figure 3.7: A comparison of SMC viability vs. cooling rate in suspension, monolayer and fibrin TE determined 3hrs post thaw to an end temperature of -20^{o}C.

Effect of Time Post Freeze/Thaw

For SMCs in the attached states, cell viability varies with time after freeze/thaw (3, 24 and 72 hrs) to an end temperature of -10^{o}C as shown in Figure 3.8. For the monolayer, viability decreases between 3 and 24hrs (93% & 86% survival at 50^{o}C/min) post freeze/thaw but a slight increase is observed at 72hrs post freeze/thaw (91% at 50^{o}C/min) (including control samples). A typical inverted U response of viability vs. cooling rate is observed at all time points of study for the fibrin TE (Figure 3.8(b)). SMC viability is lowest at 72hrs post freeze/thaw and maximum at 3hrs post freeze/thaw (except at 100^{o}C/min where no statistical significance is found in the difference between the 3hr and 72hr time points). Cell regeneration/proliferation after freeze/thaw is not observed in the fibrin TE except in the control samples at 24hrs.

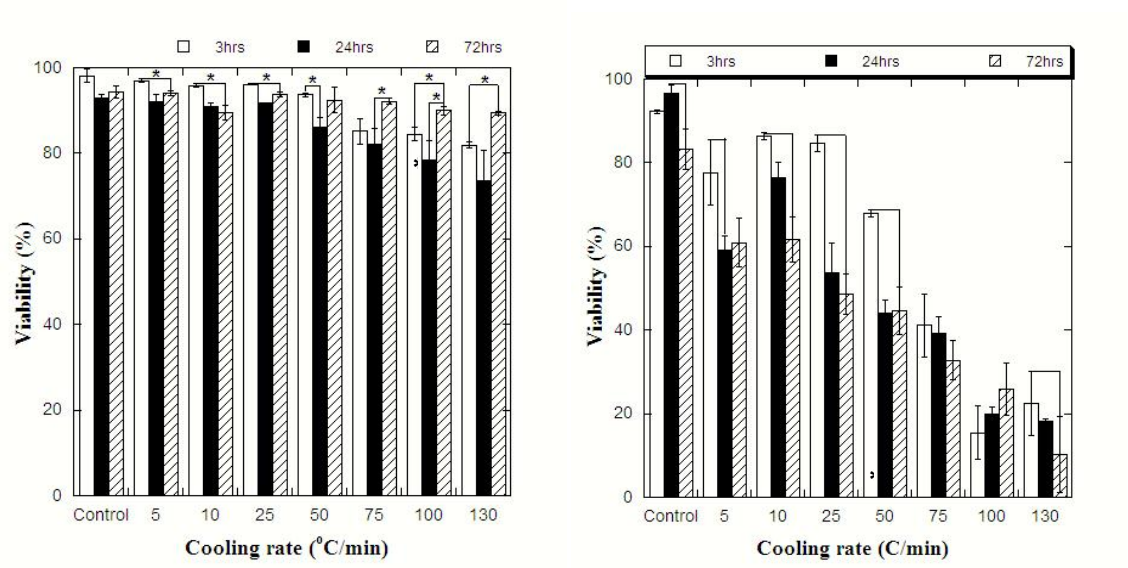

* $p < 0.05$

Figure 3.8: The effect of time post thaw (3, 24 & 72 hrs) on SMC viability at different cooling rates to an end temperature of -10°C in (a) monolayer and (b) fibrin TE. Statistical analysis using student t-test shows significant differences for $p < 0.05$.

Cell Biophysics & Viability Correlation

A correlation between the cellular biophysics and the viability was noted. Figure 3.9 shows the experimental IIF results along with the viability changes as a function of cooling rate for SMCs in all model systems to an end temperature of -20°C. In all cases, cell viability decreases as the fraction of IIF and the cooling rate increases. Cell viability is maximal when IIF is minimal in the model system and vice versa. Cell suspensions exhibited maximum cell survival and minimum IIF (53% survival and 46% IIF at 130°C/min) whereas fibrin TE had the least cell survival and maximum IIF (3% survival and 100% IIF at 130°C/min). In addition, SMCs in the fibrin TE model system exhibited a typical inverted U response of viability vs. cooling rate.

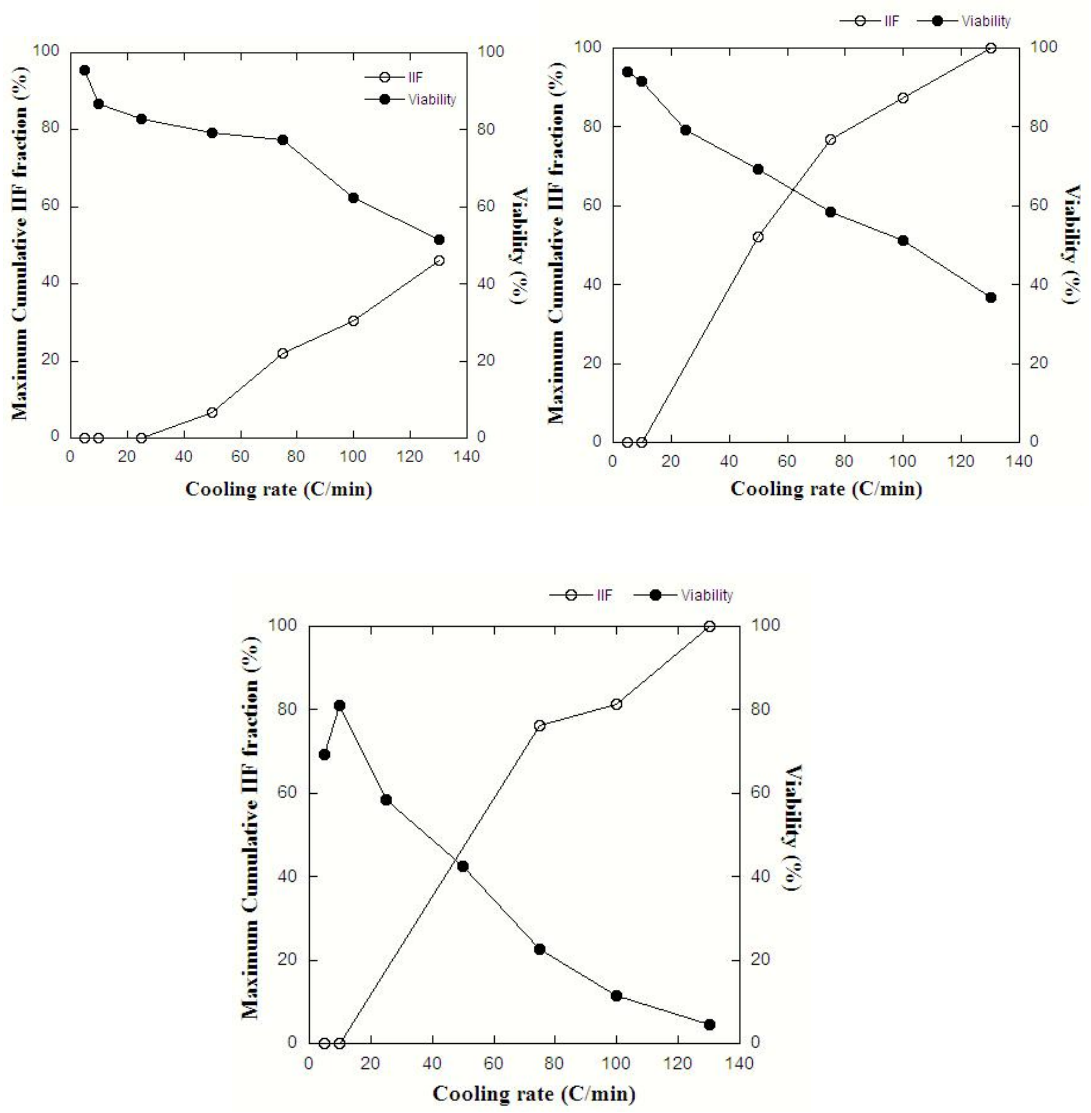

Figure 3.9: A correlation between the cumulative fraction of IIF and SMC viability as a function of freezing rate in (a) suspension, (b) monolayer and (c) fibrin TE to an end temperature of -20^{o}C.

3.5 DISCUSSION

3.5.1 Applicability of Model System

In this chapter, *in vitro* model systems have been used to help assess the effectiveness of freezing on SMCs within a simulated arterial system with the ultimate goal of treating intimal hyperplasia (restenosis). The results from the study are useful in understanding

the cellular injury responses that may help suggest mechanistically based modifications to the cryoplasty protocol for future *in vivo* studies. Additionally, an *in vitro* assessment of freezing injury and the potential mechanisms responsible for it were studied. The biophysics and cell injury are quantified using different model systems including suspensions, monolayer and fibrin TE. Cell suspensions provide a basic understanding of the freezing effects on biophysics and viability. However, additional effects to injury due to cell-cell and cell-ECM interactions need to be probed. This was analyzed using the monolayer and fibrin TE model systems in this chapter. Additionally, since fibrin is a part of the restenotic arterial wall, it may represent an improved *in vitro* system over cell suspensions to quantify freeze/thaw injury during cryoplasty. The molecular mechanisms behind freeze injury, due to apoptosis and necrosis, have been previously reported for SMC and endothelial cell suspensions (229).

3.5.2 Cellular Model System Comparison

Cells exhibit differential biophysics and injury (e.g. Chinese hamster, AT-1 tumor cells) on freezing depending on their attachment state (53; 224). The biophysics (Figure 3.5) of freezing is model system dependent. Suspensions exhibit the lowest fraction of IIF as compared to SMCs in attached systems at all cooling rates. The reason for this difference is hypothesized to be due to cell-cell or cell-ECM interactions that are absent in cell suspensions. Acker et al. have shown that cell-cell interactions promote IIF through intercellular pathways (gap junctions) present in monolayers (116; 53). In this chapter, the effect of gap junctions on the IIF kinetics was tested in monolayer using a gap junction blocker (carbenoxolone disodium). Figure 3.5 compares the difference in the IIF

kinetics for SMCs in monolayer in the presence and absence of a gap junction blocker. Though 100% of SMCs exhibited IIF in both cases, the kinetics in the presence of the gap junction blocker tended to resemble more of a cell suspension response than a monolayer response. Since this pathway of IIF injury may be important in the arterial wall, it is a potential avenue to exploit during cryoplasty to affect cell injury.

Figure 3.7 demonstrates the effect of the model system on cell viability as a function of cooling rate to an end temperature of -20^{o}C. SMCs in suspension exhibited higher viabilities post freeze/thaw as compared to SMCs in monolayer or fibrin TE (least in fibrin TE). Grassl et al. reported similar differences in SMC viability post freeze/thaw in collagen TE vs. suspensions (125). They used a directional solidification stage (DSS) to freeze SMCs in suspension and a cryoprobe for the collagen TE system. Statistically significant differences in SMC viability were reported for end temperatures of -11^{o}C (25%) and -35^{o}C (<1%) in the collagen TE. The present study observes viability results of 87% and 75% at end temperatures -10^{o}C and -20^{o}C respectively at 10^{o}C/min in the fibrin TE. This is likely due to the differences in the model systems and the freezing protocol setup. Grassl et al. used a cryoprobe (directional freezing) for the collagen TE and we used a Linkam cryostage, which is equiaxial and non-directional freezing stage for the fibrin TE. Figure 3.9 correlates the maximum cumulative fraction of IIF at different cooling rates to the SMC viability in the attached (monolayer and fibrin TE) vs. the non attached system (suspensions). SMC viability is lower and IIF is higher in the attached state as compared to suspensions at all cooling rates. This may be a consequence

of the cell-cell and cell-ECM interactions that enhance IIF and thereby reduce cell viability for the thermal conditions imposed.

3.5.3 Thermal & Biophysical Responses

The thermal model predicts initial cooling rates ranging from 2500 to 5^{o}C/min in the artery. Table 3.2 summarizes the initial cooling rates, the end temperatures and the location of the ice ball edge for the given boundary conditions in the models. In general, the results from the thermal model and the biophysics suggest that IIF is dominant in regions close to the lumen whereas both IIF and dehydration occur in the remaining sub-zero arterial regions. It should however be noted that the thermal properties used in the model are based on values reported for other tissues (1) due to the lack of applicable porcine artery thermal properties. Due care should therefore be taken when interpreting the model predictions.

Table 3.5: Water transport parameters (L_{pg} and E_{Lp}) for SMCs in monolayer and fibrin TE at different cooling rates.

COOLING RATE (^{O}C/MIN)	MONOLAYER		R^2	FIBRIN TE		R^2
	L_{PG} (μM/MIN.ATM)	E_{LP} (KCAL/MOL)		L_{PG} (μM/MIN.ATM)	E_{LP} (KCAL/MOL)	
130	18.6	112	0.93	19.4	127	0.97
100	17.4	98	0.98	19.4	118	0.94
50	18	121	0.94	17.1	127	0.95

As discussed previously, IIF kinetics (Table 3.4) is dependent on the model system. The thermodynamic and kinetic parameters determined were found to be higher for SMCs in monolayer and fibrin TE as compared to SMCs in suspensions. This is in agreement with observations reported previously for hepatocytes and human dermal fibroblasts (60; 5).

Differences were also observed in the dehydration response of SMCs in suspension as compared to SMCs in attached systems (Table 3.5). The WT parameters determined for SMCs in attached systems are higher as compared to suspensions. This is also in agreement with previous results reported for hepatocytes in a collagen sandwich and human dermal fibroblasts in a collagen/fibrin TE (60; 5). Care should be taken in the interpretation of these results since biophysical models developed for individual cells are used for predicting responses in attached cellular model systems (18; 44). However, these models are still useful in highlighting possible effects of cell-cell and cell-ECM interactions on the biophysical responses. Recently mathematical models have been proposed to account for intercellular mechanisms of IIF (120; 121). However, these models were developed for controlled micropatterned layer of hepatocytes where an individual cell was in contact with two neighboring cells. Unfortunately, the use of these models is currently not possible in systems where random multi-cell connections occur.

3.5.4 Cell Viability

The current study shows that cell viability is affected by the model system, the cooling rate, the end temperature and the time post freeze/thaw. Previous studies have shown an inverted U relation between viability vs. cooling rate for different cell types (e.g. lymphocytes, red blood cells, ova) (20). Solution effects injury is hypothesized to dominate at slower cooling rates whereas IIF is predominant at higher cooling rates (20; 54). This inverted U shape dependence was also observed during freezing SMCs in fibrin TE (Figure 3.7) whereas the response of cells in suspension and monolayer were

predicted to be the right hand limb (i.e. IIF) of the inverted U shaped curve since cooling rates lower than 5^{o}C/min were not studied.

The effect of end temperature on cell viability has also been extensively studied. Previous parametric studies using AT-1 tumor cells and ELT-3 uterine leiomyoma tumor cells established that end temperature and hold time are important parameters influencing cell viability (237; 101). In general, lower end temperatures result in increased cell injury. This is true for freezing SMCs in all the model systems studied (Figure 3.6), and is more pronounced in the fibrin TE as compared to the other model systems.

The effect of time post freeze/thaw was studied to quantify SMC viability post freeze/thaw in the attached state. Grassl et al. reported that SMCs did not proliferate in a collagen TE as had previously been suggested elsewhere (125; 238). However, they observed cell proliferation in the control samples of fibrin TE system which is in agreement with this study. Cell viability was observed to drop after 24hrs (especially for fibrin TE) suggesting the possibility of molecular pathways that may up regulate apoptosis. Tatsutani et al. reported apoptosis in SMC and endothelial cells for 30-120s exposure between -5 and -15^{o}C at 1hr post freeze/thaw using *in vitro* model systems (suspension) (229). Also, Hollister et al. reported apoptosis in prostate tumor cell lines 24-72hrs after freeze/thaw whereas Hanai et al. reported apoptosis in human colon carcinoma cells within 8hr after freeze/thaw (239; 240). The injury pathways and time periods for apoptosis is highly debated and needs to be addressed as a longer term (i.e. many hours or days) injury mechanism post cryoplasty.

3.5.5 Injury Predictions in Simulated Artery

Based on the thermal history, the biophysical mechanisms and the viability outcomes as discussed previously, conservative estimates of injury regimes with the artery are predicted (Table 3.2 and Figure 3.10).

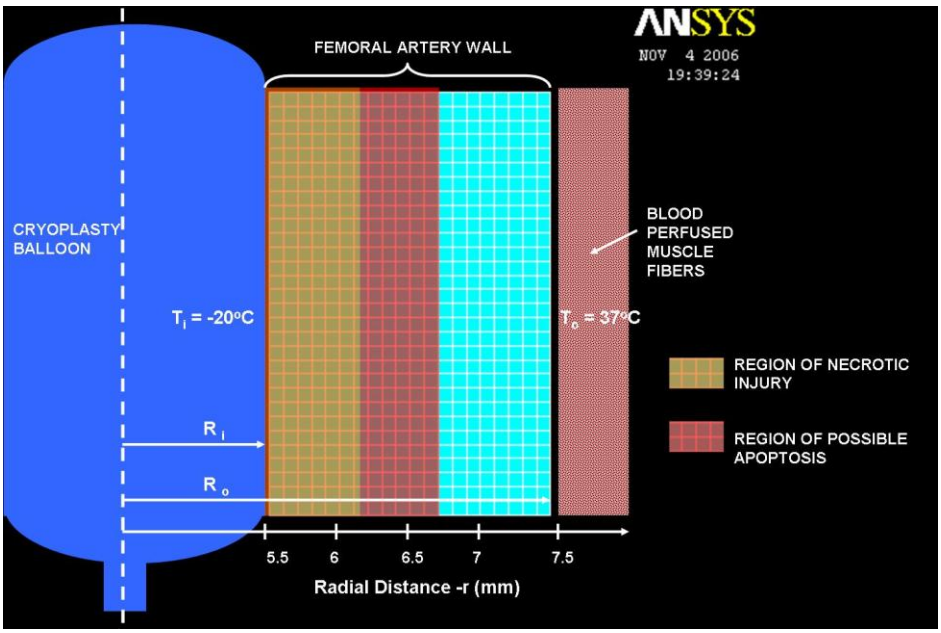

Figure 3.10: The thermal injury regimes during cryoplasty (with balloon temperature of -20°C) in a simulated femoral artery as predicted using the thermal model and the *in vitro* studies on SMC biophysics and viability. Potential regions of both necrosis and apoptosis are predicted.

Since the fibrin TE model is hypothesized to be one of the best *in vitro* model to study restenosis, thermal and biophysical effects are linked to cell survival to predict injury regimes. From our results and previous studies (229), we define temperature regimes and cooling rates that may result in necrotic or apoptotic cell injury. Necrotic injury is defined to occur in regimes experiencing 100% IIF and 20% viability and a cooling rate greater than 50°C/min (dominated by IIF). Apoptosis is defined to occur in regimes experiencing 50% or less IIF, 0 to -10°C and a cooling rate less than 50°C/min (as experienced closer

to the ice ball edge). Regions close to the inner arterial wall or to the cryoplasty balloon experience a lower end temperature (~-20^{o}C) and a high cooling rate (>130^{o}C/min) and hence are presumed to have higher necrotic injury. The thermal injury was higher as expected when a lower balloon temperature (-20^{o}C) was used. Figure 3.10 summarizes the different injury regimes, using an ANSYS model, in a simulated femoral artery of 11mm lumen diameter for a constant balloon temperature of -20^{o}C. Table 3.2 summarizes the predicted necrotic and apoptotic injury regimes for the femoral and popliteal artery due to freezing. When a constant temperature boundary condition was applied at radial distance of 15.5mm, the ice ball edge and the injury zones are expected to extend beyond the artery wall.

This study is useful in predicting possible temperature regimes that can yield higher necrotic or apoptotic cell injury by modifying the thermal conditions imposed. Arteries occlude when rapidly frozen to -80^{o}C and apoptosis and necrosis are reported for balloon temperatures of -20^{o}C and -10^{o}C for *in vitro* state (226; 229). Balloon temperatures between -80^{o}C and -20^{o}C are potential options to enhance cell injury post Cryoplasty. These results may be used in the further optimization of Cryoplasty.

3.6 SUMMARY

The impact of cell attachment on the "two factor" injury hypothesis for SMCs was assessed using three different cellular systems – suspensions, monolayer and fibrin tissue equivalents (TE). Controlled freezing experiments were conducted for cooling rates of 5 – 130^{o}C/min using a cryomicroscope. Cell biophysical models were then used to compare

the biophysics of cells in suspensions vs. attached state. The results from this study are expected to benefit Cryoplasty procedures designed to treat restenosis in patients. Important results from the study are summarized below:

i. The kinetics of IIF is enhanced in the attached state as compared to cell suspensions. In addition, water transport (L_{pg}) for SMCs in the attached state are enhanced as compared to suspensions.

ii. The kinetics of IIF for SMC monolayer is lower in the presence of a gap junction inhibitor as compared to no inhibitors.

iii. The "two factor" response for SMCs is affected by cell attachment. At rapid freezing rates, cell injury is linked to IIF. At slow freezing rates, SMCs in monolayer exhibit higher cell viability as compared to suspensions. The water transport biophysics suggests that "solution effects" injury should be higher in monolayer but it is not observed so.

The results of the study (thermal model, SMC biophysics and viability) are used to predict injury regimes in a simulated artery. At slow cooling rates, a potential interaction between solutes and cellular macromolecules is implicated in cell injury. In Chapter 4, we assess the molecular responses during slow freezing (solute effects) of cells.

4. EFFECTS OF FREEZING ON MEMBRANES AND PROTEINS IN LNCaP PROSTATE TUMOR CELLS[3]

This chapter describes the molecular events associated with the biophysics of freezing human LNCaP prostate tumor cells. Membrane phase transition and protein denaturation of LNCaP cells in suspension are characterized. The present author along with Dr. Willem Wolkers, Helena Zec and Emily Ongstad performed all the experimentation work and data analysis. The results from this chapter have been compiled, edited and published in the following citation:

I. Wolkers WF, Balasubramanian SK, Ongstad EL, Zec HC, and Bischof JC (2007) "Effects of freezing on membranes and proteins in LNCaP prostate tumor cells" *Biochimica et Biophysica Acta* 1768 (3); pp 728 - 736

[3] This part of the study was financially supported by the National Institute of Health (NIH) R01 – CA07528.

This chapter studies the molecular events – membrane phase transition & protein denaturation - associated with the biophysics of freezing malignant prostate tumor cells (LNCaP). Fourier transform infrared spectroscopy (FTIR) was used to define the process of cellular injury during freezing of LNCaP prostate tumor cells at the molecular level. Cell pellets were monitored during cooling at 2°C/min while the ice nucleation temperature was varied between -3 and -10°C. The predicted incidence of intracellular ice formation (IIF) rapidly increases at ice nucleation temperatures below -4°C and cell survival is an optimum at a nucleation temperature of -6°C. The ice nucleation temperature was found to have a great effect on the membrane phase behavior of the cells. The liquid crystalline to gel phase transition coincided with the ice nucleation temperature. In addition, ice nucleation at -3°C resulted in a much more co-operative phase transition and a concomitantly lower membrane fluidity in the frozen state compared to samples that were nucleated at -10°C. These observations were explained by the effect of the nucleation temperature on the extent of cellular dehydration and IIF. Amide-III band analysis revealed that proteins are relatively stable during freezing.

4.1 INTRODUCTION

Cryosurgery is becoming an established therapy for prostate cancer (241; 242). The general mechanisms of injury during cryosurgery typically include direct injury to the cancer cells due to the freezing event, as well as host-mediated events such as vascular injury and immunological effects, which occur after thawing.

One of the factors that determine the type of damage during freezing is the cooling rate (19). At fast cooling rates, intracellular ice formation (IIF) is primarily responsible for the destruction of cells. By contrast, at slow cooling rates, where dehydration predominates, osmotic injury due to solute effects causes damage. During slow cooling, ice forms outside the cell before propagating inside the cell (2). As soon as ice forms outside of a cell in solution, the cell dehydrates, and endogenous biomolecules are exposed to high concentrations of solutes (243). Rapid freezing, on the other hand, results in lethal IIF. The mechanism by which intracellular ice damages cells is not entirely clear, but it has been suggested that cells do not die during the freezing event itself, but during thawing (2). One other important determinant of IIF is the nucleation temperature of ice in the extracellular space (244). Studies have shown that the lower the nucleation temperature the greater is the incidence of IIF (57; 245).

At the molecular level, freezing affects membrane lipids, proteins and nucleic acids by changing the hydrophobic and hydrophilic interactions determining structure and function. It is well established that cooling alters the physical state of lipids, thus altering lipid organization and fluidity (173). Biological membranes often exhibit a liquid

crystalline to gel phase transition during cooling and vice versa during re-warming (246). The consequences of such phase transitions are thought to include increased membrane permeability and lateral phase separation of membrane components. Intracellular proteins may undergo irreversible structural alterations with freezing, due to exposure to high solute concentration (243). In addition, proteins and lipids are exposed to reactive oxygen species, because enzymatic scavenging systems are compromised by freezing. Reactive oxygen species result in lipid peroxidation and phospholipid de-esterification (247). Freezing of AT-1 Dunning tumor cells has been shown to result in the accumulation of free fatty acids (202). The changed physical properties and chemical composition of the plasma membrane may lead to leakage of cytoplasmic solutes. Proteins are also subject to free radical attack by reactive oxygen species (248). Moreover, proteins may also be degraded by proteases originating from lysosomes that lost membrane integrity during freezing or thawing (202).

One of the few suitable techniques to study freezing induced changes in structure and conformation of cellular biomolecules is Fourier transform infrared spectroscopy (FTIR). The -CH_2 stretching vibration of lipids, for example, has been used to detect lipid phase transitions in lipids, isolated biological membranes and in whole cells (246; 249). The amide -I, -II, and -III bands, arising from vibrations of the protein backbone, have been widely used to determine the protein secondary structure of isolated proteins (250; 251; 252), and are diagnostic for the overall protein secondary structure of cells and tissues (253). Most FTIR studies rely on the amide-I band for protein secondary structure analysis. Recent studies, however, have implicated the amide-III band for FTIR protein

analysis, because the different types of secondary structure are better resolved, and because this region of the spectrum does not find interference from water and water vapor bands (254; 255).

In this chapter, FTIR was used to study changes in membrane phase behavior and overall protein secondary structure during freezing of LNCaP prostate tumor cells. Samples were nucleated at temperatures ranging from -3ºC to -10ºC. It is shown that the temperature at which ice is formed in the system affects the membrane phase behavior of the cells. This is explained in terms of cellular dehydration and IIF, which both critically depend on the nucleation temperature. Proteins were found to be relatively stable during freezing.

4.2 MATERIALS & METHODS

4.2.1 LNCaP Culture

LNCaP cells were grown in DMEM F-12 media (Gibco, Grand Island, NY, USA) supplemented with 5% fetal bovine serum (FBS), 1% penicillin/streptomycin in saline (Invitrogen, Gaithersburg MD, USA), 250nM dexamethasone (Sigma-Aldrich, St. Louis, MO, USA) and 5% CO_2 at 37°C. Cells were grown in 250ml T flasks, harvested by treatment with 0.5ml Trypsin-EDTA (0.05% Trypsin, and 0.53mM EDTA (Gibco, Gaithersburg, MD, USA)) for 3 min at 37ºC. About 10ml of DMEM F-12 medium was added to neutralize the trypsin. The cells were then centrifuged at 1000 x g for 10min, the medium was removed, and the cell pellet spread between two CaF_2 IR windows for subsequent FTIR analysis.

4.2.2 FTIR Studies

Infrared absorption measurements were carried out with a Nicolet Magna 750 Fourier transform infrared spectrometer (Thermo-Nicolet, Madison, WI, USA), equipped with a TGS detector. The optical bench was continuously purged with dry air (Balston, Haverhill, MA, USA). The acquisition parameters were: $4cm^{-1}$ resolution, 32 co-added interferograms, 4000-900 cm^{-1} wavenumber range. Spectral analysis and display were carried out using Omnic software (Thermo-Nicolet, Madison, WI USA). About 10µl of cell pellet was sandwiched between two CaF_2 windows separated by a 6µm Mylar spacer (Thermo Electron North America Inc., Madison, WI USA). Samples were then mounted into a homemade variable temperature cell. Liquid nitrogen was used as a coolant, and the temperature was regulated by a temperature controller (Minco Products Inc., Minneapolis, MN USA). The temperature of the sample was recorded separately using a thermocouple that was located close to the sample. The temperature dependence of the FTIR spectra was studied by cooling the sample from ambient temperature down to temperatures as low as -80°C at a rate of approximately -2.0°C/min. Cell pellet samples that were cooled at a rate of -2°C/min showed ice formation at around -10°C. The nucleation temperature was increased using *Pseudomonas syringae* (ATCC, Rockville, MD USA) as a natural ice nucleator according to Devireddy et al. (256). Five µl of *P. syringae* (10mg/ml) was placed at the edge of the cell pellet on the IR window. This resulted in nucleation temperatures ranging from -4 to -8°C. Controlled nucleation at -3°C and -6°C was achieved by inserting a copper wire cooled with liquid nitrogen directly into the sample. The heating phase of the experiment was started after a hold

time of 5 minutes. Spectra were recorded over a temperature range from -80°C to +90°C at a heating rate of 2°C/min.

Membrane fluidity was monitored by observing the position of the -CH_2 symmetric stretching band at approximately 2850cm^{-1} as described previously (257). Wavenumber (νCH_2) versus temperature plots were constructed, and phase transition temperatures were determined from the maxima in the first derivatives of the νCH_2 versus temperature plots. The slope at the phase transition temperature, T_m, was taken as a measure for the co-operativity of the phase transition (257). Phase changes of water into ice and vice versa were determined by plotting the area of the water band between 2680 and 1950cm^{-1} (H_2O bending and libration combination band) as a function of temperature. Protein denaturation was determined as previously described (202; 258). Briefly, the spectral region between 1700 and 1500cm^{-1} containing the amide -I and -II absorption bands was selected. Heat denaturation profiles were obtained by subtracting spectra recorded at 20°C from spectra at the indicated temperatures. The second derivatives of these difference spectra were taken with a 13-point smoothing factor to resolve the different bands more clearly. Thermal denaturation of proteins was followed by monitoring the area of bands at 1625cm^{-1} (amide-I region) and 1550cm^{-1} (amide-II region) that became visible upon heating of the sample. The areas of these bands were plotted as a function of temperature, and used to determine onset and midpoint of protein denaturation. The amide-III region, located between 1350 and 1200cm^{-1}, was also analyzed to corroborate the amide -I and -II band analysis. In this case, the area under the original absorbance spectra was calculated

and plotted as a function of temperature. Bands at approximately 1315 and 1235cm^{-1} were found to decrease and increase respectively upon protein denaturation.

4.2.3 Cellular Biophysics

Previously described biophysical models (18; 47) were used to predict the cellular biophysics including cellular dehydration and IIF in LNCaP cells during freezing protocols that were used for the FTIR studies (cooling rate 2°C/min, nucleation temperature ranging from 0 to -10°C). These biophysical models are described in detail in Chapter 1 and require cell specific water transport and IIF parameters from experimentation. The specific water transport parameters for LNCaP cells were found by theoretically fitting to the dehydration behavior of n = 10 to 30 cells at 5, 10 and 25°C/min where no intracellular ice formation occurred. Similarly, the IIF model was fit for n = 50 to 75 cells at 130°C/min, a rate where cellular dehydration was minimal.

4.2.4 Cell Viability

For viability measurements, cell pellets were frozen between glass microslides using a Linkam Scientific conduction type cryostage (Linkam, Tadworth, UK). Samples were cooled at a rate of 2°C/min, and nucleated at the indicated temperatures using a liquid nitrogen cooled copper wire. The end temperature was -20°C, and after a hold time of 5min., the sample was re-warmed at a rate of 2°C/min to room temperature. After thawing, the slides were separated, dyes were loaded onto the cellular film, and the slides were covered with glass cover slips before microscopic evaluation. Both frozen and

control samples were loaded, by a 30min incubation at 37°C, with Hoechst 33258 (Sigma, St. Louis, MO, USA) which stains the DNA of all the cells, and Propidium Iodide (Molecular Probes, Eugene, OR, USA) which stains the DNA only of cells with disrupted membranes as previously described (202). The numbers of live and dead cells were counted using a BX-50 Olympus fluorescence microscope (Leeds Precision, Minneapolis, MN, USA). Three to five fields with 30-40 cells per field were counted for each sample. Based on the number of live cells obtained from the assay, viability is represented in terms of percent viability.

4.3 RESULTS

4.3.1 Cell Biophysics & Viability

Based on the experimental freezing results fit to the cellular biophysical models, the biophysical parameters of freezing LNCaP cells were obtained. This model was used to predict freezing under conditions relevant to the FTIR study (Table 4.1). The membrane permeability parameters were found to be: L_{pg} = 0.21μm $(min.atm)^{-1}$and E_{Lp} = 25.1kcal/mol. In addition, the kinetic (κ_o) and thermodynamic (Ω_o) nucleation parameters for cellular IIF were found to be: $\Omega_o = 27.7 \times 10^8 (m^2.s)^{-1}$ and $\kappa_o = 2.2 \times 10^9 K^5$. These parameters were used to construct Figure 4.1, which shows the effect of the nucleation temperature versus the predicted extent of IIF in LNCaP cells during cooling at 2°C/min as used in the FTIR studies. IIF is avoided when ice nucleation is achieved between 0 and -4ºC. At nucleation temperatures below -4ºC, the percentage of IIF increases and at a nucleation temperature of -10ºC the extent of IIF is greater than 95%. Thus, if LNCaP

cell pellets are nucleated between 0 and -4°C, IIF is avoided and the cells will be subject to dehydration, whereas nucleation below -4°C increases the incidence of IIF.

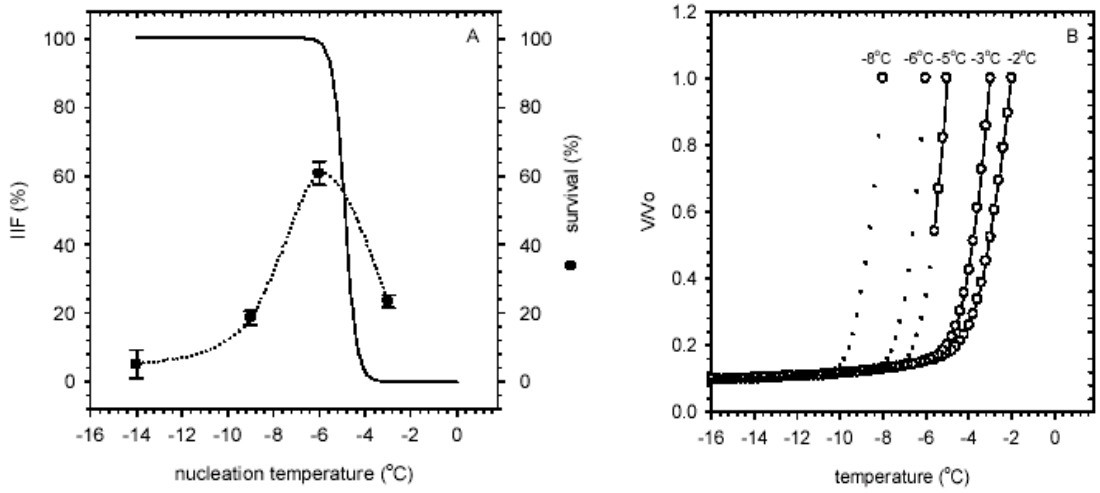

Figure 4.1: Biophysics survival of LNCaP cells after freezing at 2°C/min and nucleation at various subzero temperatures. (A) Prediction of IIF as a function of the ice nucleation temperature (solid line) and the effect of the nucleation temperature on survival (filled circles) of cells that were subsequently frozen down to an end temperature of -20°C. (B) Decrease in the volume of cells versus ice nucleation temperature. The solid lines reflect the actual decrease in volume above nucleation of -4°C, while the dotted lines represent conditions below -4°C where IIF is competing with dehydration to determine the overall cellular response

Table 4.1: Parameters used to predict IIF and cell dehydration during freezing of LNCaP cells

NOMENCLATURE	VALUE	UNIT
T = absolute temperature	Variable	K
B = cooling rate	2	K/min
V = cell volume	Variable	μm^3
V_o = initial isotonic cell volume	1806	μm^3
V_b = osmotically inactive cell volume	0.07 V_o	μm^3
L_{pg} = reference permeability at 273K	0.21	µm/(min.atm)
E_{Lp} = apparent activation energy	25.1	Kcal/mol
Ω_o = kinetic nucleation parameter	27.7×10^8	$1/(m^2.s)$
κ_o = thermodynamic nucleation parameter	2.23×10^9	K^5
PIF = probability of IIF	Variable	%
ΔT = degree of undercooling of the cytoplasm	Variable	K

Figure 4.1 also depicts the effect of the nucleation temperature on the survival of cells that were frozen to an end temperature of -20°C. Cells exhibit an optimum survival at a nucleation temperature of -6°C. Thus, optimal freezing survival coincides with intermediate levels of dehydration and IIF.

4.3.2 FTIR Spectra of LNCaP Cells

Figure 4.2 depicts the IR absorbance spectra of LNCaP cells at 20ºC, +80ºC, and -80ºC. Overall, the IR spectrum of the cells in media is dominated by the signal from water or from ice. Water exhibits strong vibrational bands at around 3300cm^{-1}, 2200cm^{-1}, and 1650cm^{-1} arising from the stretching, the libration and bending combination, and the scissoring vibrational modes, respectively. The frozen sample exhibits clear differences in spectral shape compared to the other samples. This is seen throughout the spectrum and is mostly due to shape changes of the water absorption bands upon transition into ice. In the 3000 – 2800cm^{-1} region, the symmetric and asymmetric CH_2 stretching vibrations of lipid acyl chains are visible. Characteristic protein bands are visible at 1655cm^{-1} (amide-I band) and at 1550cm^{-1} (amide-II band). The amide-I band overlaps with the scissoring vibrational mode of water. In the amide-III region of the spectrum (1330 and 1200cm^{-1}) several weak bands are visible.

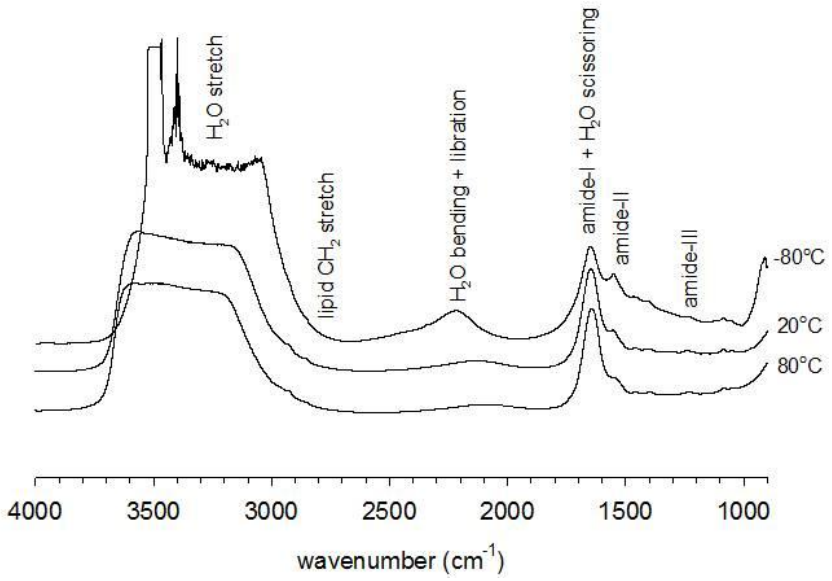

Figure 4.2: In situ absorption spectra of LNCaP prostate tumor cells at -80, 20 and 80°C. Characteristic molecular group vibrations are indicated.

4.3.3 FTIR Assessment Method

IR spectra of LNCaP cells as a function of temperature show shifts of bands, associated with gel formation of membrane lipids during cooling (Figure 4.3(A)), formation of ice during cooling (Figure 4.3(B)), and denaturation of proteins during heating (Figure 4.3(C,D)). Second derivative analysis was used to show the small lipid bands in the 3000-2800cm^{-1} region more clearly. The symmetric CH_2 stretching mode arising from membrane lipids exhibits a shift to lower wavenumber with decreasing temperature, indicating a decrease in membrane fluidity during cooling (Figure 4.3(A)). The band around 2200cm^{-1}, which arises from a combination of H_2O bending and libration motions shifts to higher wavenumber upon ice formation and the band width decreases (Figure 4.3 (B)).

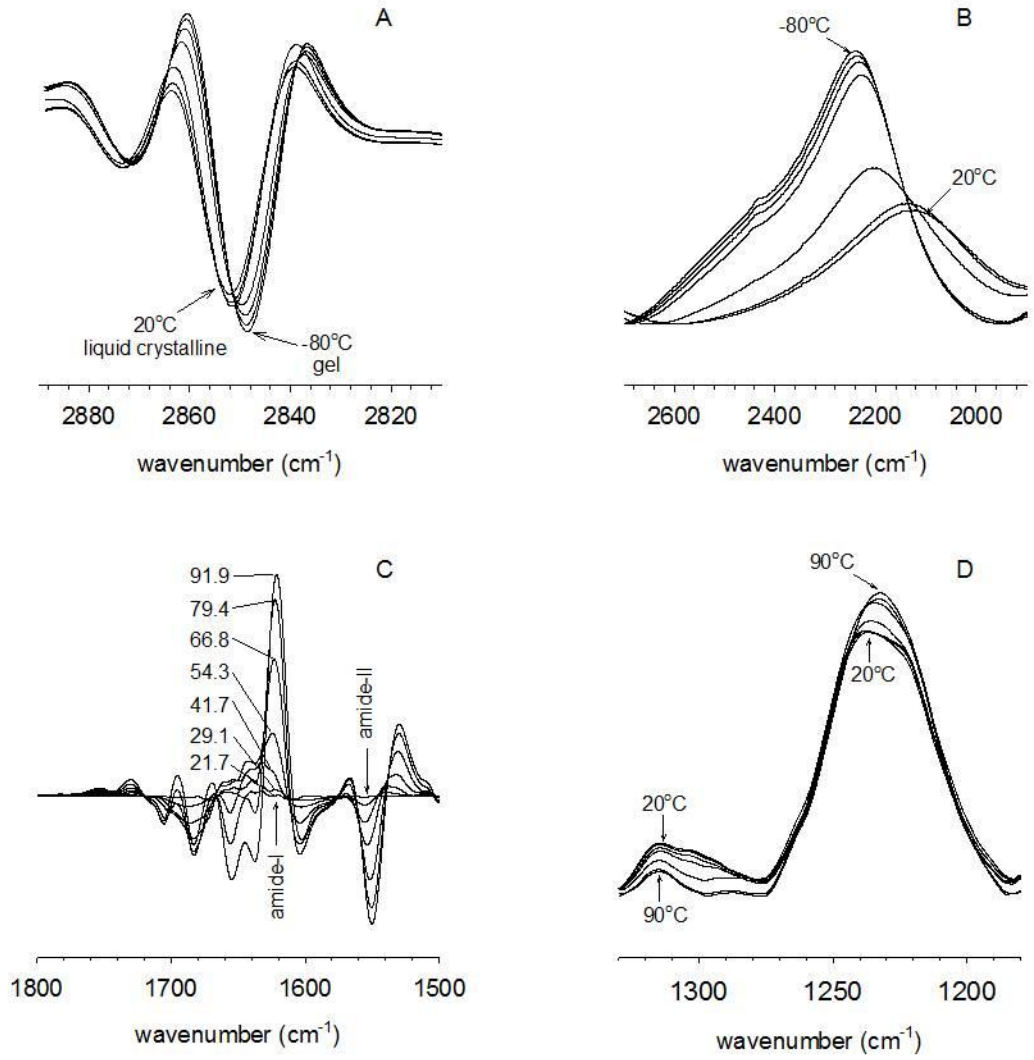

Figure 4.3: Thermal FTIR analysis of LNCaP cells. (A) Second derivative spectra in the lipid region shows a decrease in wavenumber of the symmetric CH_2 stretching band during cooling (nucleated at -3°C). Spectra are shown between 20 and -80°C at increments of 16°C. (B) The libration and bending combination mode of H_2O shows a shape change during cooling upon transition of water into ice. Spectra are shown between 20 and -80°C at increments of 16°C. (C) Protein denaturation at various temperatures, showing difference spectra in the amide I and II region. Each trace shown represents the spectrum obtained at a given temperature after the 20°C spectrum was subtracted from it. (D) Shape changes in the amide-III region during heating associated with protein denaturation. The temperature of the spectra in panel D correspond to those in panel C (increment 12°C)

Figure 4.3 also shows the spectra from cells recorded at various elevated temperatures after subtracting the spectrum taken at 20°C. Protein denaturation coincides with an abrupt increase in the formation of extended β-sheet structures as is evident from the increase of the band at around 1625cm^{-1}. In the amide-II region, denaturation is visible as a sudden decrease of the band at 1550cm^{-1}. Inspection of the amide-III region shows that a band around 1315cm^{-1} decreases upon heating, while a band at around 1235cm^{-1} increases (Figure 4.3(D)). Bands at 1315cm^{-1} and 1235cm^{-1} have been assigned to α-helical and β-sheet structures respectively (254).

4.3.4 Membrane Phase Behavior

The thermotropic response of the symmetric CH_2 stretching vibration shows that the membrane phase behavior of LNCaP cells during cooling is affected by the nucleation temperature (Figure 4.4). When the sample is nucleated at -3°C, the membranes undergo a highly co-operative phase transition with an onset temperature that coincides with the nucleation temperature of ice in the system. The sample that nucleated at -10°C exhibited a much less co-operative phase transition with an onset temperature at approximately -10°C. In addition, the sample that nucleated at -10°C shows a considerably higher wavenumber at -80°C indicating greater membrane fluidity compared to the sample nucleated at -3°C. The sample that was nucleated at -6°C shows intermediate membrane phase behavior. The highly co-operative phase transition under dehydrating conditions was only observed in intact viable cells (Figure 4.4(B)). Cells that were lysed by pelleting

and resuspending in pure water showed a much less co-operative transition and a concomitantly higher wavenumber of the CH_2 stretching vibration in the frozen state.

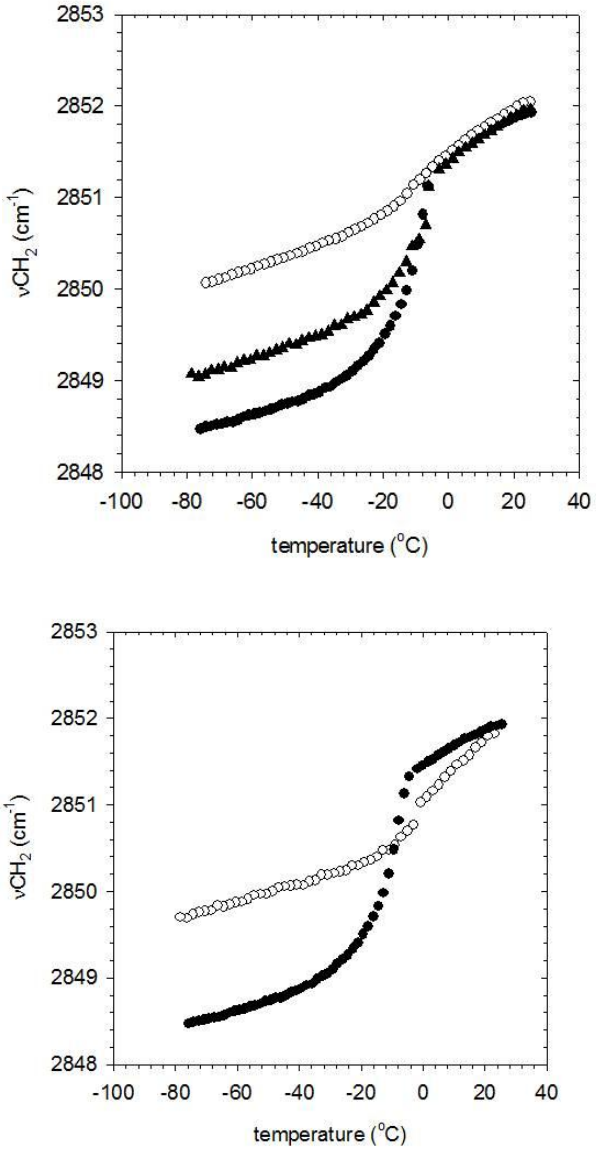

Figure 4.4: Membrane phase behavior of LNCaP cells during cooling and nucleation at various subzero temperatures. (A) νCH_2 versus temperature plot during freezing the cells down to -80°C. Samples were nucleated at -3°C (filled circles), -6°C (filled triangles) or at -10°C (open circles). (B) Membrane phase behavior of cells during cooling and nucleation at -3°C. The data points reflect those of viable control cells (filled circles) and lysed cells (open squares).

The co-operativity of the membrane phase transition, expressed as the slope at the midpoint of the transition, showed a correlation with the ice nucleation temperature. The co-operativity decreases with decreasing nucleation temperature (Figure 4.5). Taken together, these observations indicate that the onset temperature of the membrane phase transition coincides with the temperature at which ice is formed in the system and that the nucleation temperature affects the co-operativity of the membrane phase transition and the membrane fluidity in the frozen state.

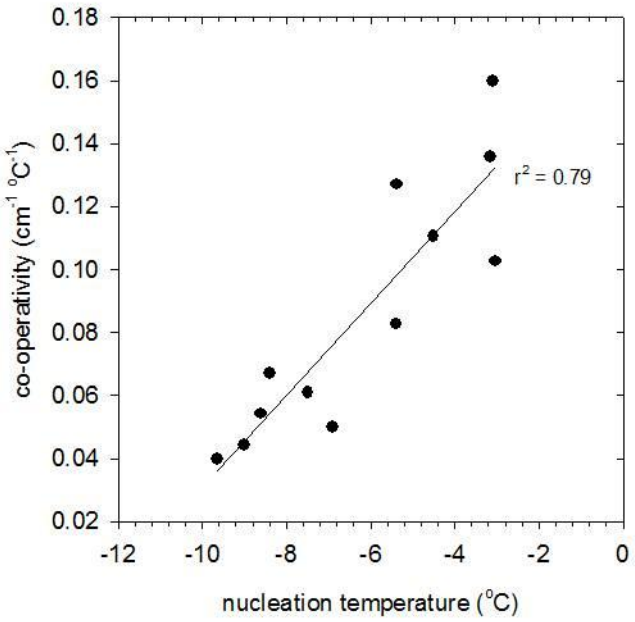

Figure 4.5: Correlation between the co-operativity of the membrane phase transition of LNCaP cellular membranes during cooling and the ice nucleation temperature

4.3.5 Protein Stability During Freezing & Heating

Changes in the amide-I, -II, and -III regions of the spectra upon heating from 20 to 90°C were used to determine the protein denaturation profile of the cells (Figure 4.6). The formation of extended β-sheet structures upon protein denaturation is evident from the

sudden increase in band area of the band at 1625cm^{-1} in the amide-I region (Figure 4.6 (A)). Protein denaturation commences at an onset temperature of 48ºC, and the rate of β-sheet accumulation reaches a maximum at 66ºC (midpoint temperature). Figure 4.6 (B) shows that the amide-II band area shows a sudden decrease in area upon denaturation of the sample. This likely reflects a combined effect of a decrease in α-helical structures and a concomitant increase in β-sheet structures. The onset and midpoint temperature that were determined from this plot were 48ºC and 64ºC, respectively. Two distinct bands in the amide-III region were found to be sensitive for protein denaturation. The band at 1235 cm^{-1} shows an abrupt increase in area upon denaturation (Figure 4.6 (C)), likely reflecting an increase in β-sheet structures (254). The band at 1315 cm^{-1} shows a decrease in area upon protein denaturation (Figure 4.6 (D)), likely due to a decrease in α-helical structures (254). The denaturation profiles that were derived using amide-III band analysis closely matched those that were determined using the amide-I or -II region. The various amide band areas were also monitored during cooling the sample back from 90ºC to 20ºC to verify that protein denaturation is irreversible. As expected, the changes in band area that were observed during heating did not reverse during cooling (data not shown).

Amide-III band analysis was also used to detect protein structural changes during freezing and thawing of the cells. Figure 4.7 shows the area of the band at 1235cm^{-1} during freezing down to -80ºC and subsequent thawing of the cells using a nucleation temperature of -3ºC. The decrease in amide-III band area coincided with the formation of

ice in the system. The thawing profile closely matched the freezing profile indicating that the freezing induced changes in amide-III band area were reversible.

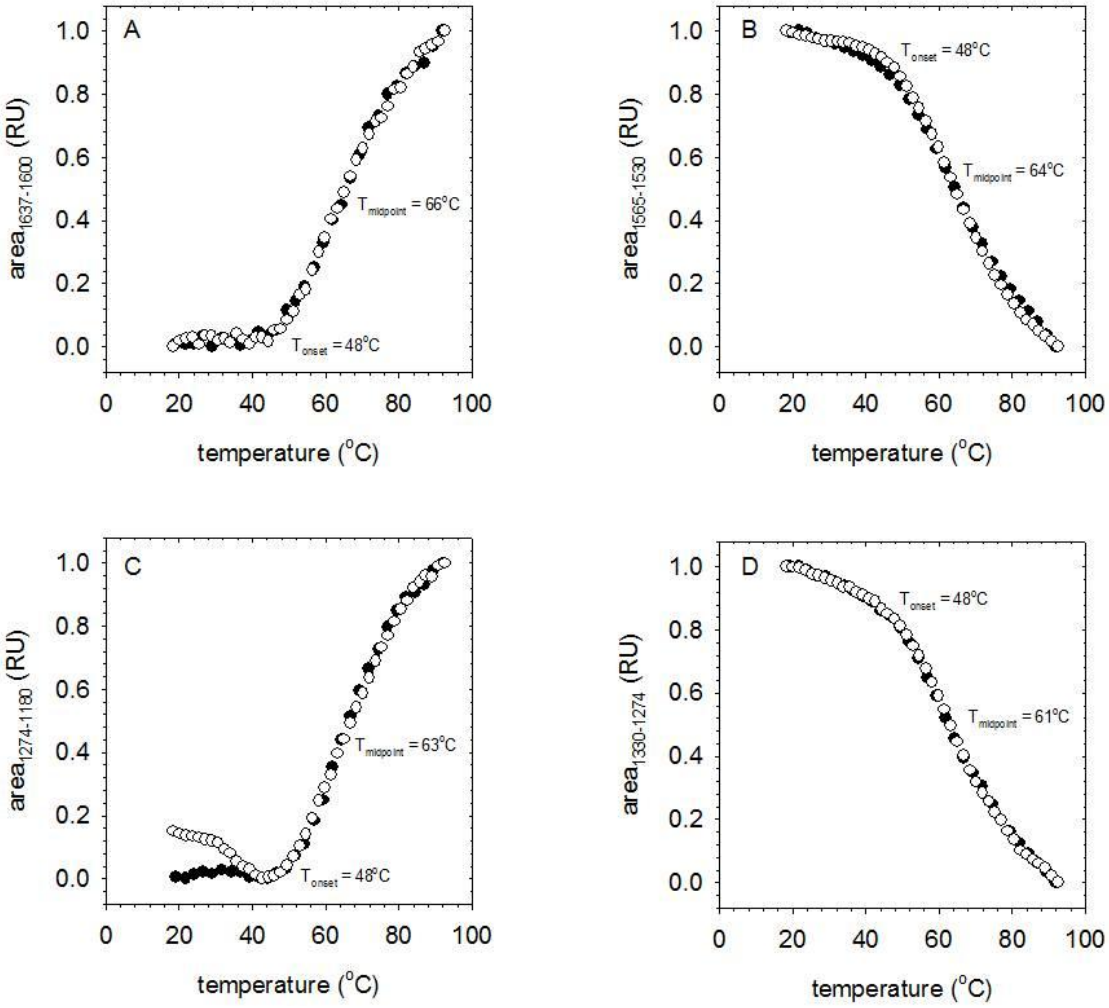

Figure 4.6: Heat induced protein denaturation in LNCaP cells using amide-I, II and III band analysis. Characteristic band areas were calculated and plotted as a function of temperature. (A) Area of the band at ~1625cm^{-1} in the amide-I region (β-sheet structures). (B) Area of the band at ~ 1550cm^{-1} in the amide-II region (α-helical + β-sheet structures). (C) Area of the band at ~ 1235cm^{-1} in the amide-III region (β-sheet structures). (D) Area of the band at ~ 1315cm^{-1} in the amide-III region (α-helical structures). The data points reflect band areas during heating of non frozen control cells (closed circles), and cells that were subjected to a freeze-thaw cycle to -80°C (open circles).

The heat denaturation profile of cells that were subjected to a freeze-thaw cycle was found to be very similar to that of non frozen control cells (Figure 4.7), indicating that the freeze-thaw cycle did not affect the cells' heat denaturation characteristics.

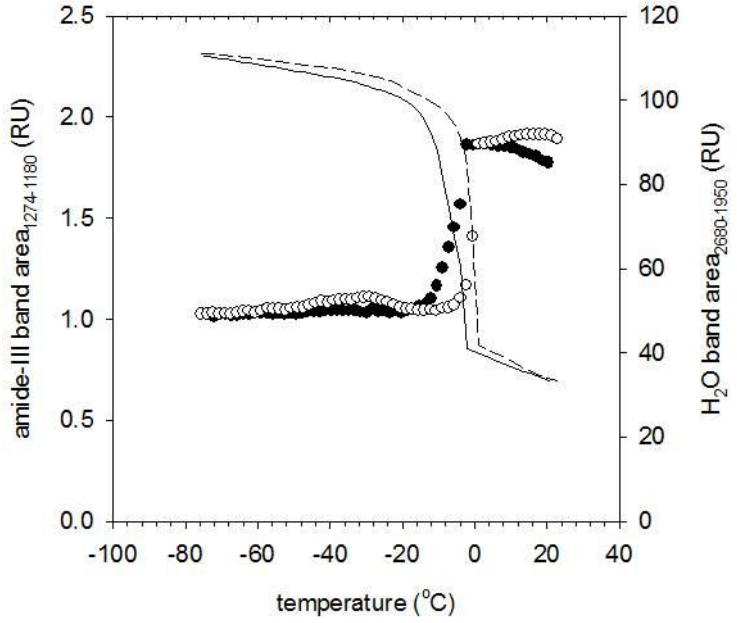

Figure 4.7: Area changes in the amide-III region during freezing and thawing of LNCaP cells nucleated at -3°C. The data points reflect the area of the band at ~1235cm^{-1} during freezing (closed circles) and re-warming (open circles). The area of the H_2O libration and bending combination band is also shown during freezing (solid line) and thawing (dashed line) is also shown to indicate ice nucleation and ice melting

4.4 DISCUSSION

FTIR was used to monitor membrane phase behavior and changes in overall protein secondary structure in LNCaP prostate tumor cells during cooling at 2°C/min while varying the ice nucleation temperature between -3 and -10°C. The predicted incidence of IIF rapidly increases at ice nucleation temperatures below -4°C and cell survival exhibits an optimum at intermediate levels of dehydration and intracellular ice formation. The ice

nucleation temperature was found to have a great effect on the membrane phase behavior of the cells. The onset of the liquid crystalline to gel phase transition coincides with the ice nucleation temperature. In addition, the ice nucleation temperature determines the co-operativity of the transition and the membrane fluidity in the frozen state. Proteins are relatively stable during freezing. Heat-induced protein denaturation is visible as an abrupt decrease in α-helical structures and a concomitant increase in β-sheet structures.

Intracellular ice formation (IIF) is regarded to be lethal at low nucleation temperatures or high cooling rates for different cell types (19). Exposure to high solute concentrations (dehydration effect) is the other main cause of cell death during freezing (259). Cells typically show optimal freezing survival at intermediate levels of dehydration and intracellular ice formation (19), which was also observed here. The effect of the nucleation temperature on the rate of IIF has been quantified for various cell types (57; 245). These studies have established that the lower the nucleation temperature the greater is the incidence of IIF in cells. The effect of the nucleation temperature on IIF could explain the observed effects on the membrane phase behavior of the cells. LNCaP cell membranes exhibit a liquid-crystalline to gel phase transition during cooling. The membrane phase behavior, however, is strongly affected by the temperature at which ice is formed in the system. The effect of the nucleation temperature on the thermotropic response of the membranes can likely be attributed to differences in the extent of cellular dehydration. Dehydration during air-drying or freeze-drying is known to affect lipid phase behavior of liposomes and biological membranes (101; 5; 26; 260). Removal of water from the phospholipid head groups causes lyotropic phase transitions. Relatively

few studies have been done on the effects of freezing on lipid phase behavior. A study on the effects of ice on the lipid phase behavior of pure phosphatidyl ethanolamine lipids revealed that the presence of ice affected the onset temperature of the main phase transition but had little effect on the co-operativity of the transition (261). These effects were attributed to osmotic dehydration. Interestingly, in LNCaP cells the nucleation temperature not only affected the onset temperature of the membrane phase transition but also the co-operativity and the membrane fluidity in the frozen state, which we suggest is due to the extent of cellular dehydration. When nucleation is initiated between 0 and -4°C, IIF is avoided and the cells will start to dehydrate upon ice formation in the extracellular space. Dehydration is manifested as a decrease in membrane fluidity in the frozen state due to a decrease in hydration level of the water around the phospholipid head groups. When ice nucleation occurs below -4°C the incidence of IIF increases, resulting in a greater membrane fluidity of the cells in the frozen state, indicating that membranes remain relatively hydrated under those conditions. Lysed cells that are nucleated at temperatures were IIF is avoided in intact cells show membrane phase behavior indicative of IIF. This is likely due to a loss of membrane integrity upon lyses of the cells, which is expected to increase the incidence of IIF.

Denaturation of proteins can be brought about by both heat and cold. Heat denaturation of many proteins typically occurs at measurable rates above 50°C (262). On the other hand, cold denaturation typically occurs in the range of 0 to 20°C (263; 264), although this was not observed in this study. Several driving forces exist during freezing of cells that can change the protein secondary structure. These include freezing-induced

concentration of solutes, free radical attack by reactive oxygen species, and release of intracellular stores of proteolytic enzymes.

It was previously showed that heat induced protein denaturation in cells can be measured in situ using changes in amide-I band profile (202). This approach yields denaturation profiles that closely resemble those determined by DSC (265). The denaturation profile is cell or tissue specific and can be used as a thermal fingerprint. The amide-III region is shown to be useful to detect protein denaturation in cells. The amide-III region has the advantage that the different types of secondary structure are better resolved and that water bands do not interfere (254; 199). The shape changes in amide-III band profile that were observed during heat denaturation of LNCaP cells have also been observed during denaturation of isolated proteins (199). It should be noted that the amide-III region of cells may also contain contributions from other molecular group vibrations, particularly the asymmetric phosphate stretching vibration. Nevertheless, the denaturation profiles that were derived using amide-III band analysis closely matched those that were determined using amide-I or -II band analysis, which indicates that the thermotropic response of the bands in the amide-III region for the most part can be assigned to protein denaturation. The observed reduction in α-helical structures and concomitant increase in β-sheet structures is typically observed during heat denaturation of proteins (202; 253; 258; 266). The overall protein secondary structure of LNCaP cells was found to be relatively stable during freezing. During cooling, a decrease in amide-III band area was observed at the ice nucleation temperature, likely because the amide vibrational modes form different hydrogen bonds with water upon ice formation in the system. The effect of

ice nucleation on the amide-III band area was found to be reversible. The heat denaturation profile of frozen cells closely resembled that of non frozen control cells, suggesting that freezing only had minor effects on the overall protein secondary structure. In AT-1 Dunning cells, freezing to -80ºC partially denatured cellular proteins, which affected the heat denaturation profile (202). The freezing and thawing conditions, however, were different from the conditions that were used here.

4.5 SUMMARY

In this chapter, the molecular events associated with the biophysics of freezing cells were studied. Specifically, membrane phase transition and protein denaturation of LNCaP tumor cells during freezing using Fourier transform infrared spectroscopy (FTIR). Important results from the study are summarized below:

i. A highly co-operative membrane phase transition is noted when ice is nucleated at -3°C. The phase transition temperature of the membranes coincides with the ice nucleation temperature. Lysed cells or cells nucleated at approximately -10^{o}C showed a much less co-operative phase transition.

ii. Proteins are relatively stable following freeze/thaw. Protein denaturation for LNCaP is reversible following freeze/thaw.

iii. The predicted incidence of intracellular ice formation (IIF) increases at ice nucleation temperatures below -4°C. LNCaP survival is optimum at a nucleation temperature of -6°C, which matches intermediate levels of dehydration and IIF.

The results of this chapter show that membrane phase transition and protein denaturation are associated with the biophysics of freezing LNCaP cells. However, the link to cellular biophysical responses is missing. This is addressed in Chapter 5 where molecular events during freezing are correlated to cellular biophysical changes.

5. MEMBRANE HYDRATION CORRELATES TO CELLULAR BIOPHYSICS DURING FREEZING IN MAMMALIAN CELLS[4]

This chapter describes the molecular events during the freezing as cell specific events that can be linked to cellular biophysics. The present author along with Dr. Willem Wolkers performed all the experiments and data analysis. The results from this chapter have been compiled, edited and published in the following citation:

I. Balasubramanian SK, Wolkers WF, and Bischof JC (2009) "Membrane hydration correlates to cellular biophysics during freezing in mammalian cells" *Biochimica et Biophysica Acta* 1788 (5); pp 945 – 953

[4] The authors would like to acknowledge grant support from National Institute of Health (NIH) R01-CA07528. The authors would also like to thank Dr. Alptekin Aksan for his inputs, Dr. Joel Slaton and the MD Anderson Cancer Center for the LNCaP Pro5 line cells.

This chapter characterizes the molecular events during freezing of multiple cell types and links the state of membrane hydration to cellular biophysical changes. Cell membranes are known to play a significant role in cell injury, but a clear correlation between the membrane molecular state and the surrounding intracellular and extracellular water/ice is still lacking. The previous chapter showed that lipid packing in LNCaP prostate tumor cells is related to cellular dehydration. In this chapter, the molecular state of the membrane and the surrounding water is linked to cellular biophysical events for three different mammalian cells types: human prostate tumor cells (LNCaP), human dermal fibroblasts (HDF), and porcine smooth muscle cells (SMC) using Fourier Transform Infrared spectroscopy (FTIR). Variable cooling rates were achieved by controlling the degree of supercooling prior to ice nucleation (between -3^{o}C and -10^{o}C) while the sample was cooled at a set rate of 2°C/min. Membranes displayed a highly cooperative fluid to gel phase transition under dehydrating conditions (i.e. NT = -3°C), which was not observed under IIF conditions (NT = -10^{o}C). Spectral analysis showed a consistently greater amount of ice forming during dehydrating vs. IIF conditions in all cells. This is hypothesized to be due to the extreme loss of membrane hydration in dehydrating cells that exhibits itself in excess water available for phase change. Interestingly, membrane dehydration correlates strongly with cellular dehydration as assessed by cryomicroscopy. A strong correlation was found between the activation energies for freezing induced lyotropic membrane phase changes determined using FTIR and the water transport measured by cryomicroscopy.

5.1 INTRODUCTION

Cryogenic temperatures are used to preserve cells and tissues during cryopreservation, and to destroy cells in cryosurgery. The success of these applications depends on understanding the damaging effects of freezing at both the cellular and molecular level. At the cellular level, seminal work suggests a two factor hypothesis of injury during freezing – 'solution effects injury' due to exposure to increasing solute concentrations during slow freezing and intracellular ice formation (IIF) due to cytoplasmic supercooling and nucleation during rapid freezing (19). At the macromolecular level, although model (267) and protoplast membrane dehydration and phase change have been measured and modeled during freezing the link to cellular biophysics and injury is still not clear (29; 172).

The mechanisms of cell injury and consequent death are highly debated topics and are an actively investigated area of research. One of the primary sites for thermal injury is attributed to cell membranes (29; 194; 268). The mechanisms of cell injury during dehydration has long been debated but membrane damage resulting from high solute concentration (26), from structural changes (269), and/or from mechanical constraints (270), have generally been implied. The membrane is in dynamic equilibrium with its environment and freezing affects the physical states of membrane lipids due to changes in hydration level (lyotropism) and temperature (thermotropism) (271). The reorganization of lipids and changes in its fluidity due to phase transitions from liquid crystalline to gel phase (172; 173; 3) or from liquid crystalline to hexagonal phase (29) under different thermal and/or hydrated conditions have been implicated in injury. The consequences of

these phase changes are thought to include increased membrane permeability and lateral phase separation of membrane components. In addition, exposure to reactive oxygen species could result in lipid peroxidation and phospholipid de-esterification (247). Alterations in the lipid composition of the plasma membrane have been causally related to cold acclimation of plant protoplasts (29).

Fourier Transform Infra-Red (FTIR) spectroscopy is increasingly being applied to study cells in a wide variety of physical sample states, including hydrated, frozen and dried. FTIR can be used to quantify thermotropic and lyotropic membrane phase changes of cells and tissues (260). Previously, we have characterized and related the effect of nucleation temperature during slow cooling on the lyotropic response of human LNCaP prostate tumor cell membranes to cell viability (3). The highest cell viability was observed under freezing conditions with intermediate dehydration and IIF. Under conditions that cause freeze-induced cellular dehydration, membranes display a highly cooperative phase transition resulting in a strongly packed gel phase of the membranes in the frozen state. This indicates that lipid packing may play a role in determining viability outcome (3). Membrane lipid phase changes in cellular systems can be monitored using the symmetric -CH_2 stretching vibration (249; 246). In addition, the state of water during freezing can be interrogated using the libration and bending combination vibration mode of H_2O.

The behavior of cell membranes during freezing and how the response correlates to cellular biophysical events has not yet been clearly established. The goal of the present study is to build upon our previous results (3) to correlate cellular biophysical events

during slow freezing (dehydrating conditions) and uncontrolled fast freezing (IIF conditions) to the state of water and the cell membrane. The molecular state of the membrane refers to the condition of existence of the membrane lipids at a particular temperature as a consequence of the imposed freezing constraints. To that end membrane and water spectra were investigated during controlled freezing using FTIR in three different cell types: human dermal fibroblasts (HDF), porcine smooth muscle cells (SMC) and human LNCaP prostate tumor cells (from (3)). The results show: (1) a unique membrane phase change for each cell that correlates to injurious cellular biophysical events; and (2) a consistently greater amount of ice formed during dehydrating vs. IIF conditions in all cells.

5.2 MATERIALS & METHODS

5.2.1 Cell Culture

Neonatal human dermal fibroblasts (HDF) were obtained from cryopreserved stock (Cambrex, East Rutherford, NJ) and cultured in Dulbecco's modified Eagle medium (DMEM) (Gibco, Grand Island, NY) containing 10% fetal bovine serum (FBS) (company) and 1% penicillin/streptomycin (p/s) in saline (Invitrogen, Carlsbad, CA).

LNCaP prostate tumor cells were obtained from cryopreserved stock (MD Anderson Cancer center, Houston, TX) and cultured in DMEM F-12 media (Gibco, Grand Island, NY) supplemented with 10% FBS and 1% p/s in saline.

Porcine smooth muscle cells (SMC) were isolated from explanted porcine femoral arteries as described previously (234). Briefly, the arteries were cut into small pieces and placed in Petri dishes allowing cells to grow out of the tissues (125). SMC media was composed of DMEM F-12 (Gibco, Grand Island, NY) containing 10% FBS, 1% p/s in saline and 1% L-glutamine. All SMC cells used for experiments were from passage 4 of culture.

Cells were cultured in T-75 flasks for 3-4 days up to 80% confluency. All cells were then trypsinized using 0.05% Trypsin with 0.53mM EDTA (Gibco, Gaithersburg, MD). The trypsin was inactivated using serum filled media. Cells were then centrifuged at 400g for 10min, the media removed and 12µL of the cell pellet was sandwiched between CaF_2 windows for FTIR analysis.

5.2.2 Cell Biophysical Models

Previously described biophysical models (18; 47) were used to predict the cellular biophysics including cellular dehydration and intracellular ice formation (IIF) the cells. The models are described in detail in Chapter 1 and require cell specific water transport and IIF parameters, which require experimentation. To properly apply the cell biophysical models and compare to FTIR data, the following parameters from previous cryomicroscopy studies are used: V_o = 716, 1806, 932µm^3; V_b/V_o = 0.24, 0.07, 0.24; L_{pg} = 0.12, 0.21 and 0.10µm/min.atm; and E_{Lp} = 24.1, 25.1 and 42.0kcal/mol for SMC, LNCaP and HDF, respectively (4; 3; 5).

5.2.3 FTIR Setup

FTIR spectra were obtained using a Nicolet Magna 6700 spectrometer (Thermo-Nicolet, Madison, WI) equipped with a TGS detector. Spectra were acquired at 4cm^{-1} resolution using 32 co-added interferograms between wavenumber ranges of 4000-900cm^{-1}. The cell pellet samples were mounted onto a specialized temperature cell that was regulated using a temperature controller (Minco products Inc., Minneapolis, MN). Sample temperature, also monitored separately using a thermocouple, was decreased from room temperature to -80^{o}C at 2^{o}C/min. The phase change temperature of the cell media upon thawing is ~-0.6^{o}C, and depends only on its osmolality. However, the temperature of phase change during cooling depends on nucleation, which is a stochastic process. Hence all of the samples reported here are nucleated at temperatures well below the equilibrium phase change temperature (or melt) of the system. For example, all for IIF studies reported here nucleation occurred below -10^{o}C following supercooling of the system. For all dehydration studies, controlled ice nucleation was done at -3^{o}C. Dehydration of cells is a consequence of phase change of water to ice and not a precursor.

5.2.4 Membrane Lipid Analysis

Spectral analysis was carried out using Omnic software (Thermo-Nicolet, Madison, WI). Membrane phase behavior during freezing was monitored by observing the peak position of the νCH_2 symmetric stretching band at ~2850 cm^{-1} as described previously (257). Ice formation induces strong phase transitions causing a strong decrease in membrane fluidity (or decrease in membrane conformational disorder). Fluidity is the term we have

chosen to represent the dramatic changes in wavenumber between cells that have been cooled rapidly vs. slowly (i.e. IIF vs. dehydrated cases). Wavenumber (νCH_2) versus temperature plots were constructed to capture freezing induced phase transitions. Since only one peak was continuously monitored and its wavenumber excursion was less than $4cm^{-1}$ during phase change, the chosen resolution did not affect the recorded data. The initial slope of νCH_2 versus temperature upon ice nucleation was taken as a measure for the dehydrating (lyotropic) effect of ice formation on membrane packing. Arrhenius plots were constructed by plotting the natural logarithm of the initial rate of the membrane phase change upon ice formation versus the inverse of the nucleation temperature. The slope of the Arrhenius plots was used to calculate the activation energy of the freezing induced membrane phase changes.

5.2.5 Water Band Analysis

The phase change of water into ice and vice versa was monitored using the H_2O bending and libration combination band between 2680 and $1950cm^{-1}$ (272). The area under the H_2O band (water or ice) was calculated and plotted as a function of temperature. The intensity of this band increases upon ice formation due to the changes in hydrogen bonding interactions as water changes phase into ice. In addition to showing the onset of ice in the system, this approach reveals differences between IIF and dehydrating freezing conditions. For comparison amongst cell types, the FTIR data were corrected and normalized. Briefly, the ice band area change is measured from directly prior to ice nucleation (i.e. at or near -3°C for dehydration and -10°C for IIF). All further increase in the ice band area for dehydration and IIF cases are then measured with respect to this

origin. Furthermore, to separate lyotropic from thermotropic changes a linear regression line is obtained for the ice band area change from -30°C to -80°C where no further biophysical changes are occurring in the IIF data set (NT at -10°C). The thermotropic effect is then subtracted from both the dehydration and IIF data sets which are set to 0 at NT = -3°C and NT = -10°C respectively.

5.2.6 Linking Molecular Events to Cellular Biophysics

Excess water during freezing is compared directly to cellular biophysical response as previously reported for DSC measurements (83; 273). When ice is nucleated at -3°C in the FTIR, the cells will reach equilibrium volume at this temperature as there is a time lag between ice nucleation and FTIR spectral recording. This equilibrium cell volume (V_o) at -3°C and the osmotically inactive cell volume (V_b) for the cell types in question are known or can be calculated based on previous work (3; 5; 4). This allows corrected ice band area change to be converted to cellular volumetric change by using the following equation:

$$\frac{A(T)_{NT=-3^oC} - A(T)_{NT=-10^oC}}{A(-30^oC)_{NT=-3^oC} - A(-30^oC)_{NT=-10^oC}} = \frac{V_o - V(T)}{V_o - V_b} \qquad (5.1)$$

In the above equation, A refers to the peak area under the ice band at temperature T, and V refers to the corresponding predicted cellular volume normalized between V_o and V_b. The numerator of the LHS represents variable excess water at a given temperature during dehydration, while the denominator represents the total excess water at -30 °C (i.e. total excess water available from complete dehydration vs. IIF at -30 °C). By converting this

to volumetric data (RHS of Equation 5.1) the data is directly compared to cellular cryomicroscopy data.

5.3 RESULTS

FTIR is used to measure the phase state of the membrane and surrounding water during freezing of three mammalian cell types with different size and biophysical properties: human dermal fibroblasts (HDF), porcine smooth muscle cells (SMC), and human LNCaP prostate tumor cells.

Figure 5.1 depicts the IR absorbance spectra of HDF cells at −2°C and−4°C (1°C above and below, respectively, the ice nucleation temperature at −3°C). The IR spectrum of the cells in media is dominated by the signal from water or from ice. Water exhibits strong vibrational bands at around 3300cm^{-1}, 2200cm^{-1}, and 1650cm^{-1}, arising from stretching, libration and bending combination, and scissoring vibrational modes, respectively (247). The frozen sample exhibits clear differences in spectral shape compared to the unfrozen cell samples. This is mostly due to shape changes of the water absorption bands upon transition into ice. The characteristic water band at 2200cm^{-1} exhibits a clear change in its shape and position upon ice nucleation of the sample. In the 3000–2800cm^{-1} region, the symmetric and asymmetric $–CH_2$ stretching vibrations of lipid acyl chains are clearly visible on taking second derivative of the spectra (Figure 5.1 (B)). The lipid bands shift to lower wavenumber with decreasing temperature.

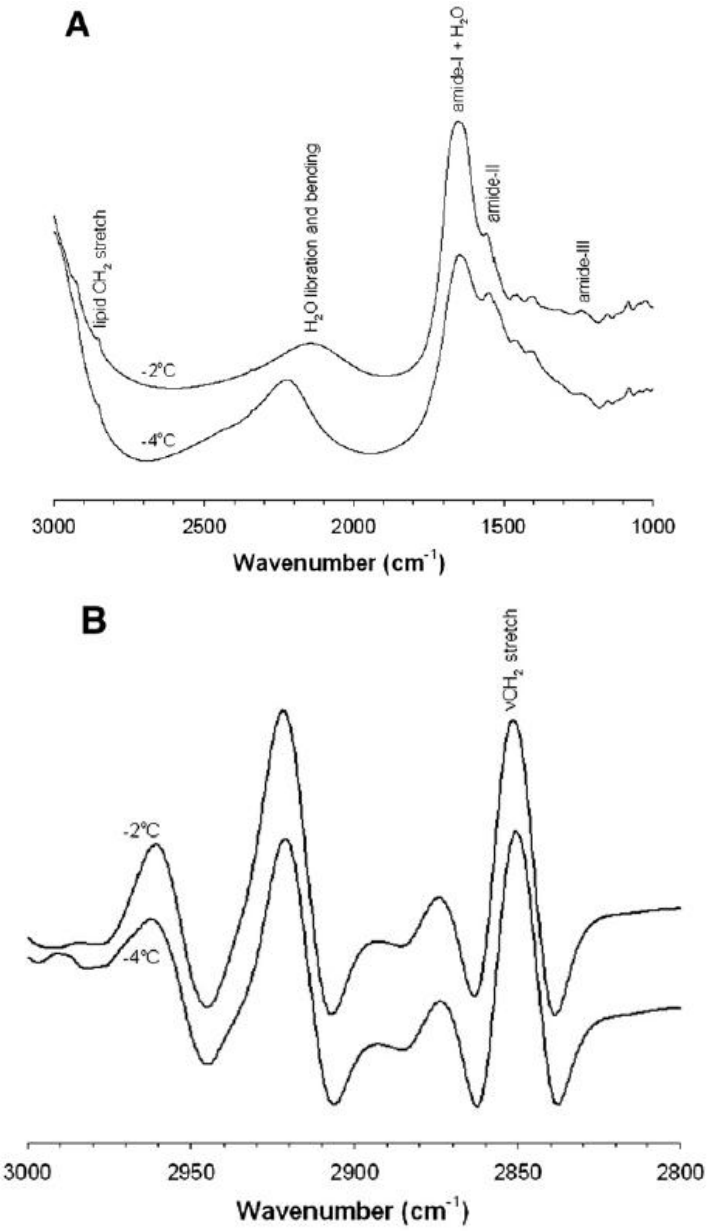

Figure 5.1: In situ IR absorption spectra of HDF cells at -2°C and -4°C just before and after ice nucleation of the sample at -3°C, respectively. Characteristic molecular group vibrations are indicated. (B) Second derivative profile of the spectra is included to highlight the characteristic $-CH_2$ vibrational bands associated with lipid acyl chains of the cells

5.3.1 Membrane Phase Behavior

The effect of freezing on membrane fluidity was monitored by tracking the shift in the wavenumber position of the symmetric νCH_2 stretching band at ~2850cm^{-1} for the three cell types. Figure 5.2 shows that ice nucleation at high sub zero temperatures (dehydrating conditions at NT = -3^{o}C) coincides with a drastic change in the membrane fluidity for all cell types, which is not observed under IIF conditions (NT = -10^{o}C). Hence, the membrane phase behavior of SMC, HDF and LNCaP cells during freezing depends on the ice nucleation temperature. In all cases, the cells display a highly cooperative membrane phase transition with nucleation at -3^{o}C whereas ice nucleation at -10^{o}C causes a much less pronounced effect on membrane fluidity. This implies that cell membranes tend to pack in a highly ordered gel phase under freezing conditions that cause cellular dehydration, whereas under freezing conditions that cause IIF, membranes remain relatively fluid in the frozen state. Dehydrating conditions result in the removal of water from phospholipid head-groups that cause membranes to undergo a lyotropic liquid crystalline to gel phase transition. The sharp decrease in νCH_2 following nucleation at -3^{o}C continues down to ~-30^{o}C before leveling off to a constant slope. This initial effect of ice nucleation on membrane fluidity is cell specific. In addition, the magnitude of change in νCH_2 is cell specific and is the highest for HDFs and the least for SMCs. Note that SMCs exhibit a thermotropic phase transition upon cooling prior to ice formation, which is not observed in the other cells.

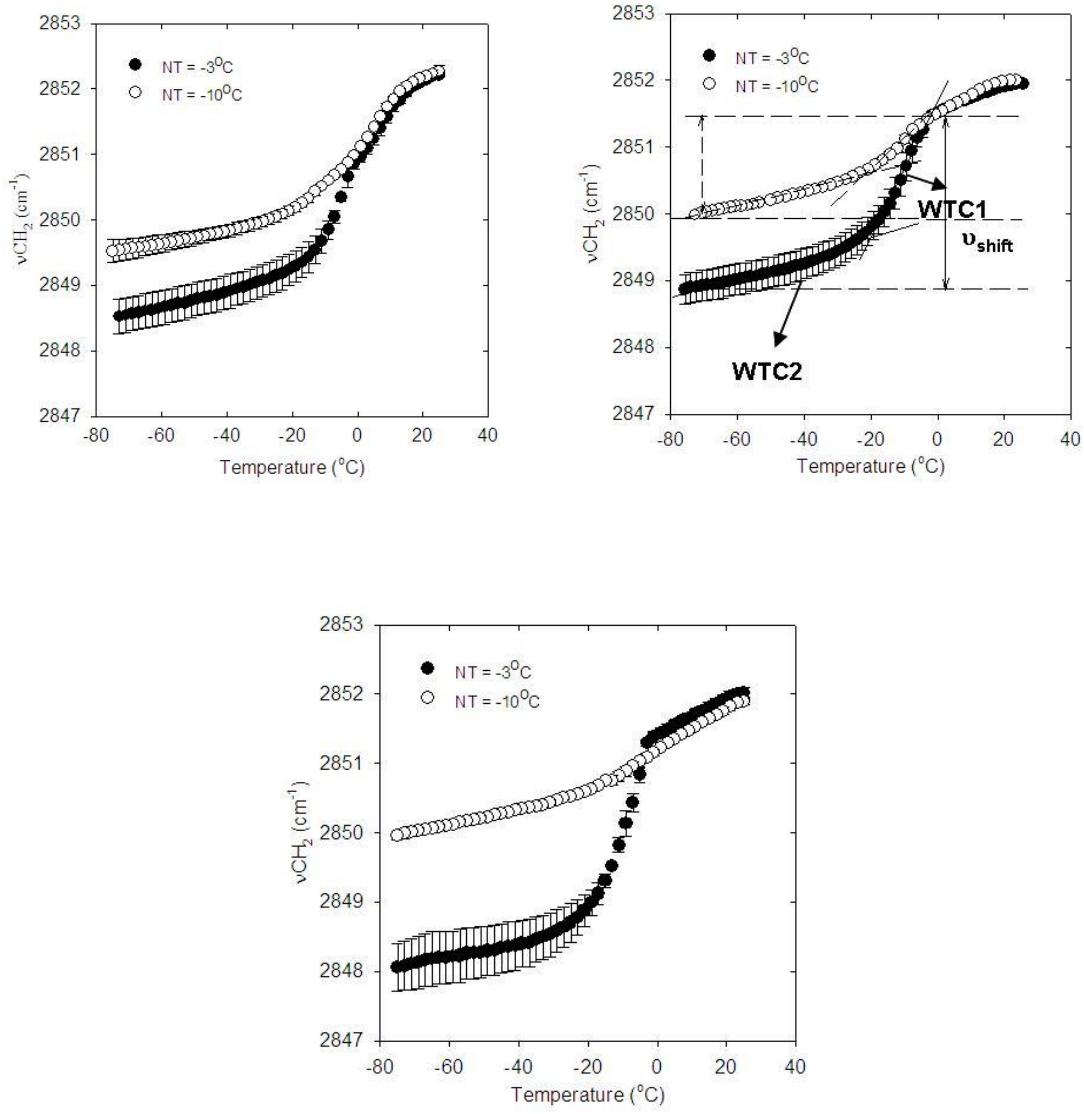

Figure 5.2: Membrane phase behavior of (A) SMC, (B) LNCaP and (C) HDF cells during cooling and nucleation at -3°C (filled circles) and -10°C (open circles). The data points reflect the wavenumber position of the symmetric -CH_2 stretching vibration (νCH_2) arising from the lipid acyl chains with corresponding standard error (n = 3).

Cell specific events that occur in membranes include the initial slope of νCH_2 versus temperature from NT to ~-30°C (wavenumber temperature coefficient, WTC1), the wavenumber temperature coefficient from -30°C to -80°C (WTC2) and the magnitude of

the shift in wavenumber position from the ice nucleation temperature till -80°C (ν_{shift}). Table 5.1 lists WTC1, WTC2, and ν_{shift} for the three cell types under dehydrating (NT = -3°C) and IIF conditions (NT = -10°C). WTC1 and ν_{shift} are greatest for HDFs and smallest for SMCs whereas the thermotropic lipid response below -30°C (WTC2), where cellular dehydration and IIF responses diminish or cease, is approximately the same irrespective of the cell type or the nucleation temperature.

Table 5.1: Characteristic cell specific molecular parameters extracted from the membrane phase behavior of SMC, LNCaP and HDF cells following spectral analysis of the FTIR freezing data. WTC1 reflects the initial Wavenumber Temperature Coefficient at the onset of ice nucleation, WTC2 refers to the Wavenumber versus Temperature Coefficient below –30°C and ν_{shift} is the wavenumber shift from the nucleation temperature to –80°C. ν_{shift} refers to the shift in wavenumber position from the ice nucleation temperature till -80°C.

	DEHYDRATING CONDITIONS (ICE FORMATION AT -3°C)			**IIF CONDITIONS (ICE FORMATION AT -10°C)**		
CELL TYPE	**WTC1 ($cm^{-1}/°C$)**	**WTC2 ($cm^{-1}/°C$)**	**νshift (cm^{-1})**	**WTC1 ($cm^{-1}/°C$)**	**WTC2 ($cm^{-1}/°C$)**	**νshift (cm^{-1})**
SMC	0.105 ± 0.012	0.107 ± 0.002	2.13 ± 0.74	0.080 ± 0.015	0.015 ± 0.004	1.34 ± 0.25
LNCaP	0.13 ± 0.03	0.02 ± 0.003	2.61± 0.34	0.058 ± 0.003	0.020 ± 0.002	1.43 ± 0.07
HDF	0.221 ± 0.005	0.017 ± 0.008	3.24 ± 0.53	0.039 ± 0.004	0.013 ± 0.001	1.13 ± 0.16

The initial slope of νCH_2 change at each NT between -3 and -10°C (WTC1) shows Arrhenius behavior for a representative cell type (LNCaP) as shown in Figure 5.3. The activation energies that are thus determined for the three cell types are depicted in Table 5.2 and this closely matches the activation energies for water transport (E_{Lp}) as determined by cryomicroscopy.

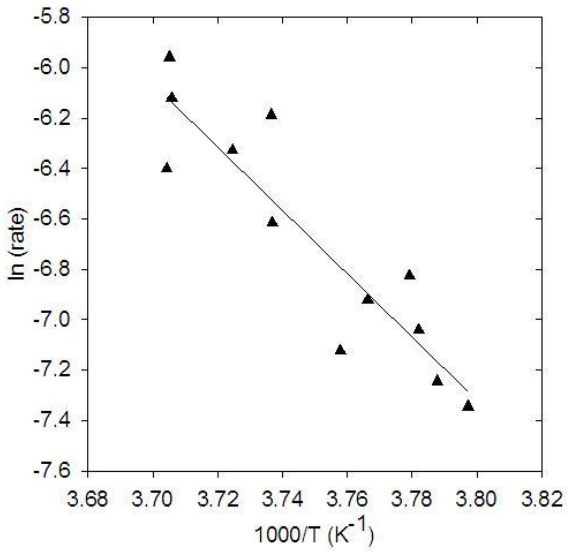

Figure 5.3: Arrhenius plot of the initial rate of the membrane phase change upon ice nucleation and the ice nucleation temperature for LNCaP cells. Data from Wolkers et al. **(3)** were used to construct the plot.

Table 5.2: The membrane hydraulic permeability (L_{pg}) and the activation energy for water transport (E_{Lp}) as determined from FTIR data compared to previously determined cryomicroscopy data on these parameters.

CELL TYPE	CELL PERMEABILITY L_{PG} (μM/MIN.ATM)		ACTIVATION ENERGY E_{LP} (KCAL/MOL)	
	CRYOMICROSCOPE (MODEL PREDICTION)	FTIR	CRYOMICROSCOPE (MODEL PREDICTION)	FTIR
SMC	0.12	0.07	24.1	22.5
LNCAP	0.21	0.24	25.1	25.0
HDF	0.10	0.08	42.0	41.0

5.3.2 State of Water/Ice

The extreme loss of lipid hydration in the membrane under dehydrating conditions is expected to result in a greater amount of ice in the sample, when compared to IIF conditions. The formation of intracellular ice under dehydrating and IIF conditions was studied here by inspection of the libration and bending combination band of water. Figure 5.4 shows the 3D spectral plots of the water and ice bands during freezing of LNCaP cell pellets for NT = -3^{o}C (dehydrating conditions) and NT ~ -10^{o}C (IIF conditions) respectively. On ice formation, the spectral peak shifts to a higher wavenumber position while the width of the spectra narrows and the associated band area increases, denoting a change in the hydrogen bonding interactions. Figure 5.4 (A) shows that ice nucleation at high sub zero temperatures (-3^{o}C) results in a gradual increase in the ice band area before leveling off at -30^{o}C. In contrast at NT ~ -10^{o}C, there is minimal increase in the ice band area upon further temperature drop. The difference in the water/ice band between dehydrating and IIF conditions is further illustrated in Figure 5.5, where the band area of the water/ice band is plotted from room temperature till -80^{o}C.

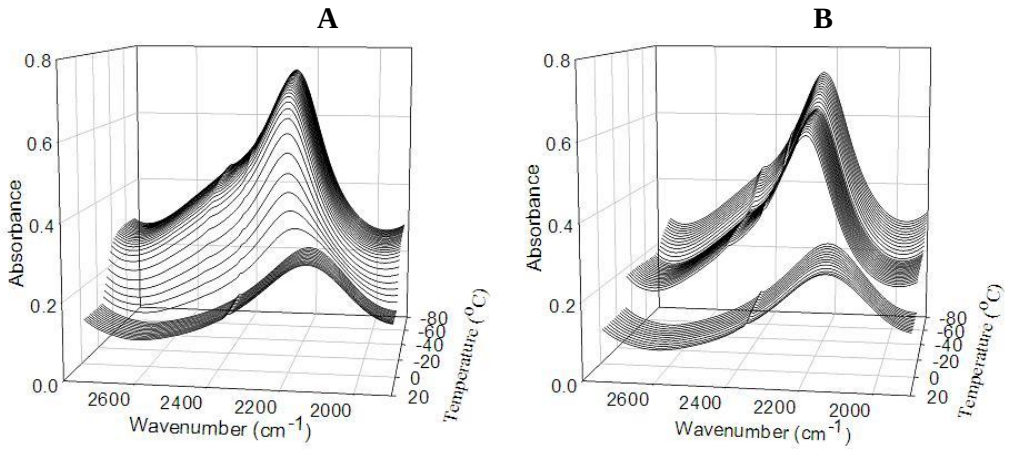

Figure 5.4: Contour plot of the H_2O spectral band during cooling of LNCaP cell pellets from room temperature to –80°C at 2°C/min with ice nucleation at (A) -3°C and (B) -10°C. The phase change of water to ice during freezing manifests itself as a narrowing of the H_2O spectral band with a corresponding shift of the peak to higher wavenumber, and an increase in the band intensity.

In Figure 5.5, the total increase in the H_2O band area from room temperature to -80°C is plotted. For all cell types, there is an increase in the total amount of water changing phase under dehydrating conditions as compared to IIF nucleating conditions. The magnitude of the increase in the excess ice formed is cell type dependent and is the highest for HDFs and the least for SMCs. Under IIF conditions (NT~-10°C), a relatively small increase in ice band area is observed with decreasing temperature, irrespective of cell type. This increase is not due to ice formation, but to changes in hydrogen bonding interactions upon cooling (thermotropic effect). The thermotropic change in ice band area is also observed below –30°C under dehydrating conditions (slopes are the same below -30°C). The thermotropic effect can be subtracted from the data, and then be compared to cryomicroscopy data according to Equation 5.1. The solid lines in Figure 5.6 are plots of

cell volume changes for each cell type at 2°C/min predicted from previously published cryomicroscopy studies (4; 3; 5). The slight lag of the FTIR data at temperatures from -4 to -10°C is likely due to differences in the experimental set-up.

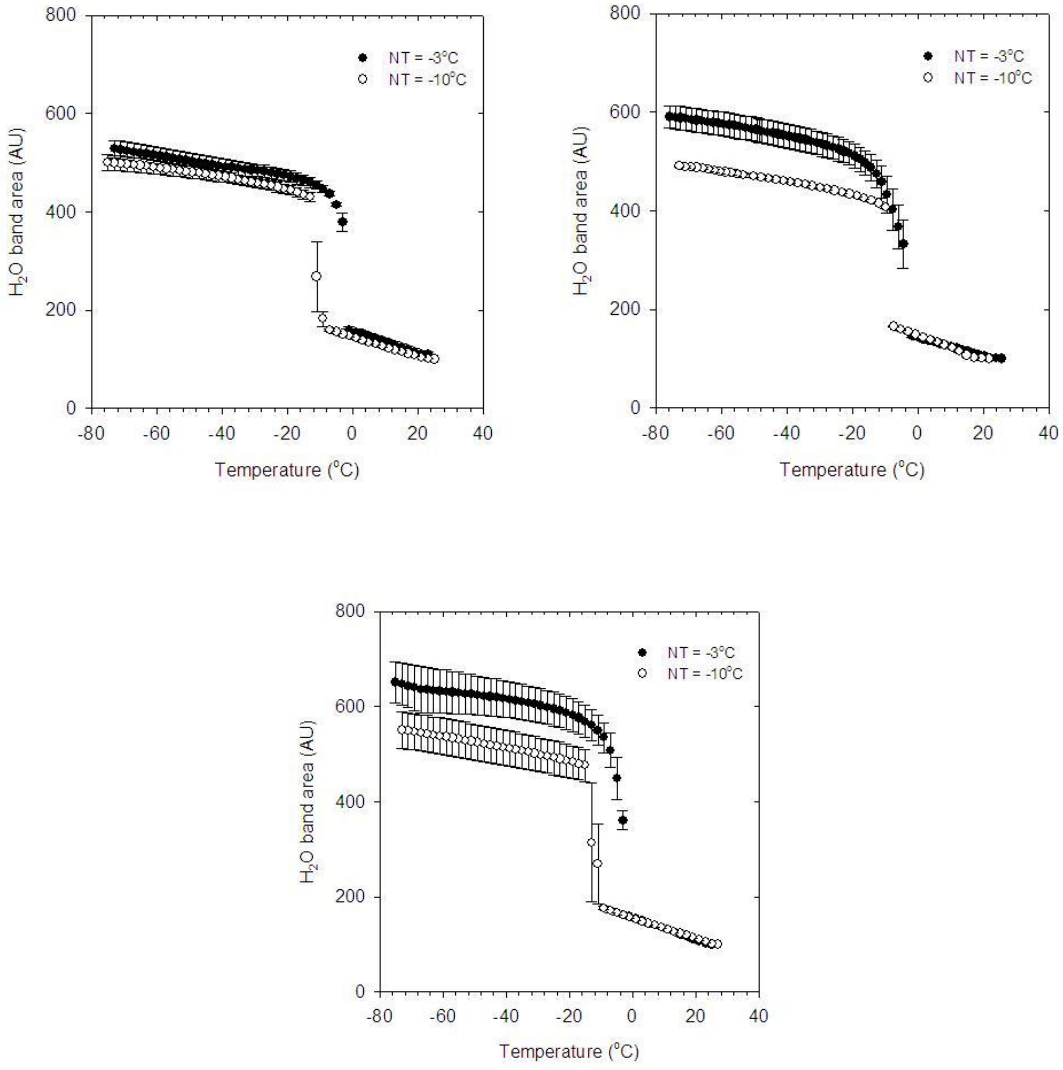

Figure 5.5: H_2O (water or ice) spectral band area versus temperature plots from room temperature to -80°C for (A) SMC, (B) LNCaP and (C) HDF cells with ice nucleation temperatures of –3°C (filled circles) and –10°C (open circles) with corresponding standard error (n = 3). In all cases, the total amount of ice that is formed under dehydrating freezing conditions (NT = -3°C) is greater than that under IIF conditions (NT = -10°C).

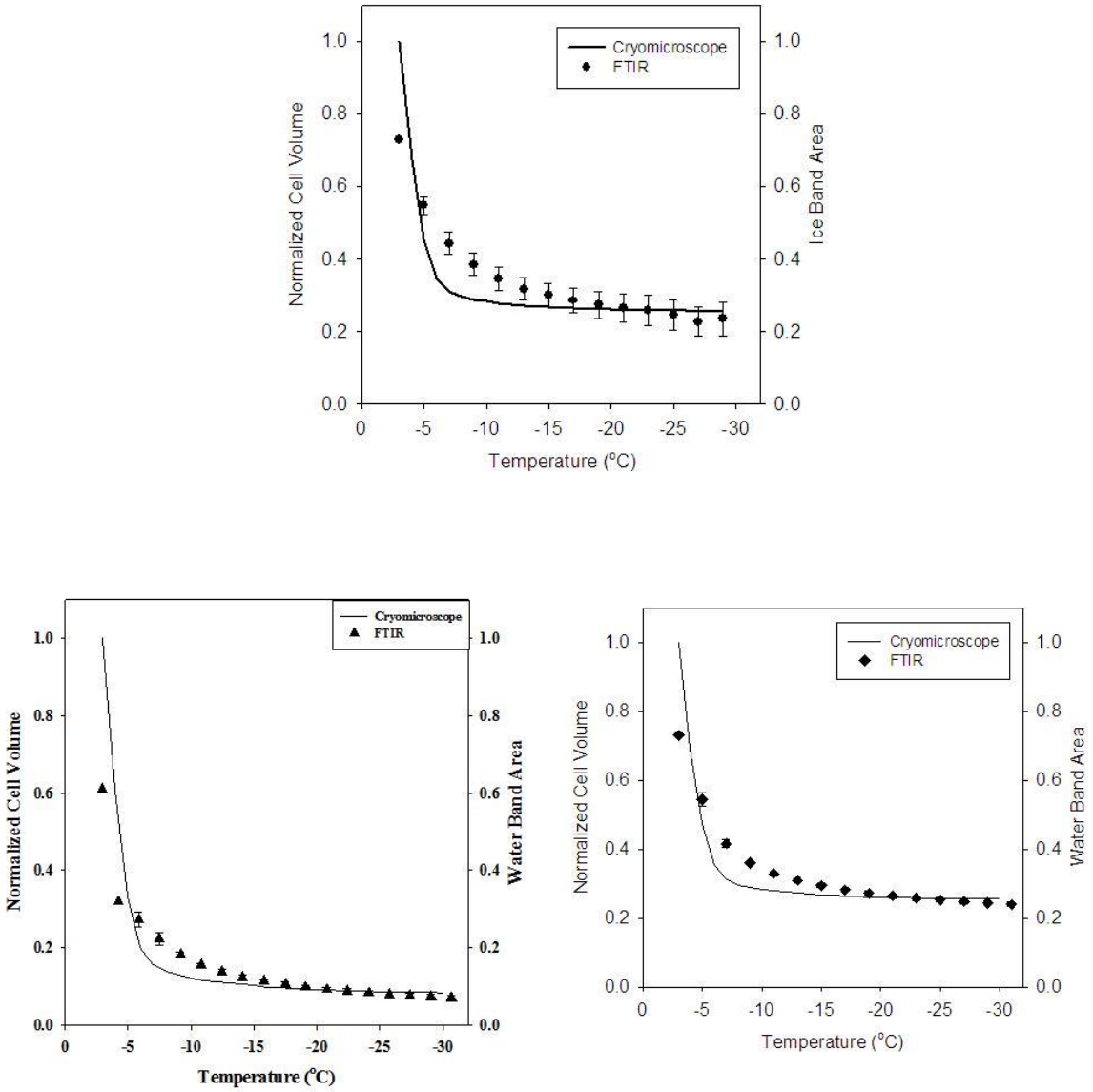

Figure 5.6: Comparison of the cellular volumetric changes as a result of freeze induced dehydration as predicted from FTIR spectral ice band area with cellular volume predicted from cryomicroscopy measurements **(4; 3; 5)** for (Top) SMC, (Bottom) LNCaP and HDF cells.

Figure 5.7 shows that the increased ice formation under dehydrating conditions coincides with strong membrane dehydration, suggesting that the extra ice in the system comes from bound or membrane associated water around lipids (and other biomolecules). A comparison of the first derivatives demonstrates that the maximum of water/ice band area

change during freezing closely coincides with the maximum of the membrane phase change, suggesting that the membrane phase change is lyotropic and the consequence of macromolecular dehydration.

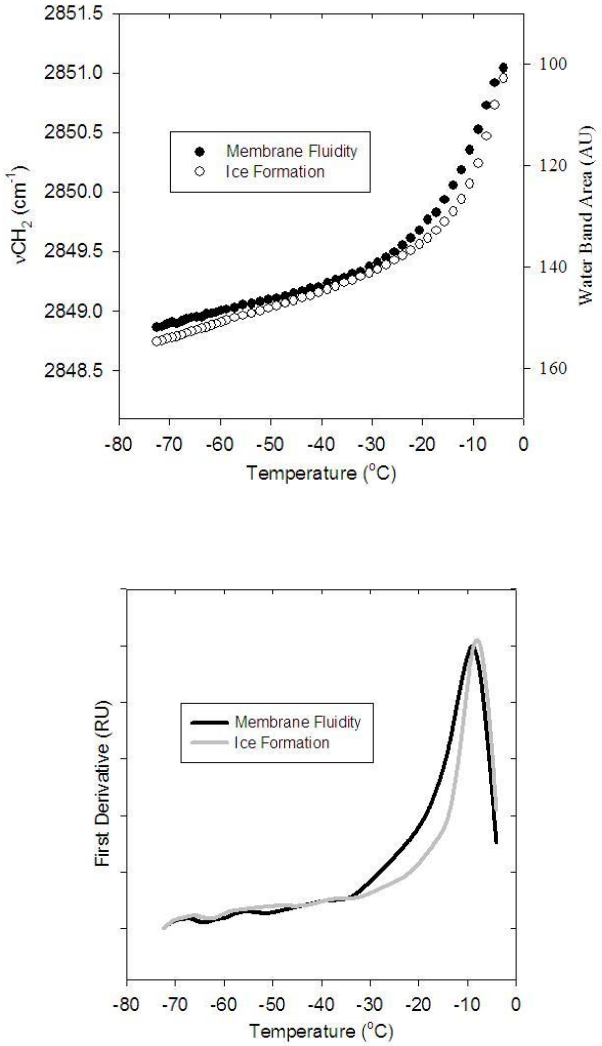

Figure 5.7: (Top) Cell membrane fluidity changes in LNCaP cells concomitantly with dehydration during freezing from -3°C to –80°C. (Bottom) First derivative of the changes in membrane fluidity and the water band area with temperature decrease for LNCaP cells.

5.4 DISCUSSION

Results from Chapter 4 shows that membrane lipid phase state during freezing correlates with cellular biophysics (i.e. dehydration and intracellular ice formation (IIF)) and viability post-freeze of LNCaP prostate cancer cells (3). Here we show the generality of this result in a variety of mammalian cells of varying size and biophysical properties (i.e. porcine smooth muscle cells (SMC) and human dermal fibroblasts (HDF)). In addition, we show that this lipid packing is a likely source of excess water/ice during phase change and the mechanism for reduction in water transport at subzero temperatures. Finally, the dramatic lipid packing during dehydration suggests a possible link to "solution effects" injury mechanism(s) (19).

5.4.1 Cell Biophysics

Unlike cryomicroscopy and DSC techniques that permit faster cooling rates, the FTIR method currently only allows for varying nucleation temperature while cooling rate is limited to 2°C/min. For ice nucleation at -3^{o}C and subsequent temperature decrease, the cells are subjected to increasing solute concentrations. To achieve chemical equilibrium the cells lose water to the extracellular media. However, this is not the case when ice nucleation occurs at -10^{o}C. In this case, all the supercooled water is trapped inside the cells leading to IIF. Thus, excess water from the dehydrating cell available from altered packing of macromolecular structures is expected to increase the total amount of extracellular ice when NT = -3^{o}C vs. -10^{o}C or below. This increased ice content under dehydrating conditions is captured in the increase in H_2O area during cooling. This

dehydration also coincides with a fluid to gel phase transition of the membranes (Figure 5.7). Specifically, a strong freezing induced lyotropic phase transition is observed during dehydrating conditions (NT = -3°C) indicating the removal of bound water predominantly around the lipid head groups that is otherwise unfrozen and unavailable for phase change during IIF conditions (NT = -10°C).

The excess H_2O band area is linked to cellular biophysics since this water is derived from the membrane during cellular dehydration, and is proportional to the normalized cell volume. This hypothesis is supported by DSC studies that suggested that excess heat is released from intact cells and tissues during freezing induced dehydration but not during IIF or lyses, and that this heat release correlates strongly to normalized cellular volume in the sample (83; 146). Applying this hypothesis to the FTIR data, the excess ice peak can be correlated to cellular dehydration. This data is then compared directly to cellular biophysical data to obtain a correlation to measurements from cryomicroscopy.

Cell dehydration during slow freezing as measured by FTIR matches reasonably well with cryomicroscopy data (Figure 5.6). It should be noted that the starting volumes are different and there is a slight lag in FTIR data vs. the cryomicroscopy data in the intermediate subzero temperature range (roughly -4 to -10°C). The starting volume difference can be explained by the fact that cryomicroscopy typically starts after seeding and equilibration at -1°C while FTIR is seeded at -3°C and below during continuous cooling. Additionally, the lag is attributed to cryomicroscopy being carried out on a cell suspension while FTIR is carried out on a cell pellet where cell density is expected to reduce dehydration kinetics as previously reported (39). With these caveats in mind FTIR

can be used to measure cellular biophysics provided the initial and non-solvent volumes of the given cell are known (V_o and V_b in Equation 5.3). Interestingly, the membrane phase change and corresponding lipid packing during cell freezing yield cell specific activation energies (Table 5.2) match closely to the activation energy of water transport (E_{Lp}) as measured by cryomicroscopy. This is highly suggestive that the lipid packing is in fact the mechanism that inhibits water transport at subzero temperatures.

5.4.2 Correlation to Cell Injury

Ice nucleation temperature has a profound effect on the membrane lipid phase behavior of the cells. It has been established that removal of water predominantly from the phospholipid head groups causes lyotropic phase transitions during air-drying (261). Freezing also has a dehydrating effect on liposomal systems (191). Here, we show that freezing can also cause such lyotropic phase changes in a variety of cells during freezing. The magnitude of freezing induced lyotropic membrane phase changes decreases with the extent of supercooling. During supercooling more water will be trapped inside the cells, which increases the incidence of IIF. For all cell types studied, the onset of the liquid crystalline to gel phase transition coincided with the ice nucleation temperature. It is shown that freezing induced water transport and membrane phase changes are closely associated events. The membrane phase behavior during freezing is a cell specific response, and must be associated with the cell's lipid composition and cholesterol content. In the case of the SMC, a thermotropic phase transition is evident prior to ice formation in the sample. However, the lyotropic phase transition upon ice nucleation is still greater than the thermotropic phase transition. Steponkus suggested that freezing

induced lamellar to hexagonal phase transition is responsible for cell death during freeze/thaw of plant protoplasts using freeze fracture analysis (29; 268). Our results in mammalian cells do not indicate formation of hexagonal phase during freezing but point to a tight gel phase packing. It has been established that lipid bilayers in liposomal systems exhibit maximal leakage of intra-liposomal contents right at the phase transition temperature (191). Hence, it is possible that freezing induced dehydration damage occurs as a result of leakage of cytoplasmic compounds during the phase transition either during cooling or rewarming. Nucleation at high subzero temperatures followed by slow cooling, which is known to cause 'solution effects injury', causes membranes to become severely dehydrated (19). These data suggests that a part of 'solution effects injury' is associated with extreme lipid packing due to loss of normally bound or membrane associated water around the phospholipid head groups.

In addition to quantifying the state of water and the membrane lipid phase changes in cells during freezing, FTIR can be used to simultaneously probe possible mechanisms of cellular injury. Figure 5.8 depicts the normalized lipid wavenumber (membrane phase state) of LNCaP cells under different nucleation temperatures against observed cell viability. An inverted U shape dependence (dotted line represents a typical cryobiological viability outcome) is predicted from experimental data (3). Minimal survival is obtained at the extremes (i.e. NT = -3 vs -10^{o}C) as a consequence of solution effects injury and IIF respectively which are linked here to residual membrane fluidity in the frozen state. The LNCaP membrane lipid wavenumber at -30^{o}C increases from its lowest during dehydration (2849.4 cm^{-1} @ -3^{o}C nucleation temperature NT) to its highest during IIF

(2850.5 cm^{-1} @ -10°C NT). At an intermediate nucleation temperature (-6°C), the lipid wavenumber observed is in between the dehydrated and the IIF conditions (2849.7 cm^{-1}). This is a consequence of a reduction in cell dehydration which allows a certain amount of cellular (and membrane) bound water to remain in the cell. It is this intermediary condition (for both NT and membrane fluidity) that we observed cell viability to be at its highest (3).

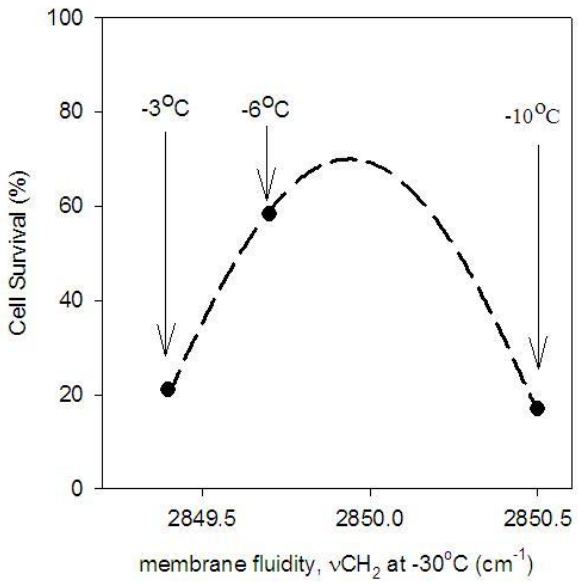

Figure 5.8: Membrane fluidity of LNCaP cells at -30°C under different ice nucleation temperatures vs. experimentally determined cell viability after freezing and thawing. The dotted line represents an inverted U shaped fit (generally associated with cellular viability under different nucleating conditions) to the representative points. Cell viability data on freeze survival obtained from Wolkers et al. (2007) were used to construct the plot.

The nucleation temperature yielding optimal survival coincides with intermediate residual membrane fluidity levels in the frozen state between dehydrating and IIF conditions. At room temperature equilibrium exists between the hydration forces and the

compressive stress of the lipid lamellae that maintains the rigidity of the lipid structure. However, as dehydration occurs, the lipid membrane adjusts to a new equilibrium state wherein it experiences an increase in the lateral compressive and hydration stresses. The increased lateral compressive stresses transition the lipid membrane from a liquid lamellar to a gel phase (172). When cell dehydration becomes more severe, the loss of lipid hydration and head group area correlates with increased cell death. This will lead to a continual decrease in the distance between lipid head groups and lipid lamellae as compared to its initial liquid state.

The reduction in head group area or hydration layers of the lipids below some critical value is therefore suggested by our studies as a possible cause of cell injury for the -3^{o}C NT cooling cases. These conditions expose the cell, and the biomolecules of the cell (including the membrane), to conditions of higher solute concentrations than during more rapid cooling where supercooling prevents high solutes exposure. This is believed to be at the heart of the "solution effects" mechanism of injury in cryobiology (19; 20). The current data is the one of the first to show the connection between cellular dehydration and membrane dehydration. We propose that this connection is also linked to a molecular mechanism of injury in "solution effects" injury that would suggest that membranes tolerate dehydration only to a certain extent. For instance, at -6^{o}C, the extent of lipid packing is not be as tight as for -3^{o}C NT and is more favorable for cell survival. This state is indeed intermediate between the highly fluid conditions found for IIF conditions (NT < -10 °C) and the extreme dehydration conditions (NT = -3 °C). Under

IIF conditions, ice formation appears to have little effect on the membrane, leaving lipids hydrated and in high conformation disorder.

5.5 SUMMARY

In this chapter, the molecular events associated with freezing of cells were studied for multiple cell types using FTIR. These molecular events are shown to be cell specific, and changes to membrane hydration during freezing are linked to cellular biophysical responses. Important results from the study are summarized below:

i. A highly co-operative membrane phase transition is noted when ice is nucleated at -3°C. The phase transition temperature of the membranes coincides with the ice nucleation temperature. Lysed cells or cells nucleated at approximately -10^{o}C showed a much less co-operative phase transition.

ii. Cell specific events associated with membrane hydration during freezing are identified. An Arrhenius relation was detected from the slope of the membrane hydration events, which linked well to the cellular activation energy for water transport across the membrane.

iii. Changes to the water band area of cells during freezing obtained from FTIR spectral analysis are linked to cell dehydration measured using a cryomicroscope. Membrane phase transition appears to be a lyotropic event resulting from the removal of bound water from membranes during slow freezing.

iv. The results show a connection between cellular dehydration and membrane dehydration. This connection is proposed to be linked to a molecular mechanism

of injury in “solution effects” injury that would suggest that membranes tolerate dehydration only to a certain extent.

6. RESEARCH SUMMARY

In this dissertation, studies were undertaken to investigate the effect of cell attachment on the "two factor" hypothesis of freezing. Additionally, molecular events – membrane phase transition and protein denaturation – associated with the biophysics of freezing cells were investigated and linked to potential injury events. The important results from the work are summarized below.

Impact of Cell Attachment on the Freezing Biophysics (Chapter 2 & 3)

The impact of cell attachment state - suspensions, monolayer, and tissue equivalents – on the biophysics of freezing was assessed for human dermal fibroblasts (HDF) and porcine smooth muscle cells (SMC).

i. The kinetics of intracellular ice formation (IIF) is higher for cells in the attached state as compared to suspensions (Tissue equivalents > Monolayer > Suspensions). At any given temperature and cooling rate, the incidence of IIF is higher in the attached state vs. suspensions.

ii. Permeability parameters, estimated using the cell biophysical models, are higher for cells in the attached state as compared to suspensions. Results indicate that both water transport and IIF are enhanced in the attached state as compared to suspensions.

iii. Cell-cell interactions are shown to play a role in the increased kinetics of IIF in the attached state. In the presence of a gap junction inhibitor, experimental data and the predicted IIF kinetics is lower for SMC in monolayer.

iv. The viability of cells post freeze/thaw is affected by the attachment state and the thermal conditions. Cell injury is linked to IIF at rapid freezing rates. At slow freezing rates, the biophysics would suggest cell viability to be markedly lower for attached cells. However, SMC exhibit higher viability in monolayer vs. suspension at slow freezing rates.

Molecular Events Linked to the Cellular Biophysical Responses (Chapter 4 & 5)

The molecular events associated with the biophysics of freezing cells were studied. More specifically, changes to the membrane phase transition and protein denaturation were studied using FTIR. Salient results from the studies are included below.

i. A highly co-operative membrane phase transition is noted when ice is nucleated at -3°C. The phase transition temperature of the membranes coincides with the ice nucleation temperature. Lysed cells or cells nucleated at approximately -10^{o}C showed a much less co-operative phase transition.

ii. Cell specific events associated with membrane hydration during freezing are identified. An Arrhenius relation was detected from the slope of the membrane hydration events, which linked well to the cellular activation energy for water transport across the membrane.

iii. Changes to the water band area of cells during freezing obtained from FTIR spectral analysis are linked to cell dehydration measured using a cryomicroscope. Membrane phase transition appears to be a lyotropic event resulting from the removal of bound water from membranes during slow freezing.

iv. Proteins are observed to be stable following freeze/thaw. Protein denaturation for LNCaP is reversible following freeze/thaw since subsequent heat denaturation profile is similar to control cells that did not undergo freezing.

v. The results show a connection between cellular dehydration and membrane dehydration. This connection is proposed to be linked to a molecular mechanism of injury in "solution effects" injury that would suggest that membranes tolerate dehydration only to a certain extent.

Future Directions

i. Our results indicate that water transport and IIF are both enhanced for attached cells as compared to suspensions. However, current experimental techniques limit our capability to measure cell volume in a 3D configuration to verify the model predictions. Future work involving the development of novel experimental techniques to measure cell volume changes and freezing biophysics in a 3D configuration would be highly beneficial to the field.

ii. Molecular events associated with the biophysics of freezing cell suspensions were studied. Future work is needed to study the same for cells in the attached state including monolayer and tissue equivalents. Development of experimental techniques in parallel is needed to further the understanding of molecular events associated with freezing. For example, Dong et al. (2010) have used Confocal Raman spectroscopy to assess changes at the molecular level to attached cells during freezing (167).

7. BIBLIOGRAPHY

1. *Revival of spermatozoa after vitrification and dehydration at low temperatures.* **Polge, C, Smith, A.U and Parkes, A.S.** 1949, Nature, Vol. 164, p. 666.

2. *Frozen red cells.* **Meryman, HT.** 2, April 1989, Transfusion Medicine Reviews, Vol. 3, pp. 121 - 127.

3. *Cryopreservation of red blood cells.* **Rowe, AW.** Suppl 3, 1994, Vox Sang, Vol. 67, pp. 201 - 206.

4. *Cryopreservation of human oocytes: A review of current problems and perspectives.* **Bernard, A and Fuller, BJ.** 3, 1996, Human Reprod Update, Vol. 2, pp. 193 - 207.

5. *Cryopreservation of human granulocytes: Study of granulocyte function and ultrastructure.* **Boonlayangoor, P, et al.** 2, August 1980, Blood, Vol. 56, pp. 237 - 245.

6. *Cryopreservation of vascular endothelial cells as isolated cells and as monolayers.* **Pegg, DE.** 1, February 2002, Cryobiology, Vol. 44, pp. 46 - 53.

7. *Cryopreservation of equine sperm: Optimal cooling rates in the presence and absence of cryoprotective agents determined using Differential Scanning Calorimetry.* **Devireddy, RV, et al.** 1, January 2002, Biology of Reproduction, Vol. 66, pp. 222 - 231.

8. *The cryobiology of cryosurgical injury.* **Hoffmann, NE and Bischof, JC.** 2 Suppl 1, August 2002, Urology, Vol. 60, pp. 40 - 49.

9. *Experimental cryosurgery investigations in vivo.* **Gage, AA, Baust, JM and Baust, JG.** 3, December 2009, Cryobiology, Vol. 59, pp. 229 - 243.

10. *Biopreservation of red blood cells: Past, present and future.* **Scott, KL, Lecak, J and Acker, JP.** 2, April 2005, Transfusion Medicine Reviews, Vol. 19, pp. 127 - 142.

11. *History of cryosurgery.* **Gage, AA.** 1998, Sem Surg Oncology, Vol. 14, pp. 99 - 109.

12. *Cryosurgery.* **Rubinsky, B.** 2000, Annual Rev Biomed Eng, Vol. 2, pp. 157 - 187.

13. *Freezing of living cells: Mechanisms and implications.* **Mazur, P.** 1984, American J of General Physiology, Vol. 247, pp. C125 - 142.

14. *Nucleation and growth of ice crystals inside cultured hepatocytes during freezing in the presence of dimethyl sulfoxide.* **Karlsson, JO, et al.** 6, December 1993, Biophysical J, Vol. 65, pp. 2524 - 2536.

15. *A parametric study of freezing injury in ELT-3 uterine leiomyoma tumour cells.* **Bischof, JC, et al.** 2, 2001, Human Reproduction, Vol. 16, pp. 340 - 348.

16. *A parametric study of freezing injury in AT-1 rat prostate tumor cells.* **Smith, DJ, et al.** 1, August 1999, Cryobiology, Vol. 39, pp. 13 - 28.

17. *Quantitative measurement and prediction of biophysical response during freezing in tissues.* **Bischof, JC.** 2000, Annual Reviews Biomedical Engineering, Vol. 2, pp. 257 - 288.

18. *A two factor hypothesis of freezing injury.* **Mazur, P, Leibo, S and Chu, E.H.Y.** 1972, Experimental Cell Research, Vol. 71, pp. 345 - 355.

19. *Basic investigations on the freezing of human lymphocytes.* **Scheiwe, MW and Korber, C.** 3, June 1983, Cryobiology, Vol. 20, pp. 257 - 273.

20. *Kinetics of water loss from cells at subzero temperatures and the likelihood of intracellular freezing.* **Mazur, P.** November 1963, J General Physiology, Vol. 47, pp. 347 - 369.

21. *Intracellular freezing of glycerolized red cells.* **Diller, KR.** 2, April 1979, Cryobiology, Vol. 16, pp. 125 - 131.

22. *The effect of various cooling rates on the membrane ultrastructure of frozen human erythrocytes and its relation to the extent of haemolysis after thawing.* **Fujikawa, S.** June 1981, J Cell Sci, Vol. 49, pp. 369 - 382.

23. *Cryopreservation of cultured skin cells.* **Kearney, JN.** 5, October 1991, Burns, Vol. 17, pp. 380 - 383.

24. *Cryopreservation of isolated rat hepatocytes.* **Novicki, DL, et al.** 4, 1982, In Vitro, Vol. 18, pp. 393 - 399.

25. *Cooling rate dependent biophysical and viability response shift with attachment state in human dermal fibroblast cells.* **Choi, J and Bischof, JC.** 3, October 2011, Cryobiology, Vol. 63.

26. *Thermodynamic analysis of the permeability of biological membranes to non-electrolytes.* **Kedem, O and Katchalsky, A.** 2, February 1958, Biochim Biophys Acta, Vol. 27, pp. 229 - 246.

27. *Water transport in a cluster of closely packed erythrocytes at subzero temperatures.* **Levin, RL, Cravalho, EG and Huggins, CE.** 5, October 1977, Cryobiology, Vol. 14, pp. 549 - 558.

28. *Simplified calculation of cell water content during freezing and thawing in nonideal solutions of cryoprotective agents and its possible application to the study of "solution effects" injury.* **Fahy, GM.** 5, October 1981, Cryobiology, Vol. 18, pp. 473 - 482.

29. *Thermodynamics and kinetics of intracellular ice formation during freezing of biological cells.* **Toner, M, Cravalho, EG and Marcus, K.** 3, February 1990, J Applied Physics, Vol. 67, pp. 1582 - 1593.

30. *Intracellular ice formation: Causes and consequences.* **Karlsson, JO, Cravalho, EG and Toner, M.** 1993, Cryo-Letters, Vol. 14, pp. 323 - 334.

31. *Cryobiology of rat embryos II: A theoretical model for the development of interrupted slow freezing procedures.* **Liu, J, et al.** 5, November 2000, Biol Reprod, Vol. 63, pp. 1303 - 1312.

32. *A membrane model describing the effect of temperature on the water conductivity of erythrocyte membranes at subzero temperatures.* **Levin, RL, Cravalho, EG and Huggins, CE.** 4, August 1976, Cryobiology, Vol. 13, pp. 415 - 429.

33. **McGrath, JJ.** Preservation of biological material by freezing and thawing. [book auth.] A Shitzer and RC Eberhart. *Heat Transfer in Medicine and Biology.* New York : Plenum Press, 1985.

34. *The role of intracellular freezing in the death of cells cooled at supraoptimal rates.* **Mazur, P.** 3, June 1977, Cryobiology, Vol. 14, pp. 251 - 272.

35. **McGrath, JJ.** Membrane transport properties. [ed.] JJ McGrath and KR Diller. *Low Temperature Biotechnology: Emerging Applications and Engineering Contributions.* New York : ASME, 1988, pp. 273 - 330.

36. **Mazur, P.** Principles of cryobiology. [ed.] BJ Fuller, N Lane and EE Benson. *Life in the Frozen State.* s.l. : CRC Press LLC, 2004, 1, pp. 3 - 67.

37. *Membrane permeability modeling: Kedem-Katchalsky vs a two-parameter formalism.* **Kleinhans, FW.** 4, 1998, Cryobiology, Vol. 37, pp. 271 - 289.

38. *Osmotic transport across cell membranes in nondilute solutions: A new nondilute solute transport equation.* **Elmoazzen, HY, Elliott, JA and McGann, LE.** 7, April 2009, Biophysical J, Vol. 96, pp. 2559 - 2571.

39. *Hepatic tissue engineering. Development of critical technologies.* **Yarmush, ML, et al.** 665, October 1992, Annals of the New York Academy of Sciences, Vol. 13, pp. 238 - 252.

40. *Cryobiology: The freezing of biological systems.* **Mazur, P.** 934, May 22, 1970, Science, Vol. 168, pp. 939 - 949.

41. *Osmotic properties of the erythrocyte: III. The applicability of osmotic laws to the rate of hemolysis in hypotonic solutions of non-electrolytes.* **Jacobs, MH.** 1932, Biol Bull, Vol. 62, pp. 178 - 194.

42. *Frost injury in living cells.* **Asahina, E.** November 3, 1962, Nature, Vol. 196, pp. 445 - 446.

43. *The role of cell membranes in the freezing of yeast and other singe cells.* **Mazur, P.** 1965, Annals of the New York Academy of Sciences, Vol. 125, pp. 658 - 676.

44. *Physical factors implicated in the death of micro-organisms at subzero temperatures.* **Mazur, P.** 1960, Annals of the New York Academy of Sciences, Vol. 85, pp. 610 - 629.

45. **Mazur, P.** Physical and chemical basis of injury in single-celled micro-organisms subjected to freezing and thawing. [ed.] HT Meryman. *Cryobiology.* San Diego : Academic Press, 1966, pp. 214 - 315.

46. *Intercellular ice propagation: Experimental evidence for ice growth through membrane pores.* **Acker, JP, Elliott, JA and McGann, LE.** September 2001, Biophysical Journal, Vol. 81, pp. 1389 - 1397.

47. *Transport phenomena during freezing of isolated hepatocytes.* **Toner, M, et al.** 10, October 1992, AIChE J, Vol. 38, pp. 1512 - 1522.

48. *Quantitative analysis of the probability of intracellular ice formation during freezing of isolated protoplasts.* **Pitt, RE and Steponkus, PL.** 1, February 1989, Cryobiology, Vol. 26, pp. 44 - 63.

49. *Subfreezing volumetric behavior and stochastic modeling of intracellular ice formation in Drosophila melanogaster embryos.* **Pitt, RE, et al.** 1, February 1991, Cryobiology, Vol. 28, pp. 72 - 86.

50. *Performance of a kinetic model for intracellular ice formation based on the extent of supercooling.* **Pitt, RE, Chandrasekaran, M and Parks, JE.** 3, June 1992, Cryobiology, Vol. 29, pp. 359 - 373.

51. *Freezing characteristics of isolated pig and human hepatocytes.* **Darr, TB and Hubel, A.** 2, April 1997, Cell Transplantation, Vol. 6, pp. 173 - 183.

52. *Subzero osmotic characteristics of intact and disaggregated hepatocyte spheroids.* **Korniski, B, Darr, TB and Hubel, A.** 4, June 1999, Cryobiology, Vol. 38, pp. 339 - 352.

53. *Ice formation in isolated human hepatocytes and human liver tissue.* **Bischof, JC, et al.** 4, August 1997, ASAIO J, Vol. 43, pp. 271 - 278.

54. *Evaluation of freezing effects on human microvascular-endothelial cells (HMEC).* **Berrada, MS and Bischof, JC.** 6, December 2001, Cryo Letters, Vol. 22, pp. 353 - 366.

55. *Effects of freezing on membranes and proteins in LNCaP prostate tumor cells.* **Wolkers, WF, et al.** 3, March 2007, Biochimica et Biophysica Acta, Vol. 1768, pp. 728 - 736.

56. *Freezing characteristics of genetically modified lymphocytes for the treatment of MPS II.* **Hubel, A, Darr, TB and Norman, JA.** 5, October 1999, Cell Transplantation, Vol. 8, pp. 521 - 530.

57. *Thermal injury prediction during Cryoplasty through in vitro characterization of smooth muscle cell biophysics and viability.* **Balasubramanian, SK, et al.** 1, Januart 2008, Annals of Biomedical Engineering, Vol. 36, pp. 86 - 101.

58. *Water transport and IIF parameters for a connective tissue equivalent.* **Balasubramanian, S.K, Bischof, J.C and Hubel, A.** 2005, Cryobiology, Vol. 52, pp. 62 - 73.

59. *Nonequilibrium freezing of one-cell mouse embryos. Membrane integrity and developmental potential.* **Toner, M, et al.** 6, June 1993, Biophysical J, Vol. 64, pp. 1908 - 1921.

60. *Water transport and estimated transmembrane potential during freezing of mouse oocytes.* **Toner, M, Cravalho, EG and Armant, DR.** 3, May 1990, J Membrane Biology, Vol. 115, pp. 261 - 272.

61. *Cryobiophysical characteristics of genetically modified hematopoietic progenitor cells.* **Hubel, A, Norman, J and Darr, TB.** 2, March 1999, Cryobiology, Vol. 38, pp. 140 - 153.

62. *Cryobiology of non-human primate oocyte.* **Younis, A, et al.** 1, January 1996, Human Reproduction, Vol. 11, pp. 156 - 165.

63. *Pioneers in cryobiology: Julius von Sachs (1832 - 1897).* **Diller, KR.** 1996, Cryo-Letters, Vol. 17, pp. 201 - 212.

64. *[English Translation: Investigations into the freezing of plants].* **Molish, H.** 1897 [1982], [Cryo-Letters], Vol. [3], pp. [331 - 390].

65. *Untersuchungen uber das Auswintern des Getreides.* **Schander, R and Schaffnit, E.** 1918, Landwirt. Jahrb. , Vol. 52, pp. 1 - 66.

66. *Apparatus for cinemicrography during rapid freezing.* **Rapatz, G and Luyet, B.** 1957, Biodynamica, Vol. 7, pp. 347 - 355.

67. *Microscopic observation of living cells during freezing and thawing.* **Smith, AU, Polge, C and Smiles, J.** 2, September 1951, J Royal Microscopical Society, Vol. 71, pp. 186 - 195.

68. *Freezing of nonwoody plant tissues: III. Videotape micrography and the correlation between individual cellular freezing events and temperature changes in the surrounding tissue.* **Brown, MS and Reuter, MW.** 1974, Cryobiology, Vol. 11, pp. 185 - 191.

69. *A cryomicroscope for the study of freezing and thawing processes in biological cells.* **Diller, KR and Cravalho, EG.** 4, December 1970, Cryobiology, Vol. 7, pp. 191 - 199.

70. *An experimental comparison of intracellular ice formation and freeze-thaw survival of HeLa S-3 cells.* **McGrath, JJ, Cravalho, EG and Huggins, CE.** 6, December 1975, Cryobiology, Vol. 12, pp. 540 - 550.

71. *Engineering-based contributions in cryobiology.* **Diller, KR.** 4, June 1997, Cryobiology, Vol. 34, pp. 304 - 314.

72. *Quantitative measurement of cell membrane transport: Technology and applications.* **McGrath, JJ.** 4, June 1997, Cryobiology, Vol. 34, pp. 315 - 334.

73. *Computer recognition and analysis of freezing cells in noisy, cluttered images.* **Dietz, TE, et al.** 5, October 1982, Cryobiology, Vol. 19, pp. 539 - 549.

74. *Automated computer evaluation of time-varying cryomicroscopical images.* **Dietz, TR, Diller, KR and Aggarwal, JK.** 2, April 1984, Cryobiology, Vol. 21, pp. 200 - 208.

75. *Automated computer analysis of cell size changes during cryomicroscope freezing: A biased trident convolution mask technique.* **Diller, KR and Knox, JM.** 1983, Cryo-Letters, Vol. 4, pp. 77 - 92.

76. *Formation and melting of intracellular ice in granulocytes.* **Scheiwe, MW and Korber, C.** 1982, Cryo-Letters, Vol. 3, pp. 275 - 284.

77. *Visualization of intracellular ice formation using high-speed video cryomicroscopy.* **Stott, SL and Karlsson, JOM.** 1, February 2009, Cryobiology, Vol. 58, pp. 84 - 95.

78. *Measurement of water transport during freezing in cell suspensions using a Differential Scanning Calorimeter.* **Devireddy, RV, Raha, D and Bischof, JC.** 2, March 1998, Cryobiology, Vol. 36, pp. 124 - 155.

79. **Devireddy, RV and Bischof, JC.** Recent advances in cryobiology using calorimetry. [book auth.] S Kakac, HF Smirnov and MR Avelino. *Low temperature and cryogenic refrigeration.* Dordrecht : Kluwer Academic Publishers, 2003, pp. 265 - 295.

80. *A microscope diffusion chamber for the determination of the equilibrium and non-equilibrium osmotic response of individual cells.* **McGrath, JJ.** Pt 3, September 1985, J Microscopy, Vol. 139, pp. 249 - 263.

81. *Quantitative light microscopy of combined perfusion and freezing processes.* **Walcerz, DB and Diller, KR.** Pt 2, February 1991, J Microscopy, Vol. 161, pp. 297 - 311.

82. *Development of a novel microperfusion chamber for determination of cell membrane transport properties.* **Gao, DY, et al.** 1, July 1996, Biophysical J, Vol. 71, pp. 443 - 450.

83. *Osmotic shrinkage of giant egg-lecithin vesicles.* **Boroske, E, Elwenspoek, M and Helfrich, W.** 1, April 1981, Biophysical J, Vol. 34, pp. 95 - 109.

84. *Osmotic water permeability of human red cells.* **Terwilliger, TC and Solomon, AK.** 5, May 1981, J Gen Physiol, Vol. 77, pp. 549 - 570.

85. *Effect of osmolality on the hydraulic permeability coefficient of red cells.* **Rich, GT, et al.** 6, December 1968, J Gen Physiol, Vol. 52, pp. 941 - 954.

86. *Water permeability and its activation energy of fertilized and unfertilized mouse ova.* **Leibo, SP.** 3, 1980, J Membrane Biology, Vol. 53, pp. 179 - 188.

87. *The influence of cooling rate on survival of frozen cells differs in monolayers and in suspensions.* **Armitage, WJ and Juss, BK.** 1996, Cryo-Letters, Vol. 17, pp. 213 - 218.

88. *Microcomputer interface for rapid measurements of average volume using an electronic particle counter.* **McGann, LE, Turner, AR and Turc, JM.** 1, January 1982, Med Biol Eng Comput, Vol. 20, pp. 117 - 120.

89. *Fundamental cryobiology of selected African mammalian spermatozoa and its role in biodiversity preservation through the development of genome resource banking.* **Gilmore, JA, et al.** 1 - 4, 1998, Animal Reproduction Science, Vol. 53, pp. 277 - 297.

90. *Analysis of the water permeability of human granulocytes at subzero temperatures in the presence of extracellular ice.* **Schwartz, GJ and Diller, KR.** 4, November 1983, J Biomechanical Engineering, Vol. 105, pp. 360 - 366.

91. *Thermodynamic modeling and cryomicroscopy of cell-size, unilamellar, and paucilamellar liposomes.* **Callow, RA and McGrath, JJ.** 3, June 1985, Cryobiology, Vol. 22, pp. 251 - 267.

92. *Cryomicroscopic determination of the membrane osmotic properties of human monocytes at subfreezing temperatures.* **McCaa, C, et al.** 4, August 1991, Cryobiology, Vol. 28, pp. 391 - 399.

93. *Hydraulic permeability and activation energy of human keratinocytes at subzero temperatures.* **Aggarwal, SJ, Diller, KR and Baxter, CR.** 3, June 1988, Cryobiology, Vol. 25, pp. 203 - 211.

94. *The osmotic rupture hypothesis of intracellular freezing injury.* **Muldrew, K and McGann, LE.** 2 Pt 1, February 1994, Biophysical J, Vol. 66, pp. 532 - 541.

95. *Cryopreservation and biophysical properties of articular cartilage chondrocytes.* **Wu, WT, Lyu, SR and Hsieh, WH.** 3, December 2005, Cryobiology, Vol. 51, pp. 330 - 338.

96. *The effect of dimethylsulfoxide on the water transport response of rat hepatocytes during freezing.* **Smith, DJ, Schulte, M and Bischof, JC.** 5, October 1998, J Biomechanical Engineering, Vol. 120, pp. 549 - 558.

97. *Microscopic and calorimetric assessment of freezing processes in uterine fibroid tumor tissue.* **Devireddy, RV, Coad, JE and Bischof, JC.** 4, June 2001, Cryobiology, Vol. 42, pp. 225 - 243.

98. *Osmometric behavior, hydraulic conductivity, and incidence of intracellular ice formation in bovine oocytes at different developmental stages.* **Ruffing, NA, Steponkus, PL, Pitt, RE and Parks, JE.** 6, 1993, Cryobiology, Vol. 30, pp. 562 - 580.

99. *Subzero water transport characteristics of boar spermatozoa confirm observed optimal cooling rates.* **Devireddy, RV, et al.** 4, April 2004, Molecular Reproduction and Development, Vol. 67, pp. 446 - 457.

100. *Cryopreservation of canine spermatozoa: Theoretical prediction of optimal cooling rates in the presence and absence of cryoprotective agents.* **Thirumala, S, et al.** 2, October 2003, Cryobiology, Vol. 47, pp. 109 - 124.

101. *Effect of glycerol and cholesterol-loaded cyclodextrin on freezing-induced water loss in bovine spermatozoa.* **Li, G, et al.** 5, May 2006, Reproduction, Vol. 131, pp. 875 - 886.

102. *Cellular biophysics during freezing of rat and mouse sperm predicts post-thaw motility.* **Hagiwara, M, et al.** 4, October 2009, Biology of Reproduction, Vol. 81, pp. 700 - 706.

103. *Subzero water permeability parameters of mouse spermatozoa in the presence of extracellular ice and cryoprotective agents.* **Devireddy, RV, et al.** 3, September 1999, Biology of Reproduction, Vol. 61, pp. 764 - 775.

104. *Water transport in epididymal and ejaculated rhesus monkey (Macaca Mulatta) sperm during freezing.* **Alapati, R, et al.** 2, October 2008, Cryobiology, Vol. 57, pp. 182 - 185.

105. *The effect of extracellular ice and cryoprotective agents on the water permeability parameters of human sperm plasma membrane during freezing.* **Devireddy, RV, et al.** 5, May 2000, Human Reproduction, Vol. 15, pp. 1125 - 1135.

106. *Subzero water permeability parameters and optimal freezing rates for sperm cells of the southern platyfish, Xiphophorus maculatus.* **Pinisetty, D, et al.** 3, June 2005, Cryobiology, Vol. 50, pp. 250 - 263.

107. *The haemolysis of human red blood-cells by freezing and thawing.* **Lovelock, JE.** 3, March 1953, Biochimica Biophysica Acta, Vol. 10, pp. 414 - 426.

108. *Cryopreservation of spinach chloroplast membranes by low-molecular-weight carbohydrates.II. Discrimination between colligative and noncolligative protection.* **Santarius, KA and Giersch, C.** 1, February 1983, Cryobiology, Vol. 20, pp. 90 - 99.

109. *Modified model for the mechanism of freezing injury in erythrocytes.* **Meryman, HT.** 5139, April 1968, Nature, Vol. 218, pp. 333 - 336.

110. *Freezing injury from "solution effects" and its prevention by natural or artificial cryoprotection.* **Meryman, HT, Williams, RJ and Douglas, MS.** 3, June 1977, Cryobiology, Vol. 14, pp. 287 - 302.

111. *The osmometric behavior of human erythrocytes.* **Wiest, SC and Steponkus, PL.** 1, February 1979, Cryobiology, Vol. 16, pp. 101 - 104.

112. *On the mechanism of injury to slowly frozen erythrocytes.* **Pegg, DE and Diaper, MP.** 3, September 1988, Biophysical J, Vol. 54, pp. 471 - 488.

113. *Physical instability and thermal shock in red cells.* **Lovelock, JE.** 4406, April 10, 1954, Nature, Vol. 173, pp. 659 - 661.

114. *Effects of cooling rate on thermal shock hemolysis.* **Morris, GJ and Farrant, J.** 2, June 1973, Cryobiology, Vol. 10, pp. 119 - 125.

115. *Freeze/thaw-induced destabilization of the plasma membrane and the effects of cold acclimation.* **Steponkus, PL and Lynch, DV.** 1, February 1989, J Bioenergetics Biomembranes, Vol. 21, pp. 21 - 41.

116. *The salting-in hypothesis of post-hypertonic lysis.* **Muldrew, K.** 3, December 2008, Cryobiology, Vol. 57, pp. 251 - 256.

117. *The formation of ice in protoplasm.* **Chambers, R and Hale, HP.** 1932, Proc. Roy. Soc. London B, Vol. 110, pp. 336 - 352.

118. *A theoretical model of intracellular devitrification.* **Karlsson, JO.** 3, May 2001, Cryobiology, Vol. 42, pp. 154 - 169.

119. *Mechanisms of intracellular ice formation.* **Muldrew, K and McGann, LE.** 3, March 1990, Biophysical J, Vol. 57, pp. 525 - 532.

120. *Thermal shock and dilution shock as the causes of freezing injury.* **Farrant, J and Morris, GJ.** 2, June 1973, Cryobiology, Vol. 10, pp. 134 - 140.

121. *Use of two-step cooling procedures to examine factors influencing cell survival following freezing and thawing.* **Farrant, J, et al.** 3, June 1977, Cryobiology, Vol. 14, pp. 273 - 286.

122. *A sulfhydryl-disulfide hypothesis of frost injury and resistance in plants.* **Levitt, J.** 1962, J Theoret Biol, Vol. 3, pp. 355 - 391.

123. *Phenomenology of intracellular ice nucleation in isolated protoplasts.* **Steponkus, PL and Dowgert, MF.** 1981, Plant Physiology, Vol. 67, pp. S-58.

124. *The response of multilamellar liposomes to freezing and thawing.* **Morris, GJ and McGrath, JJ.** 4, 1981, Cryobiology, Vol. 18, pp. 390 - 398.

125. *Innocuous intracellular ice improves survival of frozen cells.* **Acker, JP and McGann, LE.** 6, 2002, Cell Transplant, Vol. 11, pp. 563 - 571.

126. *A stable state of frozen protoplasm with invisible intracellular ice crystals obtained by rapid cooling.* **Asahina, E, Shimada, K and Hisada, Y.** 3, 1970, Exp Cell Res, Vol. 59, pp. 349 - 358.

127. *Survival of higher animal cells after the formation and dissolution of intracellular ice.* **Sherman, JK.** 1962, Anat Rec, Vol. 144, pp. 171 - 189.

128. *Visualization of intracellular ice crystals formed in very rapidly frozen cells at -27 degree C.* **Shimada, K and Asahina, E.** 3, 1975, Cryobiology, Vol. 12, pp. 209 - 218.

129. *Large ice crystals in the nucleus of rapidly frozen liver cells.* **Bischof, JC and Rubinsky, B.** 6, 1993, Cryobiology, Vol. 30, pp. 597 - 603.

130. *Studies on cellular structure and ice location in frozen organs and tissues: The use of freeze-substitution and related techniques.* **Hunt, CJ.** 4, August 1984, Cryobiology, Vol. 21, pp. 385 - 402.

131. *Cell-cell contact affects membrane integrity after intracellular freezing.* **Acker, JP and McGann, LE.** 1, February 2000, Cryobiology, Vol. 40, pp. 54 - 63.

132. *Membrane damage occurs during the formation of intracellular ice.* **Acker, JP and McGann, LE.** 4, 2001, Cryo-Letters, Vol. 22, pp. 241 - 254.

133. *Morphological and phenotypical characterization of human endothelial progenitor cells in an early stage of differentiation.* **Bellik, L, Ledda, F and Parenti, A.** 2005, FEBS Letters, Vol. 579, pp. 2731 - 2736.

134. *Geometric control of cell life and death.* **Chen, CS, et al.** 5317, May 30, 1997, Science, Vol. 276, pp. 1425 - 1428.

135. *The influence of extracellular matrix on gene expression: Is structure the message?* **Bissell, MJ and Barcellos-Hoff, MH.** 1987, J Cell Sci Suppl, Vol. 8, pp. 327 - 343.

136. *Expression of extracellular matrix components is regulated by substratum.* **Streuli, CH and Bissell, MJ.** 4, April 1990, J Cell Biol, Vol. 110, pp. 1405 - 1415.

137. *The organizing principle: Microenvironmental influences in the normal and malignant breast.* **Bissell, MJ, et al.** 9 - 10, December 2002, Differentiation, Vol. 70, pp. 537 - 546.

138. *Phospholipids undergo hop diffusion in compartmentalized cell membrane.* **Fujiwara, T, et al.** 6, June 2002, J Cell Biol, Vol. 157, pp. 1071 - 1081.

139. *Mediation, modulation, and consequences of membrane-cytoskeleton interactions.* **Doherty, GJ and McMahon, HT.** 2008, Annu Rev Biophys, Vol. 37, pp. 65 - 95.

140. *The cytoskeleton and cell volume regulation.* **Pedersen, SF, Hoffmann, EK and Mills, JW.** 3, October 2001, Comp Biochem Physiol A Mol Integr Physiol, Vol. 130, pp. 385 - 399.

141. *Direct observations of the mechanical behaviors of the cytoskeleton in living fibroblasts.* **Heidemann, SR, et al.** 1, April 1999, J Cell Biol, Vol. 145, pp. 109 - 122.

142. *Cytoskeletal regulation of membrane transport events.* **Mills, JW and Mandel, LJ.** 14, November 1994, FASEB J, Vol. 8, pp. 1161 - 1165.

143. *Mutations of the red blood cell membrane proteins: From clinical evaluation to detection of the underlying genetic defect.* **Palek, J and Sahr, KE.** 2, July 1992, Blood, Vol. 80, pp. 308 - 330.

144. *Response of the cell-membrane cytoskeleton complex to osmotic and freeze/thaw stresses.* **Ragoonan, V, Hubel, A and Aksan, A.** 3, December 2010, Cryobiology, Vol. 61, pp. 335 - 344.

145. *Ice formation and the death of plant cells by freezing.* **Stuckey, IH and Curtis, OF.** 1938, Plant Physiology, Vol. 13, pp. 815 - 833.

146. *Freeze-induced shrinkage of individual cells and cell-to-cell propagation of intracellular ice in cell chains from salivary glands.* **Berger, WK and Uhrik, B.** 9, September 15, 1996, Experientia, Vol. 52, pp. 843 - 850.

147. *Intracellular ice formation is affected by cell interactions.* **Acker, JP, et al.** 1999, Cryobiology, Vol. 38, pp. 363 - 371.

148. *Liver freezing response of the freeze-tolerant wood frog, Rana Sylvatica, in the presence and absence of glucose. II. Mathematical modeling.* **Devireddy, RV, et al.** 4, June 1999, Cryobiology, Vol. 38, pp. 327 - 338.

149. *A mathematical model for the freezing process in biological tissues.* **Rubinsky, B and Pegg, DE.** 1276, August 1988, Proc Royal Soc London B Biol Sci, Vol. 234, pp. 343 - 358.

150. *Water transport through a multicellular tissue during freezing: A network thermodynamic modeling analysis.* **Diller, KR and Raymond, JF.** 1990, Cryo-Letters, Vol. 11, pp. 151 - 162.

151. *Network thermodynamic model of coupled transport in a multicellular tissue - The islet of Langerhans.* **de Freitas, RC, et al.** 858, September 1998, Annals of New York Academy of Sciences, Vol. 11, pp. 191 - 204.

152. *A model of low-temperature water transport for hepatocyte spheroids.* **Korniski, B and Hubel, A.** September 11, 1998, Annals of the New York Academy of Sciences, Vol. 858, pp. 183 - 190.

153. *Kinetics and mechanism of intercellular ice propagation in a micropatterned tissue construct.* **Irimia, D and Karlsson, JOM.** 4, 2002, Biophysical Journal, Vol. 82, pp. 1858 - 1868.

154. *Kinetics of intracellular ice formation in one-dimensional arrays of interacting biological cells.* **Irimia, D and Karlsson, J.O.M.** January 2005, Biophysical Journal, Vol. 88, pp. 647 - 660.

155. *Modeling of cryopreservation of engineered tissue with one-dimensional geometry.* **Cui, ZF, et al.** 2, 2002, Biotechnology Progress, Vol. 18, pp. 354 - 361.

156. **Ball, P.** *H2O: A biography of water.* s.l. : Weidenfeld & Nicolson, 1999. p. 387. 0297643142, 9780297643142.

157. *Dielectric modulation of biological water.* **Despa, F, Fernandez, A and Berry, RS.** 22, November 2004, Physical Review Letters, Vol. 93, p. 228104.

158. *Probing the role of water in protein conformation and function.* **Rand, RP.** 1448, August 2004, Philos Trans R Soc Lond B Biol Sci, Vol. 359, pp. 1277 - 1284.

159. *Surface topography dependence of biomolecular hydrophobic hydration.* **Cheng, YK and Rossky, PJ.** 6677, April 1998, Nature, Vol. 392, pp. 696 - 699.

160. *Hydration structure of deoxyribonucleic acid and its physiochemical properties.* **Jacobson, B.** 4380, October 1953, Nature, Vol. 172, pp. 666 - 667.

161. *Is there a "hydrophobic effect"?* **Hildebrand, JH.** 1, January 1979, Proc Natl Acad Sciences USA, Vol. 76, p. 194.

162. *The origin of long-range attraction between hydrophobes in water.* **Despa, F and Berry, RS.** 2, January 15, 2007, Biophysics J, Vol. 92, pp. 373 - 378.

163. *Melting and freezing of water in ordered mesoporous silica materials.* **Schreiber, A, Ketelsen, I and Findenegg, GH.** 2001, Phys Chemistry Chem Phys, Vol. 3, pp. 1185 - 1195.

164. *First-order transition in confined water between high-density liquid and low-density amorphous phases.* **Koga, K, Tanaka, H and Zeng, XC.** 6812, November 30, 2000, Nature, Vol. 408, pp. 564 - 567.

165. *Freezing in yeast cells.* **Wood, TH and Rosenberg, AM.** 1, July 1957, Biochimica Biophysica Acta, Vol. 25, pp. 78 - 87.

166. *Interaction of cord factors (alpha, alpha'-trehalose-6,6'-dimycolate) with phospholipids.* **Crowe, LM, et al.** 1, August 1994, Biochim Biophys Acta, Vol. 1194, pp. 53 - 60.

167. *Use of nuclear magnetic-resonance to model thermophysical properties of frozen and unfrozen model food gels.* **Cornillon, P, et al.** 1995, J Food Eng, Vol. 25, pp. 1 - 19.

168. *Calorimetric properties of dehydrating pollen (Analysis of a dessication-tolerant and an intolerant species).* **Buitink, J, et al.** 1, May 1996, Plant Physiology, Vol. 111, pp. 235 - 242.

169. *Physical properties of cell water in partially dried Saccharomyces Cerevisiae.* **Koga, S, Echigo, A and Nunomura, K.** 5, September 1966, Biophysical J, Vol. 6, pp. 665 - 674.

170. *Calorimetric studies of freeze-induced dehydration of phospholipids.* **Bronshteyn, VL and Steponkus, PL.** 5, November 1993, Biophysical J, Vol. 65, pp. 1853 - 1865.

171. *Structure and dynamics of primary hydration shell of phosphatidylcholine bilayers at subzero temperatures.* **Hsieh, CH and Wu, WG.** 6, December 1996, Biophysical J, Vol. 71, pp. 3278 - 3287.

172. *Spatial distribution of the state of water in frozen mammalian cells.* **Dong, J, et al.** October 2010, Biophysical J, Vol. 99, pp. 2453 - 2459.

173. *State and phase transition behaviors of Querus Rubra seed axes and Cotyledonary tissues: Relevance to the dessication sensitivity and cryopreservation of recalcitrant seeds.* **Sun, WQ.** 4, June 1999, Cryobiology, Vol. 38, pp. 372 - 385.

174. *On bimolecular layers of lipoids on the chromocytes of the blood.* **Gorter, E and Grendel, F.** 1925, JEM, Vol. 41, p. 493.

175. *A contribution to the theory of permeability of thin films.* **Danielli, JF and Davson, H.** 4, 1935, J Cell Comp Phys, Vol. 5, p. 495.

176. *Physical principles of membrane organization.* **Israelachvili, JN, Marcelja, S and Horn, RG.** 2, May 1980, Q Reviews of Biophysics, Vol. 13, pp. 121 - 200.

177. *Freezing, drying, and/or vitrification of membrane-solute-water systems.* **Wolfe, J and Bryant, G.** 1999, Cryobiology, Vol. 39, pp. 103 - 129.

178. *The effects of temperature on biological membranes and their models.* **Lee, DC and Chapman, D.** 1987, Symposia of the Society for Experimental Biology, Vol. 41, pp. 35 - 52.

179. *Changes of membrane permeability due to extensive cholesterol depletion in mammalian erythrocytes.* **Grunze, M and Deuticke, B.** 1, July 12, 1974, Biochimica Biophysica Acta, Vol. 356, pp. 125 - 130.

180. *New insights into water-phospholipid model membrane interactions.* **Milhaud, J.** 1-2, May 27, 2004, Biochimica Biophysica Acta, Vol. 1663, pp. 19 - 51.

181. *The combined and separate effects of low temperature and freezing on membrane lipid mesomorphic phase behavior: Relevance to cryobiology.* **Caffrey, M.** 1, January 9, 1987, Biochimica Biophysica Acta, Vol. 896, pp. 123 - 127.

182. *Induction of anhydrobiosis: Membrane changes during drying.* **Crowe, JH and Crowe, LM.** 3, June 1982, Cryobiology, Vol. 19, pp. 317 - 328.

183. *The mechanical properties of the cell surface: I. The cell elastimeter .* **Mitchison, JM and Swann, MM.** 3, 1954, J Experimental Biology, Vol. 31, pp. 443 - 460.

184. *The mechanical properties of the cell surface: II. The unfertilized sea-urchin egg.* **Mitchison, JM and Swann, MM.** 3, September 1954, J Experimental Biology, Vol. 31, pp. 461 - 472.

185. *Mechanical properties of the plasma membrane of isolated plant protoplasts:Mechanism of hyperosmotic and extracellular freezing injury.* **Wolfe, J and Steponkus, PL.** 2, February 1983, Plant Physiology, Vol. 71, pp. 276 - 285.

186. *Hydration forces.* **Leikin, S, et al.** 1993, Annual Reviews of Physical Chemistry, Vol. 44, pp. 369 - 395.

187. *Measurement of forces between lecithin bilayers.* **LeNeveu, DM, Rand, RP and Parsegian, VA.** 5544, February 19, 1976, Nature, Vol. 259, pp. 601-603.

188. *Measurement of the lateral compressibility of several phospholipid bilayers.* **Lis, LJ, et al.** 3, March 1982, Biophysical J, Vol. 37, pp. 667 - 672.

189. *Role of hydration and water structure in biological and colloidal interactions.* **Israelachvili, J and Wennerstrom, H.** 6562, January 18, 1996, Nature, Vol. 379, pp. 219 - 225.

190. *Are lipid phase transitions responsible for chilling damage in human platelets?* **Crowe, JH, et al.** 3, May 1999, Cryobiology, Vol. 38, pp. 180 - 191.

191. *Thermotropic transitions in biomembranes.* **Melchior, DL and Steim, JM.** 1976, Annual Review of Biophysics Bioengineering, Vol. 5, pp. 205 - 238.

192. *Interactions of sugars with membranes.* **Crowe, JH, et al.** 2, June 9, 1988, Biochimica Biophysica Acta, Vol. 947, pp. 367 - 384.

193. *Phase transitions and fluidity characteristics of lipids and cell membranes.* **Chapman, D.** 2, May 1975, Q Reviews Biophysics, Vol. 8, pp. 185 - 235.

194. *Can hydration forces induce lateral phase separataions in lamellar phases?* **Bryant, G and Wolfe, J.** 6, 1989, Eur Biophysical J, Vol. 16, pp. 369 - 374.

195. *Dehydration-induced lamellar-to-hexagonal-II phase transitions in DOPE/DOPC mixtures.* **Webb, MS, Hui, SW and Steponkus, PL.** 1, January 18, 1993, Biochimica Biophysica Acta, Vol. 1145, pp. 93 - 104.

196. *Lamellar-to-hexagonal II phase transitions in the plasma membrane of isolated protoplasts after freeze-induced dehydration.* **Gordon-Kamm, WJ and Steponkus, PL.** 20, October 1984, Proceedings National Academy of Sciences USA, Vol. 81, pp. 6373 - 6377.

197. *Freeze-fracture cytochemistry: A new fracture-labeling method for topological analysis of biomembrane molecules.* **Takizawa, T and Robinson, JM.** 2, April 2000, Histology Histopathology, Vol. 15, pp. 515 - 522.

198. *Freeze-fracture replication techniques of human skin.* **Caputo, R and Gasparini, G.** 4, August 1982, J Cutaneous Pathology, Vol. 9, pp. 203 - 224.

199. *Water transport across biological membranes.* **Haines, TH.** 1, June 6, 1994, FEBS Letters, Vol. 346, pp. 115 - 122.

200. *Effects of lipid environment on membrane transport: The human erythrocyte sugar transport protein/lipid bilayer system.* **Carruthers, A and Melchior, DL.** 1988, Annual Review Physiology, Vol. 50, pp. 257 - 271.

201. *Erythrocyte permeability to lipophilic solutes changes with temperature.* **Garrick, RA, Patel, BC and Chinard, FP.** 1, January 1982, American J Physiology, Vol. 242, pp. C74 - C80.

202. *Permeability of lipid membranes revised in relation to freeze-thaw processes.* **Biondi, AC, Senisterra, GA and Disalvo, EA.** 3, June 1992, Cryobiology, Vol. 29, pp. 323 - 331.

203. *The structure of proteins. Two hydrogen-bonded helical configurations of the polypeptide chain.* **Pauling, L, Corey, RB and Branson, HR.** 4, April 1951, Proceedings National Academy of Sciences USA, Vol. 37, pp. 205 - 211.

204. *Principles that govern the folding of protein chains.* **Anfinsen, CB.** 96, July 20, 1973, Science, Vol. 181, pp. 223 - 230.

205. *Interfaces and the driving force of hydrophobic assembly.* **Chandler, D.** 7059, September 29, 2005, Nature, Vol. 437, pp. 640 - 647.

206. *Protein denaturation during freezing and thawing in phosphate buffer systems: Monomeric and tetrameric beta-galactosidase.* **Pikal-Cleland, KA, et al.** 2, December 15, 2000, Archives Biochemistry Biophysics, Vol. 384, pp. 398 - 406.

207. *Cold denaturation of myoglobin.* **Privalov, PL, et al.** 3, August 5, 19986, J Molecular Biology, Vol. 190, pp. 487 - 498.

208. *Cold denaturation of proteins.* **Privalov, PL.** 4, 1990, Crit Rev Biochemistry Mol Biology, Vol. 25, pp. 281 - 305.

209. *Quantification of temperature and injury response in thermal therapy and cryosurgery.* **He, X and Bischof, JC.** 5 - 6, 2003, Crit Rev Biomed Eng, Vol. 31, pp. 355 - 422.

210. *The hydrophobic effect and its role in cold denaturation.* **Dias, CL, et al.** 1, February 2010, Cryobiology, Vol. 60, pp. 91 - 99.

211. *Lipid and protein changes due to freezing in Dunning AT-1 cells.* **Bischof, JC, et al.** 1, August 2002, Cryobiology, Vol. 45, pp. 22 - 32.

212. *Tissue Engineering.* **Langer, R and Vacanti, JP.** 1993, Science, Vol. 260, pp. 920 - 926.

213. *A completely biological tissue-engineered human blood vessel.* **L'Heureux, N, et al.** 1, January 1998, FASEB J, Vol. 12, pp. 47 - 56.

214. *Living tissue formed in vitro and accepted as skin-equivalent tissue of full thickness.* **Bell, E, et al.** 4486, March 6, 1981, Science, Vol. 211, pp. 1052 - 1054.

215. *Small-diameter artificial arteries engineered in vitro.* **Isenberg, BC, Williams, C and Tranquillo, RT.** 1, January 2006, Circ Res, Vol. 98, pp. 25 - 35.

216. *Tissue engineering for anterior cruciate ligament reconstruction: A review of current strategies.* **Petrigliano, FA, McAllister, DR and Wu, BM.** 4, April 2006, Arthroscopy, Vol. 22, pp. 441 - 451.

217. *Intracellular ice formation in three-dimensional tissues: Pancreatic islets.* **de Freitas, RC and Diller, KR.** 1, July 5, 2004, Cell Preservation Technology, Vol. 2, pp. 19 - 28.

218. *Quantitative cryomicroscopic analysis of intracellular freezing of granulocytes without cryoadditive.* **Scheiwe, MW and Korber, C.** 5, October 1987, Cryobiology, Vol. 24, pp. 473 - 483.

219. **Bevington, PR and Robinson, DK.** *Data reduction and error analysis for the physical sciences.* New York : McGraw - Hill Inc, 1992.

220. *Cryomicroscope investigation and thermodynamic modeling of the freezing of unfertilized hamster ova.* **Shabana, M and McGrath, JJ.** 4, August 1988, Cryobiology, Vol. 25, pp. 338 - 354.

221. *Cryopreservation of collagen-tissue equivalents.I. Effect of freezing in the absence of cryoprotective agents.* **Devireddy, RV, et al.** 6, December 2003, Tissue Engineering, Vol. 9, pp. 1089 - 1100.

222. **Association, American Heart.** Peripheral Arterial Disease. *www.americanheart.org.* [Online] 2006.

223. **Altman, JD, Bayes, GA and Schwartz, RS.** Pathophysiology of Restenosis. [book auth.] DP Faxon. *Restenosis: A Guide to Therapy.* London : Martin Dunitz Ltd, 2001, pp. 9 - 19.

224. *Interventional therapy for coronary artery disease.* **Shah, PB and Lilly, CM.** 6, September 15, 2002, Am J Respir Crit Care Med, Vol. 166, pp. 791 - 796.

225. *Mechanisms of restenosis after coronary intervention: Difference between plain old balloon angioplasty and stenting.* **Nakatani, M, et al.** 1, 2003, Cardiovascular Pathology, Vol. 12, pp. 40 - 48.

226. *New approaches to preventing restenosis.* **Bhargava, B, et al.** 7409, August 2, 2003, BMJ, Vol. 327, pp. 274 - 279.

227. *Drug-coated stents: Preventing restenosis in coronary artery disease.* **Stanik-Hutt, JA.** 6, 2004, J Cardiovascular Nursing, Vol. 19, pp. 404 - 408.

228. **Lafontaine, DM.** *Cryoplasty Device and Method. 588735* United States, 1999.

229. *Differences in healing of skin wounds caused by burn and freeze injuries.* **Li, AK, et al.** 2, February 1980, Ann Surg, Vol. 191, pp. 244 - 248.

230. *Histologic differences between cryothermic and hyperthermic therapies.* **Coad, JE and Bischof, JC.** 2003, Proc SPIE, Vol. 4954, pp. 27 - 34.

231. *Biothermal modeling of post-cryoplasty atherosclerosis in restenotic patients.* **Men-Chi, H and Ravigururajan, TS.** 1, March 2007, Cardiovascular Engineering, Vol. 7, pp. 7 - 16.

232. *Cryosurgery - A review of recent advances and current issues.* **Gage, AA and Baust, JG.** 2002, Cryoletters, Vol. 23, pp. 69 - 78.

233. *Cryosurgery for tumors - A clinical overview.* **Gage, AA and Baust, JG.** 2, April 2004, Technol Cancer Res Treat, Vol. 3, pp. 187 - 199.

234. *Cryosurgery of normal and tumor tissue in the dorsal skin flap chamber: Part I - Thermal response.* **Hoffmann, NE and Bischof, JC.** 4, August 2001, J Biomech Engineering, Vol. 123, pp. 301 - 309.

235. *Cryosurgery of normal and tumor tissue in the dorsal skin flap chamber: Part II - Injury response.* **Hoffmann, NE and Bischof, JC.** 4, August 2001, J Biomech Eng, Vol. 123, pp. 310 - 316.

236. *Effects of intravascular cryotherapy on vessel wall repair in a balloon-injured rabbit iliac artery model.* **Cheema, AN, et al.** 1, July 1, 2003, Cardiovasc Res, Vol. 59, pp. 222 - 233.

237. *A cryoinjury model using engineered tissue equivalents for cryosurgical applications.* **Han, B, et al.** 7, July 2005, Annals of Biomedical Engineering, Vol. 33, pp. 972 - 982.

238. *In vivo analysis of microvascular injury after myocardial cryothermia.* **Huwer, H, et al.** 1, September 1998, J Surg Res, Vol. 79, pp. 1 - 7.

239. *Effects of freezing on cell viability and mechanisms of cell death in a human prostate cancer cell line.* **Hollister, WR, et al.** 1, 1998, Mol Urol, Vol. 2, pp. 13 - 18.

240. *In vitro model systems for evaluation of smooth muscle cell response to cryoplasty.* **Grassl, ED and Bischof, JC.** 2, April 2005, Cryobiology, Vol. 50, pp. 162 - 173.

241. *In vitro evaluation of vascular endothelial and smooth muscle cell survival and apoptosis in response to hypothermia and freezing.* **Tatsutani, KN, et al.** 1, 2005, Cryo Letters, Vol. 26, pp. 55 - 64.

242. *Analysis of thermal stress in cryosurgery of kidneys.* **He, X and Bischof, JC.** 4, August 2005, J of Biomechanical Engineering, Vol. 127, pp. 656 - 661.

243. *Thermodynamic nonequilibrium phase change behavior and thermal properties of biological solutions for cryobiology applications.* **Han, B and Bischof, JC.** 2, April 2004, J Biomech Eng, Vol. 126, pp. 196 - 203.

244. *Arterial dimensions in the lower extremities of patients with abdominal aortic aneurysms - no indications of a generalized dilating diathesis.* **Sandgren, T, et al.** 6, December 2001, J Vasc Surg, Vol. 34, pp. 1079 - 1084.

245. *An ultrasonic measurement of superficial femoral artery wall thickness.* **Beach, KW, et al.** 8, 1989, Ultrasound Med Biol, Vol. 15, pp. 723 - 728.

246. *Effects of freezing and cryopreservation on the mechanical properties of arteries.* **Venkatasubramanian, RT, et al.** 5, May 2006, Ann Biomed Eng, Vol. 34, pp. 823 - 832.

247. *Heterogeneity of smooth muscle cell populations cultured from pig coronary artery.* **Hao, H, et al.** 7, July 1, 2002, Arteriscler Thromb Vasc Biol, Vol. 22, pp. 1093 - 1099.

248. *Involvement of gap junctions in the manifestations and control of the duration of seizures in rats in vivo.* **Gajda, Z, et al.** 12, December 2003, Epilepsia, Vol. 44, pp. 1596 - 1600.

249. *Vascular gap junctions and implications for hypertension.* **Rummery, NM and Hill, CE.** 10, October 2004, Clin Exp Pharmacol Physiol, Vol. 31, pp. 659 - 667.

250. *Aortic smooth muscle cells in collagen lattice culture: Effects on ultrastructure, proliferation and collagen synthesis.* **Thie, M, et al.** 2, August 1991, Eur J Cell Biol, Vol. 55, pp. 295 - 304.

251. *Cellular components of the coronary vasculature exhibit differential sensitivity to low temperature insult.* **Hollister, WR, et al.** 4, July 5, 2004, Cell Preservation Technology, Vol. 1, pp. 269 - 280.

252. *Induction of apoptosis in human colon carcinoma cells HT29 by sublethal cryo-injury: Mediation by cytochrome c release.* **Hanai, A, Yang, WL and Ravikumar, TS.** 4, August 2001, Int J Cancer, Vol. 93, pp. 526 - 533.

253. *Introduction: Thermal ablation therapy.* **Stauffer, PR and Goldberg, SN.** 7, November 2004, Int J Hyperthermia, Vol. 20, pp. 671 - 677.

254. **Porter, A, et al.** Radiotherapy and cryotherapy for prostate cancer. [ed.] P Walsh, et al. *Campbell's Urology.* Philadelphia : Saunders Co, 1998, pp. 2605 - 2626.

255. *Roles of unfrozen fraction, salt concentration, and changes in cell volume in the survival of frozen human erythrocytes.* **Mazur, P and Cole, KW.** 1, February 1989, Cryobiology, Vol. 26, pp. 1 - 29.

256. *Extra- and intracellular ice formation in mouse oocytes.* **Mazur, P, et al.** 1, August 2005, Cryobiology, Vol. 51, pp. 29 - 53.

257. *Preservation of membranes in anhydrobiotic organisms: The role of trehalose.* **Crowe, JH, Crowe, LM and Chapman, D.** 4637, February 17, 1984, Science, Vol. 223, pp. 701 - 703.

258. *In situ detection and localization of lipid peroxidation in individual bovine sperm cells.* **Brouwers, JF and Gadella, BM.** 11, December 2003, Free Radic Biol Med, Vol. 35, pp. 1382 - 1391.

259. *Protein oxidation in aging, disease, and oxidative stress.* **Berlett, BS and Stadtman, ER.** 33, August 15, 1997, J Biol Chem, Vol. 272, pp. 20313 - 20316.

260. *Membrane isolation alters the gel to liquid crystal transition of Acholeplasma laidlawii B.* **Cameron, DG, Martin, A and Mantsch, HH.** 4581, January 1983, Science, Vol. 219, pp. 180 - 182.

261. *Amide modes and protein confirmation.* **Bandekar, J.** 2, April 8, 1992, Biochimica Biophysica Acta, Vol. 1120, pp. 123 - 143.

262. *Determination of protein secondary structure by Fourier transform infrared spectroscopy: A critical assessment.* **Surewicz, WK, Mantsch, HH and Chapman, D.** 2, January 1993, Biochemistry, Vol. 32, pp. 389 - 394.

263. *Determination of soluble and membrane protein structure by Fourier transform infrared spectroscopy. III. Secondary structures.* **Goormaghtigh, E, Cabiaux, V and Ruysschaert, JM.** 1994, Subcell Biochem, Vol. 23, pp. 405 - 450.

264. *In situ FTIR assessment of dessication-tolerant tissues.* **Wolkers, WF and Hoekstra, FA.** 2003, Spectroscopy, Vol. 17, pp. 297 - 313.

265. *A distinct utility of the amide III infrared band for secondary structure estimation of aqueous protein solutions using partial least squares method.* **Cai, S and Singh, BR.** 9, March 9, 2004, Biochemistry, Vol. 43, pp. 2541 - 2549.

266. *Fourier transform infrared spectrometric analysis of protein conformation: Effect of sampling method and stress factors.* **van de Weert, M, et al.** 2, October 15, 2001, Analytical Biochem, Vol. 297, pp. 160 - 169.

267. *Measured effect of collection and cooling conditions on the motility and the water transport parameters at subzero temperatures of equine spermatozoa.* **Devireddy, RV, et al.** 5, November 2002, Reproduction, Vol. 124, pp. 643 - 648.

268. *In situ assessment of erythrocyte membrane properties during cold storage.* **Wolkers, WF, et al.** 1, 2002, Mol Membr Biol, Vol. 19, pp. 59 - 65.

269. *Heat stability of proteins in dessication-tolerant cattail (Typha latifolia L.) pollen: A Fourier transform infrared spectroscopic study.* **Wolkers, WF and Hoekstra, FA.** 1997, Comp Biochem Physiol, Vol. 117, pp. 349 - 355.

270. *In situ thermal denaturation of proteins in Dunning AT-1 prostate cancer cells: Implication for hyperthermic cell injury.* **He, X, et al.** 10, October 2004, Ann Biomed Eng, Vol. 32, pp. 1384 - 1398.

271. *Lipid phase transitions measured in intact cells with Fourier transform infrared spectroscopy.* **Crowe, JH, et al.** 1, February 1989, Cryobiology, Vol. 26, pp. 76 - 84.

272. *Stabilization of dry membranes by mixtures of hydroxyethyl starch and glucose: The role of vitrification.* **Crowe, JH, et al.** 1, August 1997, Cryobiology, Vol. 35, pp. 20 - 30.

273. *Effects of the sugar headgroup of a glycoglycerolipid on the phase behavior of phospholipid model membranes in the dry state.* **Popova, AV and Hincha, DK.** 11, November 2005, Glycobiology, Vol. 15, pp. 1150 - 1155.

274. *Freezing and dessication tolerance in the moss Physcomitrella patens: An in situ Fourier transform infrared spectroscopic study.* **Oldenhof, H, et al.** 8, August 2006, Biochimica Biophysica Acta, Vol. 1760, pp. 1226 - 1234.

275. *The effect of ice on membrane lipid phase behavior.* **Sanderson, PW, et al.** 2, June 1993, Biochimica Biophysica Acta, Vol. 1148, pp. 278 - 284.

276. **Eyring, H.** Temperature. [ed.] FH Johnson, H Eyring and BJ Stover. *The Theory of Rate Processes in Biology and Medicine.* New York : John Wiley and Sons, 1974, pp. 155 - 272.

277. *The effect of stabilizers and denaturants on the cold denaturation temperatures of proteins and implications for freeze-drying.* **Tang, XC and Pikal, MJ.** 7, July 2005, Pharm Res, Vol. 22, pp. 1167 - 1175.

278. *Polymorphic phase behavior of phospholipid membranes studied by infrared spectroscopy.* **Casal, HL and Mantsch, HH.** 4, 1984, Biochimica Biophysica Acta, Vol. 779, pp. 381 - 401.

279. *Transformation of the cryobehavior of rye protoplasts by modification of the plasma membrane lipid composition.* **Steponkus, PL, et al.** 23, December 1988, Proc Natl Acad Sci USA, Vol. 85, pp. 9026 - 9030.

280. *Mechanical study of the deformation and rupture of the plasma membranes of protoplasts during osmotic expansions.* **Wolfe, J, Dowgert, MF and Steponkus, PL.** 1986, J Membrane Biol, Vol. 93, pp. 63 - 74.

281. *Freezing injury and its prevention in living cells.* **Meryman, HT.** 0, 1974, Annual Rev Biophys Bioeng, Vol. 3, pp. 341 - 363.

282. *The role of water in biomembrane structures.* **Chapman, D.** 1 - 4, 1994, J Food Eng, Vol. 22, pp. 367 - 380.

283. *Water (H2O and D2O) molar absorptivity in the 1000-4000 cm-1 range and quantitative infrared spectroscopy of aqueous solutions.* **Venyaminov, SY and Prendergast, FG.** 2, June 1, 1997, Analytical Biochem, Vol. 248, pp. 234 - 245.

284. *Measurement of water transport during freezing in mammalian liver tissue: Part II - The use of Differential Scanning Calorimetry.* **Devireddy, RV and Bischof, JC.** 5, October 1998, J Biomechanical Engineering, Vol. 120, pp. 559 - 569.

285. *Factors affecting leakage of trapped solutes from phospholipid vesicles during thermotropic phase transitions.* **Hays, LM, et al.** 2, March 2001, Cryobiology, Vol. 42, pp. 88 - 102.

8. APPENDIX A: PROTEIN DENATURATION AND MEMBRANE PHASE TRANSITION DURING THERMAL TREATMENTS OF MAMMALIAN CELLS: AN FTIR STUDY[5]

This chapter describes the molecular events during the thermal treatment of cells (freezing and heating) are cell specific and unique. A potential method to "thermal fingerprint" mammalian cells is suggested. The present author along with Dr. Willem Wolkers performed all the experiments and data analysis. The results from this chapter are being compiled and edited for publication:

I. Balasubramanian SK, Wolkers WF, and Bischof JC (In preparation) "Protein denaturation and membrane phase transition during thermal treatments of mammalian cells: An FTIR study"

[5]This project was financially supported by the National Institute of Health (NIH) R01-CA07528. W.F. Wolkers performed work in Minnesota and Hannover for this project and was supported in part by funding from the Deutsche Forschungsgemeinschaft (DFG, German Research Foundation) for the Cluster of Excellence REBIRTH (From Regenerative Biology to Reconstructive Therapy).

Thermal treatments – cryopreservation, cryosurgery or thermal ablation – aim to maximize cell survival or injury depending on the application. Protein denaturation and membrane phase transition have been implicated in cell injury during thermal treatments. However, there is a dearth of information on protein and lipid changes in the cellular environment during thermal treatments. In this study, Fourier transform infrared (FTIR) spectroscopy is used to investigate molecular events that accompany thermal stresses in three different cell types including cardiovascular cells (porcine aortic smooth muscle cells (SMC), human dermal fibroblasts (HDF)), and malignant (LNCaP prostate tumor) cells as compared to pure protein and lipid controls. Protein denaturation is found to be a cell specific response during heating. Distinct denaturation temperatures and cooperativity of denaturation are identified per cell type. Freezing induced cold denaturation of proteins is found to be reversible for HDF and LNCaP cells but not for SMC. This suggests that the proteins are more stable (or less susceptible to freeze injury) in LNCaP and HDF as compared to SMC. The cells display similar membrane phase behavior during heating that lack a distinct thermotropic phase transition. Protein denaturation during heating is suggested as a potential method to thermal fingerprint mammalian cells.

8.1 INTRODUCTION

Thermal treatment of cells is generally aimed to maximize cell survival (e.g. cryopreservation) or injury (e.g. cryosurgery or thermal ablation) depending on the desired application (1; 2; 3). The treatments lead to changes in the membranes and proteins of cells, which has been implicated in cell injury. Specifically, protein denaturation and membrane phase transition have been linked as potential cell injury mechanisms during thermal treatments (4; 5). Hence, it is important to understand the effect of the thermal stability of membranes and proteins. The thermo-physical properties of pure lipids and proteins are well studied but not a lot is known on the thermal stability of membranes and proteins in the cellular environments.

Protein denaturation during heating has been implicated as a cell injury mechanism during heating (5; 6). Protein denaturation refers to the conformational transition resulting in a partial or total unfolding of proteins from its native state. This is often characterized by secondary structure changes from alpha helix to extended beta sheet structures (7). Protein denaturation has been reported at both high and low temperatures for cells (6; 8). In addition, an enthalpy or calorimetric event has been noted to occur with protein denaturation for both isolated proteins and cells (9; 10). The denaturation peaks were noted to be dependent on cell type, and the reported multiple peaks are believed to correspond to specific protein groups within the cell (i.e. membrane, cytoskeletal etc.). In a previous study, we established that protein conformational changes and corresponding enthalpy events during heating in AT-1 tumor cells are correlated with viability changes (11).

The molecular events associated with cellular freeze injury are still highly debated. Slow freezing injury has been argued to be the result of molecular damage resulting from high solute concentration (12), membrane structural changes (13) or mechanical constraints (14). Both membrane and protein structural changes have been implicated in cellular freeze injury (4; 11). The reorganization of lipids and membrane phase transition from liquid crystalline to gel phase has been reported (15; 16). The consequences of these changes are suggested to include increased membrane leakage and lateral phase separation of membrane components (17; 18). Additional molecular events including exposure to reactive oxygen species resulting in lipid peroxidation and phospholipids de-esterification have also been linked to cell injury (19). Bischof et al. attributed protein denaturation as a potential cause of AT-1 cell injury during freezing, while Ragoonan et al. linked cytoskeletal changes to cellular freeze injury (20; 21).

Fourier transform infrared spectroscopy (FTIR) is one of the few experimental techniques that can be used to simultaneously monitor membrane phase transition and protein denaturation during thermal treatments. Protein secondary structure conformational changes can be monitored using the amide I, II or III bands (22; 23; 24). Though the amide I signal is stronger, interference from water band has to be accounted for. The amide III band is weaker but equally sensitive as compared to amide I and is free of water interference (25). We have previously established protein denaturation information measured from amide I and amide III bands for LNCaP tumor cells is similar (26). Membrane phase transition events are monitored using the symmetric and asymmetric –

CH_2 stretching bands of lipid acyl chains. This band is clearly visible in the FTIR spectra of cells and is generally free of water band interference (26; 27).

In this study, the impact of thermal treatments (heating and/or freezing) on cellular protein denaturation and membrane phase transition events in three different mammalian cell types – human dermal fibroblasts (HDF), porcine smooth muscle cells (SMC) and human LNCaP prostate tumor cells – is established. It will be shown that protein denaturation of each cell type is unique leading to a "thermal fingerprint". In the future, the knowledge of cell specific lipid and protein changes may help recognize and potentially manipulate the macromolecular make of a cell thereby influencing cellular thermal treatments to either selectively induce or mitigate cell injury.

8.2 MATERIALS & METHODS

8.2.1 Cell Culture

Human Dermal Fibroblasts (HDF)

Cells were obtained from cryopreserved stock (Cambrex, East Rutherford, NJ) and cultured in Dulbecco's modified Eagle medium (DMEM) containing 10% fetal bovine serum (FBS) and 1% penicillin/streptomycin (p/s) in saline (Invitrogen, Carlsbad, CA).

LNCaP Pro 5 tumor cells

Cells were obtained from cryopreserved stock (MD Anderson Cancer center, Houston, TX) and cultured in DMEM F-12 media (Gibco, Grand Island, NY) and supplanted with 10% FBS and 1% p/s in saline.

Porcine Smooth Muscle Cells (SMC)

Cells were isolated from explanted porcine femoral arteries as described (28). Vessels were cut into small pieces and cells were grown in Petri dishes as described earlier (29). Cell media was composed of DMEM F-12 containing 10% FBS, 1% p/s in saline and 1% L-glutamine. Cell passages 3-4 were used for experiments.

All cells were trypsinized using 0.05% Trypsin and 0.53mM EDTA (Gibco, Gaithersburg, MD). The trypsin was inactivated using serum filled media. Cells were then centrifuged at 400g for 10min, the media removed and 12µL of the cell pellet was sandwiched between CaF_2 windows for FTIR analysis.

8.2.2 FTIR setup and analysis

FTIR spectra were obtained using a Nicolet Magna 750 spectrometer (Thermo-Nicolet, Madison, WI) equipped with a TGS detector. Spectra were acquired at $4cm^{-1}$ resolution using 32 co-added interferograms between 4000-900cm^{-1} wavenumber ranges. The samples were mounted into a specialized temperature cell whose temperature was regulated using a temperature controller (Minco products Inc., Minneapolis, MN). Sample temperature, also monitored separately using a thermocouple, was increased from room temperature to 90^{o}C at 1^{o}C/min. Spectral analysis was carried out using Omnic software (Thermo-Nicolet, Madison, WI). The symmetric and asymmetric $–CH_2$ stretching bands of lipid acyl chains are visible at 3000-2800 cm^{-1}. Protein denaturation was determined by monitoring area changes of the raw spectra in the α helical (~1315cm^{-}

^{1}) and the β sheet (~1235cm^{-1}) regimes (amide III region) as a function of temperature as previously described (26).

8.3 RESULTS

8.3.1 Denaturation of Pure Proteins

Bovine serum albumin (BSA) was used to baseline the protein denaturation analysis using FTIR. Spectral analysis of the amide III band was done from 20^{o}C to 95^{o}C at 1^{o}C/min to monitor protein denaturation. Figure 8.1 depicts the increase in the extended β-sheet structures and the decrease in α-helical structures during thermal denaturation of BSA. An inverse linear correlation (R^2=0.98) is obtained between the content of α-helix and β-sheet structures (Figure 8.1– inset). This indicates that protein denaturation is associated with definitive structural changes that are captured using FTIR. The onset temperature (T_{onset}) of BSA is noted to be 66°C.

Protein denaturation profiles are unique during heating. This is shown in Figure 8.2 for egg white and lysozyme. A first derivative of the curves is obtained to differentiate maxima in the denaturation profiles of the proteins. Egg white exhibits two peaks associated with protein denaturation at 65.7^{o}C and 77.5^{o}C. In comparison, lysozyme, which is purified from egg white, has one defined denaturation peak at 79.8^{o}C.

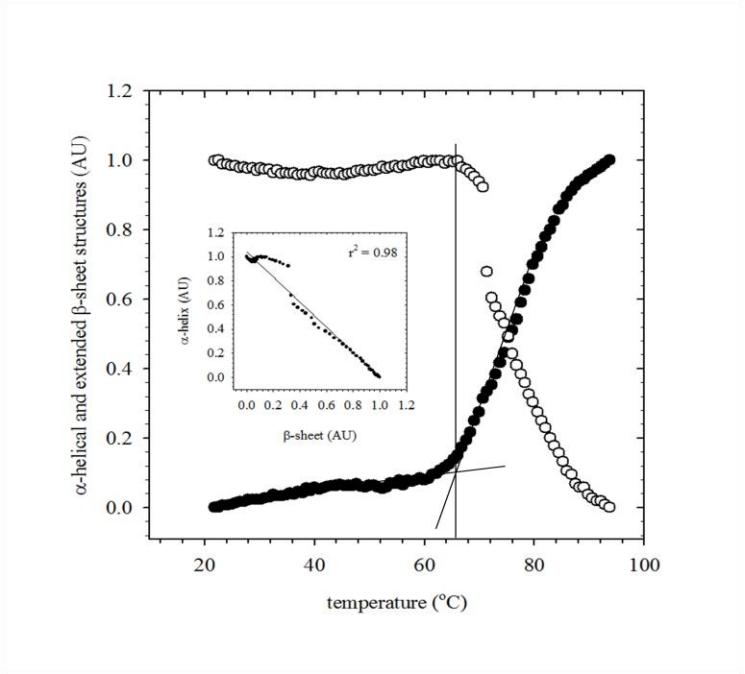

Figure 8.1: Protein denaturation of Bovine Serum Albumin (BSA) is characterized by monitoring changes to the α-helical and extended β-sheet structures as a function of temperature increases from 20°C to 95°C. The inset depicts the correlation between the decrease in α-helical and the increase in extended β-sheet content during thermal denaturation.

8.3.2 FTIR spectra of Cells

The FTIR spectra of cells show characteristic bands for water, lipids and proteins. Figure 8.3 illustrates the FTIR absorption spectra of smooth muscle cells (SMC) at 0°C and 90°C. Strong vibration bands from water are observed at ~3200-3600 cm^{-1}, ~2200 cm^{-1} and ~1650 cm^{-1} corresponding to the –OH stretching vibration, the libration and bending combination vibration, and the scissoring vibration, respectively. The symmetric and asymmetric $–CH_2$ stretching bands of lipid acyl chains are visible at 3000-2800 cm^{-1}. Characteristic protein bands are visible at ~1650 cm^{-1}, ~ 1550 cm^{-1} and ~1250 cm^{-1} corresponding to the amide-I, amide-II and amide-III regions of the spectrum

respectively. Changes to the overall protein secondary structure of the cellular proteins have been quantified using the amide III band.

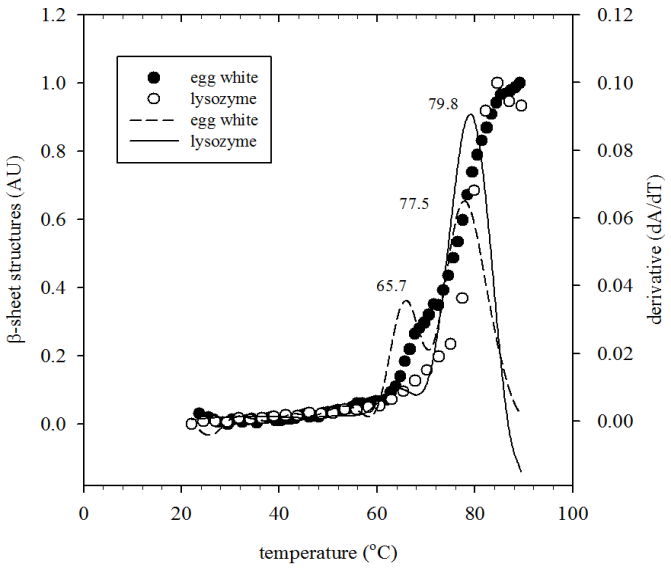

Figure 8.2: Protein denaturation of pure proteins – egg white and lysozyme - characterized by monitoring changes to the extended β-sheet structures as a function of temperature increase from 20°C to 90°C. First derivative profiles of the curves are included to elucidate the denaturation maxima

8.3.3 Protein denaturation following freeze/thaw

The thermal denaturation of control cells and following freeze/thaw to -80°C is compared for SMC and HDF cells (Figure 8.4). For the SMC control cells, denaturation is a highly cooperative event starting at an onset of 49°C ending at 63°C. Freezing decreases the onset temperature of protein denaturation (46°C) and broadens the denaturation transition (ending at 72°C). In contrast, the denaturation profiles of control and freeze/thaw HDF

cells are not statistically significant different from one another. The onset denaturation temperature (44^{o}C) and the denaturation profiles are comparable.

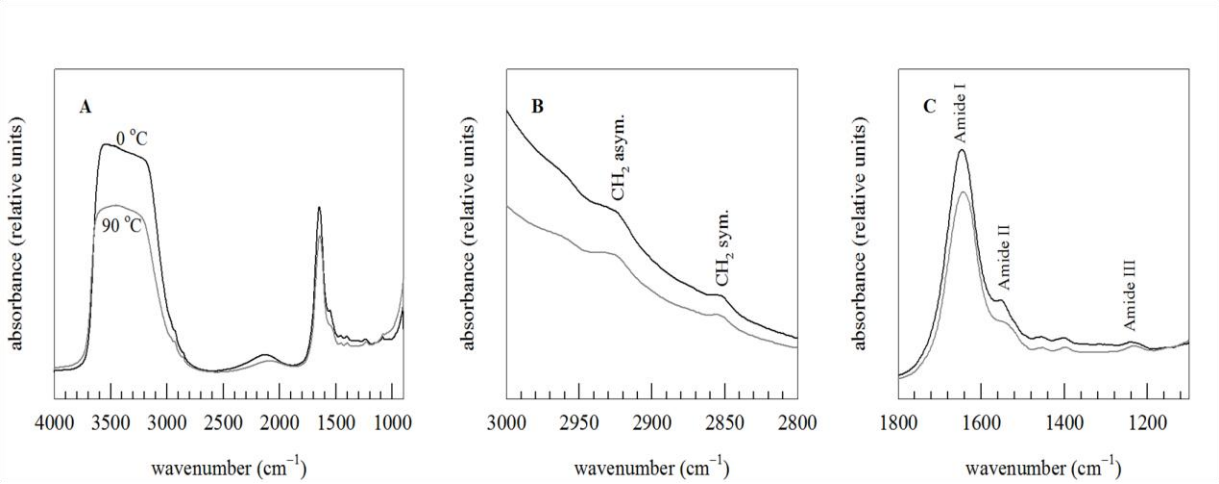

Figure 8.3: FTIR spectra of smooth muscle cells (SMC) at 0^{o}C and 90^{o}C. (A) Overall spectral profile that captures the contribution of water, lipids and proteins. (B) Enlargement of spectral region containing the asymmetric and symmetric –CH_2 stretching bands of lipid acyl chains. (C) Enlargement of the spectral region containing the Amide I, Amide II and Amide III bands.

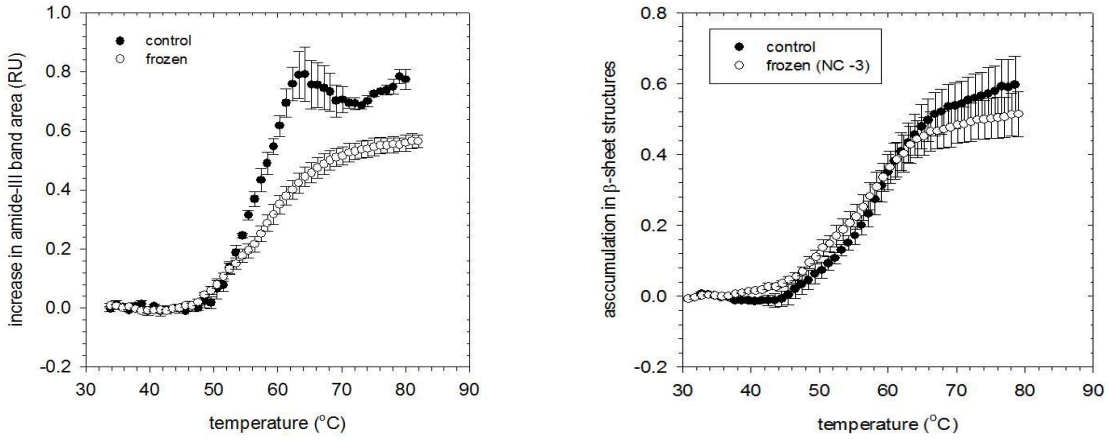

Figure 8.4: Comparison of the protein denaturation of control (non-frozen) and post freeze/thaw cells – (A) Smooth muscle cells (SMC) & (B) Human dermal fibroblasts (HDF) – characterized by monitoring changes to the extended β-sheet structures as a function of temperature increase from 20^{o}C to 90^{o}C. The error bars denote standard deviation (SD) in data obtained from testing N = 3 samples each.

8.3.4 Protein denaturation during heating

The denaturation of three different cell types (SMC, HDF & LNCaP) is quantified during heating from room temperature to 90^{o}C at a rate of 1^{o}C/min. Figure 8.5 shows the increase in the β sheet structures for these cell types as a function of temperature. First derivative plots are included to identify peaks and transition regions in the denaturation profiles. The heat denaturation profile is cell-specific with unique onset temperature of protein denaturation (T_{onset}), width of the denaturation transition ($T_{midpoint}$ and cooperativity), and the number of denaturation events. The onset denaturation temperatures for SMC, HDF and LNCaP are 49.5^{o}C, 44.5^{o}C and 45.8^{o}C respectively. Table 8.1 shows the onset and midpoint temperatures of protein denaturation and the cooperativity of the denaturation for the three cell types.

Table 8.1: A comparison of the distinctive denaturation response of cells obtained during heating from room temperature to 90^{o}C

CELL TYPE	T_{ONSET} (^{O}C)	$T_{MIDPOINT}$ (^{O}C)	COOPERATIVITY AT $T_{MIDPOINT}$ (AREA $^{O}C^{-1}$)	CORRELATION COEFFICIENT (r)
SMC	49.5	56.3	0.071	0.69
HDF	44.5	57.2	0.057	1.00
LNCaP	45.8	53.8	0.038	0.91

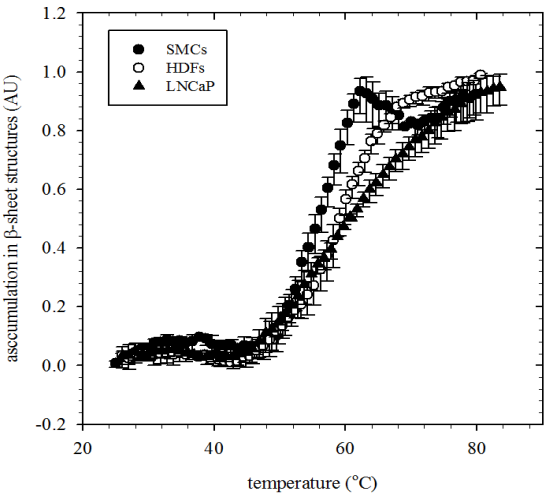

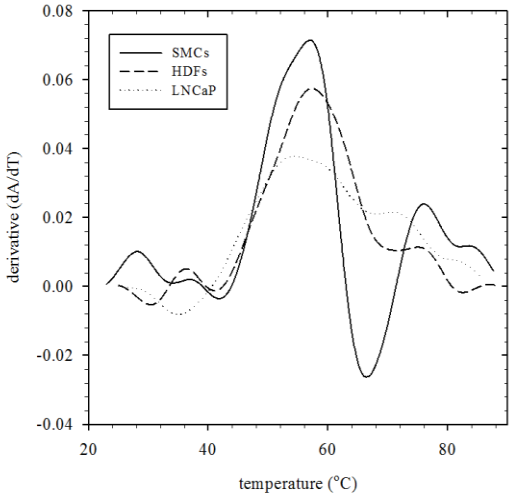

Figure 8.5: (A) Comparison of the protein denaturation of three different cell types – Smooth muscle cells (SMC), Human dermal fibroblasts (HDF), and LNCaP prostate tumor cell – characterized by monitoring changes to the extended β-sheet structures as a function of temperature increase from 20°C to 90°C. The error bars denote standard deviation (SD) in data obtained from testing N = 3 samples each. (B) First derivative of the average denaturation curves are plotted as a function of temperature

A correlation coefficient was calculated from the spectral profile with HDF as baseline as defined below. In the equation, x and y refers to the wavenumber difference (spectral

information) of HDF and other cell type (SMC or LNCaP) respectively. A lower value of correlation coefficient (r) denotes a greater difference from the HDF denaturation response. SMC denaturation has a lower correlation (0.69) as compared to LNCaP denaturation (0.91).

$$r = \frac{\sum_{i=1}^{N} x_i y_i}{\sqrt{\sum x_i^2 . \sum y_i^2}}$$

8.3.5 Membrane Fluidity Changes During Heating

Membrane phase transition events were studied during heating of the cells from room temperature to 90^{o}C. Figure 8.6 compares the membrane phase transition of the cells to two pure lipids – DOPC and DPPC. The pure lipids show thermotropic phase transitions at 41^{o}C and -22 °C for respectively DPPC and DOPC. The cells do not show thermotropic phase transitions in the suprazero temperature regime, but show a monotonous increase in νCH_2 from 2852.0 to 2852.7 cm^{-1} during heating from 20^{o}C to 90°C. The wavenumber position of νCH_2 in the suprazero temperature regime suggests that the cellular membranes of the three cell types are in the fluid phase characterized by the high conformational disorder of the lipid acyl chains.

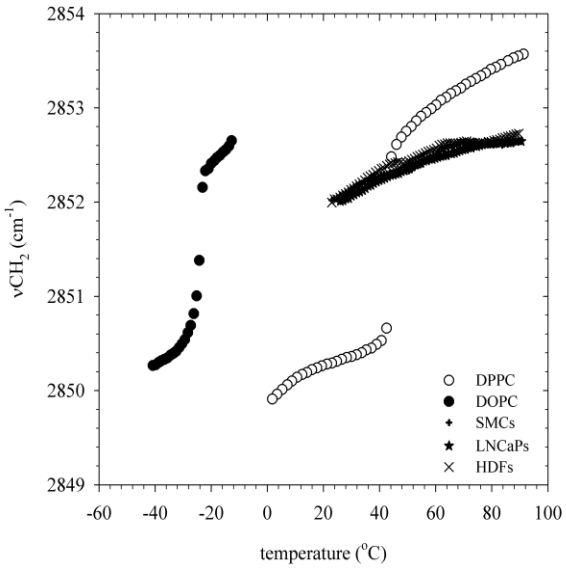

Figure 8.6: Comparison of the membrane fluidity changes of three different cell types – Smooth muscle cells (SMC), Human dermal fibroblasts (HDF), and LNCaP prostate tumor cell – with pure lipid systems DOPC and DPPC. The data points reflect the wavenumber position of the CH_2 symmetric stretching band at ~2850 cm^{-1} as a function of temperature.

8.4 DISCUSSION

FTIR is used to characterize the molecular events in three different mammalian cell types – SMC, HDF and LNCaP – during controlled heating and freezing. Protein denaturation is shown to be unique and cell specific during heating. All cells exhibit a highly conformational membrane disorder during heating, which is noted to be different from the thermotropic phase transition behavior of pure lipid systems.

Protein denaturation is generally associated with a decrease in the α-helix and a corresponding increase in the β-sheet content (25; 30). Based on the analysis of the asymptotes – indicating the onset of denaturation – of the α-helix and the β-sheet curves, the onset denaturation temperatures are predicted. The denaturation profile of pure

proteins was studied to identify the onset denaturation temperature and the number of peaks of denaturation as potentially unique events. Based on this, we identified these denaturation events for the three cell types and noted them to be unique during heating. This is in agreement with previous data where differential scanning calorimeter (DSC) was used to show that protein denaturation is a cell specific event dependent on the protein composition of the cell (10). Hence, we suggest that the thermal denaturation response can potentially be used as a thermal fingerprint of the cell.

Thermal denaturation of control cells was compared to freeze/thaw cells for SMC and HDF. The data suggests that freeze/thaw led to an irreversible denaturation event in SMCs but not for HDF (Figure 8.4). This indicates that SMCs are more susceptible to thermal freeze injury as compared to HDF and LNCaP cells. Our previous *in vitro* freezing experiments for viability of HDF and SMC suggests the same (31; 32). The increased susceptibility of SMCs to cooling has also been reported elsewhere (33; 34). The effect of freezing resulting in reversible protein denaturation has been previous noted for LNCaP cells (26). In contrast, AT-1 cells were observed to show irreversible protein denaturation based on the end temperature of freezing (20). These observations suggest that certain cell types may undergo irreversible protein denaturation during freeze/thaw, which could make them more susceptible to freeze injury.

Cellular membranes are known to be impacted by freezing. We have previously studied membrane phase transition events during freezing of multiple cell types and linked them to cellular biophysical events (27). Slow freezing was associated with both thermotropic and lyotropic phase transition events. In this study, the results indicate that the

membranes retain their high conformational disorder during heating. This is suggested when compared to the thermotropic phase transition events noted at defined temperatures for DOPC and DPPC. This hints that heating may impact cellular proteins more as compared to lipids. Additional work is needed to identify specific membrane phase transition and protein denaturation events that can be correlated to cell injury.

8.5 REFERENCES

1. *The history and principles of cryopreservation.* **Pegg, DE**., February 2002, Semin Reprod Med, Vol. 20, pp. 5 - 13.

2. *Cryosurgery.* **Rubinsky, B.** 2000, Annual Rev Biomed Eng, Vol. 2, pp. 157 - 187.

3. *Thermal therapy, part 1: An introduction to thermal therapy.* **Habash, RW, et al.** 6, 2006, Crit Rev Biomed Eng, Vol. 34, pp. 459 - 489.

4. *Destabilization of the plasma membrane of isolated plant protoplasts during a freeze-thaw cycle: The influence of cold acclimation.* **Steponkus, PL, Dowgert, MF and Gordon-Kamm, WJ.** 4, August 1983, Cryobiology, Vol. 20, pp. 448 - 465.

5. *Cellular effects of hyperthermia: Relevance to the minimum dose for thermal damage.* **Lepock, JR.** 3, 2003, Int J Hyperthermia, Vol. 19, pp. 252 - 266.

6. *Cellular responses to hyperthermia (40-46 degrees C): Cell killing and molecular events.* **Roti Roti, JL.** 1, 2008, Int J Hyperthermia, Vol. 24, pp. 3 - 15.

7. *Thermal stability of proteins.* **Bischof, JC and He, X.** 2005, Annals of NY Acad Sci, Vol. 1066, pp. 12 - 33.

8. *Cold shock injury in animal cells.* **Watson, PF and Morris, GJ.** 1987, Symp Soc Exp Biol, Vol. 41, pp. 311 - 340.

9. *Heat capacity and conformation of proteins in the denatured state.* **Privalov, PL, et al.** 4, February 1989, J Mol Biol, Vol. 205, pp. 737 - 750.

10. *Measurement of protein stability and protein denaturation in cells using differential scanning calorimetry.* **Lepock, JR.** 2, 2005, Methods, Vol. 35, pp. 117 - 125.

11. *In situ thermal denaturation of proteins in Dunning AT-1 prostate cancer cells: Implication for hyperthermic cell injury.* **He, X, et al.** 10, October 2004, Ann Biomed Eng, Vol. 32, pp. 1384 - 1398.

12. *The haemolysis of human red blood-cells by freezing and thawing.* **Lovelock, JE.** 3, March 1953, Biochimica Biophysica Acta, Vol. 10, pp. 414 - 426.

13. *Mechanical study of the deformation and rupture of the plasma membranes of protoplasts during osmotic expansions.* **Wolfe, J, Dowgert, MF and Steponkus, PL.** 1986, J Membrane Biol, Vol. 93, pp. 63 - 74.

14. *Freezing injury and its prevention in living cells.* **Meryman, HT.** 0, 1974, Annual Rev Biophys Bioeng, Vol. 3, pp. 341 - 363.

15. *The combined and separate effects of low temperature and freezing on membrane lipid mesomorphic phase behavior: Relevance to cryobiology.* **Caffrey, M.** 1, January 9, 1987, Biochimica Biophysica Acta, Vol. 896, pp. 123 - 127.

16. *Freezing, drying, and/or vitrification of membrane-solute-water systems.* **Wolfe, J and Bryant, G.** 1999, Cryobiology, Vol. 39, pp. 103 - 129.

17. *Can hydration forces induce lateral phase separataions in lamellar phases?* **Bryant, G and Wolfe, J.** 6, 1989, Eur Biophysical J, Vol. 16, pp. 369 - 374.

18. *Factors affecting leakage of trapped solutes from phospholipid vesicles during thermotropic phase transitions.* **Hays, LM, et al.** 2, March 2001, Cryobiology, Vol. 42, pp. 88 - 102.

19. *In situ detection and localization of lipid peroxidation in individual bovine sperm cells.* **Brouwers, JF and Gadella, BM.** 11, December 2003, Free Radic Biol Med, Vol. 35, pp. 1382 - 1391.

20. *Lipid and protein changes due to freezing in Dunning AT-1 cells.* **Bischof, JC, et al.** 1, August 2002, Cryobiology, Vol. 45, pp. 22 - 32.

21. *Response of the cell membrane-cytoskeleton complex to osmotic and freeze/thaw stresses.* **Ragoonan, V, Hubel, A and Aksan, A.** 3, 2010, Cryobiology, Vol. 61, pp. 335 - 344.

22. *In situ FTIR assessment of dessication-tolerant tissues.* **Wolkers, WF and Hoekstra, FA.** 2003, Spectroscopy, Vol. 17, pp. 297 - 313.

23. *Determination of protein secondary structure by Fourier transform infrared spectroscopy: A critical assessment.* **Surewicz, WK, Mantsch, HH and Chapman, D.** 2, January 1993, Biochemistry, Vol. 32, pp. 389 - 394.

24. *Determination of soluble and membrane protein structure by Fourier transform infrared spectroscopy. III. Secondary structures.* **Goormaghtigh, E, Cabiaux, V and Ruysschaert, JM.** 1994, Subcell Biochem, Vol. 23, pp. 405 - 450.

25. *A distinct utility of the amide III infrared band for secondary structure estimation of aqueous protein solutions using partial least squares method.* **Cai, S and Singh, BR.** 9, March 9, 2004, Biochemistry, Vol. 43, pp. 2541 - 2549.

26. *Effects of freezing on membranes and proteins in LNCaP prostate tumor cells.* **Wolkers, WF, et al.** 3, March 2007, Biochimica et Biophysica Acta, Vol. 1768, pp. 728 - 736.

27. *Membrane hydration correlates to cellular biophysics during freezing in mammalian cells.* **Balasubramanian, SK, Wolkers, WF and Bischof, JC.** 5, May 2009, Biochimica Biophysica Acta, Vol. 1788, pp. 945 - 953.

28. *Heterogeneity of smooth muscle cell populations cultured from pig coronary artery.* **Hao, H, et al.** 7, July 1, 2002, Arteriscler Thromb Vasc Biol, Vol. 22, pp. 1093 - 1099.

29. *In vitro model systems for evaluation of smooth muscle cell response to cryoplasty.* **Grassl, ED and Bischof, JC.** 2, April 2005, Cryobiology, Vol. 50, pp. 162 - 173.

30. *Identification of beta-turn and random coil amide III infrared bands for secondary structure estimation of proteins.* **Cai, S and Singh, BR.** 1, July 1999, Biophys Chem, Vol. 80, pp. 7 - 20.

31. *Thermal injury prediction during Cryoplasty through in vitro characterization of smooth muscle cell biophysics and viability.* **Balasubramanian, SK, et al.** 1, Januart 2008, Annals of Biomedical Engineering, Vol. 36, pp. 86 - 101.

32. *Cooling rate dependent biophysical and viability response shift with attachment state in human dermal fibroblast cells.* **Choi, J and Bischof, JC.** 3, October 2011, Cryobiology, Vol. 63.

33. *Direct comparison of endothelial cell and smooth muscle cell response to supercooling and rewarming.* **Yiu, WK, Cheng, SW and Sumpio, BE.** 3, 2007, J Vasc Surg, Vol. 46, pp. 557 - 564.

34. *In vitro evaluation of vascular endothelial and smooth muscle cell survival and apoptosis in response to hypothermia and freezing.* **Tatsutani, KN, et al.** 1, 2005, Cryo Letters, Vol. 26, pp. 55 - 64.